Development of appropriate steam turbine models in Flownex

Prepared by:

Rahendra Laljith Neerputh

NRPRAH001

Department of Mechanical Engineering

University of Cape Town

Supervisor:

Dr WF Fuls

December 2014

Submitted to the Department of Mechanical Engineering at the University of Cape Town in partial fulfilment of the academic requirements for a Masters of Science degree in Mechanical Engineering

Key Words: Thermo-hydraulic model, steam turbines, Flownex

Abstract

The Specialization Centre for Energy Efficiency at the University of Cape Town has a goal of building thermo-hydraulic models of an entire power plant. A one-dimensional thermo-hydraulic network solver, Flownex, is the software envisaged to accomplish this goal. The development of appropriate steam turbine models in Flownex supports fulfilment of this goal.

Steam turbines of fossil and nuclear power plants make up most of the generating capacity for the majority of industrialised and industrial developing countries, except for those whose power industry depends mainly on hydroelectric power plants [1]. It is therefore a matter of great interest to be able to predict the steady state and transient operation of steam turbines.

The aim of this dissertation was to use minimal data that was readily available to the end user to develop accurate models. Acceptance test data was used as the primary source because it is more reliable than plant data.

Various pressure drop correlations and methods to predict off-design efficiency were investigated. These correlations and methods were solved analytically and implemented in Flownex. Interpretation of the error analysis for the pressure drop correlations established that the general empirical law using inlet conditions and Stodola law in the volume form were the most accurate and consistent in predicting mass flow rate and pressure. The Ray method was shown to be the most accurate to predict off-design efficiency and one of the less complicated to implement.

Steady state models were built for four turbine trains using the general empirical and Stodola laws. The results produced by both correlations were similar, showing that for high vacuum conditions either correlation could be used.

The general empirical law was the chosen correlation to implement for transient analysis since it was generally more accurate and easier to implement than Stodola. The power predicted by the model was within ±1 % of that of the actual power produced.

Declaration

I, Rahendra Laljith Neerputh, hereby declare the work contained in this dissertation to be my own. All information which has been gained from various journal articles, text books or other sources has been referenced accordingly. I have not allowed, and will not allow, others to copy my work with the intention of passing it off as their own work or part thereof.

Signed by candidate

_____

Rahendra Laljith Neerputh

Acknowledgements

I am utterly indebted to the Supreme Personality of Godhead, Sri Krishna, for giving me some knowledge to be able to complete this dissertation. I am grateful to my family for their support during my studies.

I extend my sincere thanks and gratitude to my academic supervisor Dr WF Fuls for his invaluable guidance and assistance throughout this dissertation. It is much appreciated.

I am also grateful to my industrial supervisor Mr G de Klerk for his assistance in obtaining information for the Eskom power plants and for his guidance.

To all the students in the Eskom Centre for Energy Efficiency laboratory, I would like to thank you for your assistance and for making the laboratory an interesting and entertaining place.

I would like to thank my engineering manager, Ms L Kone, and my manager, Mrs D Mathebula, for sponsoring my studies and providing me with the opportunity to further my career. I would also like to thank EPPEI management and staff for considering me for the EPPEI post graduate programme.

I am indebted to many of my colleagues who assisted with gathering plant data from their power plants, especially Mr P Takane.

Table of Contents

List of Figures

List of Tables

List of Nomenclature

General symbols

C_k	Turbine loss constant [the units depend on the value of α and β]
C_ℓ	Nozzle loss co-efficient
g	Gravitational acceleration [m/s^2]
h	Static enthalpy [kJ/kg]
h_a	Static inlet enthalpy to the fixed blade [kJ/kg]
h_b	Static inlet enthalpy to the rotating blade [kJ/kg]
h_c	Static exit enthalpy from the rotating blade [kJ/kg]
h_1	Static inlet enthalpy [kJ/kg]
h_2	Static outlet enthalpy [kJ/kg]
h_{2s}	Static outlet isentropic enthalpy [kJ/kg]
h_{2sn}	Static outlet isentropic enthalpy at nominal conditions [kJ/kg]
Δh_s	Isentropic enthalpy drop [kJ/kg]
Δh_{sn}	Isentropic enthalpy drop at nominal conditions [kJ/kg]
h_o	Total enthalpy [kJ/kg]
h_{o1}	Total inlet enthalpy [kJ/kg]
h_{o2}	Total outlet enthalpy [kJ/kg]
k	Isentropic index
k_L	Pipe loss factor
L	Length [m]
m	Mass flow rate [kg/s]
m_1	Inlet mass flow rate [kg/s]
m_{1n}	Inlet mass flow rate at nominal conditions [kg/s]
m_2	Outlet mass flow rate [kg/s]
N	Turbine rotational speed [rpm]
N_n	Turbine rotational speed at nominal conditions [rpm]
p	Static pressure [Pa]
Δp	Static pressure drop [Pa]
p_1	Static inlet pressure [Pa]
p_{1n}	Static inlet pressure at nominal conditions [Pa]

p_2	Static outlet pressure [Pa]
p_{2n}	Static outlet pressure at nominal conditions [Pa]
p_s	Static pressure in the nozzle throat [Pa]
p_o	Total pressure [Pa]
p_{o1}	Total inlet pressure [Pa]
p_{o1n}	Total inlet pressure at nominal conditions [Pa]
p_{o2}	Total outlet pressure [Pa]
p_{o2n}	Total outlet pressure at nominal conditions [Pa]
Δp_o	Total pressure drop [Pa]
Q	Volume flow rate [m^3/s]
Q_1	Inlet volume flow rate [m^3/s]
Q_{1n}	Inlet volume flow rate at nominal conditions [m^3/s]
Q_2	Outlet volume flow rate [m^3/s]
Q_{ave}	Average volume flow rate [m^3/s]
$\dot{Q}$	Heat flow[J/s]
$\dot{Q}_{added}$	Heat added to steam generator [J/s]
$\dot{Q}_{rejected}$	Heat rejected by condenser [J/s]
R	Universal gas constant [J/molK]
R_{steam}	Specific gas constant for steam[kJ/kgK]
s	Entropy [kJ/kgK]
s_1	Inlet entropy [kJ/kgK]
s_2	Outlet entropy [kJ/kgK]
Δs	Change in entropy [kJ/kgK]
t	Time [s]
T	Static temperature [K]
T_1	Static inlet temperature [K]
T_{1n}	Static inlet temperature at nominal conditions [K]
T_o	Total temperature [K]
T_{o1}	Total inlet temperature [K]
T_{o1n}	Total inlet temperature at nominal conditions [K]
T_{o2}	Total outlet temperature [K]
U	Blade velocity [m/s]

v	Volume [m^3]
V	Velocity [m/s]
V_a	Absolute velocity of steam [m/s]
V_{ai}	Absolute inlet velocity of steam [m/s]
V_{ae}	Absolute exit velocity of steam [m/s]
V_{ri}	Relative inlet velocity of steam [m/s]
V_{re}	Relative exit velocity of steam [m/s]
$\dot{W}$	Work [J/s]
$\dot{W}_{in}$	Pump work in [J/s]
$\dot{W}_{out}$	Turbine work out [J/s]
x	Steam quality
z	Height [m]
z_1	Height at inlet [m]
z_2	Height at outlet [m]

Greek symbols

α	Volume flow rate index
α_i	Inlet angle of the absolute inlet velocity of the steam [°]
α_e	Exit angle of the absolute exit velocity of the steam [°]
β	Density index
β_i	Inlet angle of the relative inlet velocity of the steam [°]
β_e	Exit angle of the relative exit velocity of the steam [°]
ε	Schegliaiev factor
η	Efficiency
η_n	Efficiency at nominal conditions
$\Delta\eta$	Change in efficiency
ν	Specific volume [m^3/kg]
ν_1	Inlet specific volume [m^3/kg]
ν_{1n}	Inlet specific volume at nominal conditions [m^3/kg]
ϕ	Constant flow co-efficient [m^2]

ϕ_1	Inlet constant flow co-efficient [m^2]
ρ	Density [kg/m^3]
ρ_1	Inlet density [kg/m^3]
ρ_2	Outlet density [kg/m^3]
ρ_{ave}	Average density [kg/m^3]
σ	Schegliaiev dimensionless factor
Λ	Degree of reaction

Acronyms and Abbreviations

AC	Alternating current
ASME	American Society of Mechanical Engineers
BFPT	Boiler feed pump turbine
CFD	Computational fluid dynamics
EPPEI	Eskom Power Plant Engineering Institute
GE	General empirical
GE Ave	General empirical law using average conditions
GE Inlet	General empirical law using inlet conditions
GS	Generator side
HPT	High pressure turbine
IAPWS97	International Association for the Properties of Water and Steam industrial formulation 1997
IPT	Intermediate pressure turbine
LPT	Low pressure turbine
OEM	Original equipment manufacturer
SCC	Spencer, Cotton and Cannon
SI	International System of Units
Stodola T	Temperature form of Stodola law
Stodola Tave	Temperature form of Stodola law using average conditions
Stodola v	Volume form of Stodola law
Stodola vave	Volume form of Stodola law using average conditions
TS	Turbine side

1. Introduction

1.1 Problem description

The Specialization Centre for Energy Efficiency at the University of Cape Town has as its goal the building of thermo-hydraulic models for an entire fossil and nuclear power plants. The software identified to accomplish the modelling is Flownex. Flownex is a one-dimensional thermo-hydraulic network solver.

It is envisaged that the models will be used to analyse Eskom power plants in order to conduct fault finding, investigate methods of improving the cycle efficiency and simulate the behaviour of the power plant as a whole in transient situations, load rejection, islanding etc. The turbine systems form an integral part of the power plant model.

Turbine manufacturers rarely supply detailed steam path information about their turbines. This is done to prevent these turbines being used in reverse engineering by other turbine manufacturers and spares suppliers. This lack of information makes it difficult to model turbine systems accurately. The aim of this study was to use data that is available to the end user to develop the models.

The primary source of data for modelling is acceptance tests. Where there are gaps in the acceptance test data, the acceptance test is supplemented by heat balance diagrams and data from plant instrumentation.

Although acceptance test data is produced under stable steady state conditions, it is believed that suitable transient responses could be modelled using this data. One can assume quasi-steady conditions, and as long as the model “adjusts” for different quasi-conditions, the results should be representative. Of course this means that very fast transient results may not be valid.

The detailed geometry of the steam path through the turbine is not available for virtually all of the steam turbines in the Eskom fleet. However, if the detailed geometry were available it would require three-dimensional CFD software to model them. Flownex being a one-dimensional thermo-hydraulic network solver, it cannot model such problems.

There are various correlations available in literature to predict the pressure drop across a steam turbine and its efficiency during off-design load conditions. The accuracy and solving time of these correlations is important in modelling as it has an economic impact. Therefore a trade-off is required between accuracy and solving time.

In similar manner the level of detail required to model has an impact on accuracy, solving time and the ability to study special conditions, so once again a trade-off is required in the level of detail in the model.

The generic nature of the Flownex toolset makes it laborious to model a turbine system in an existing power plant. To overcome this problem, compound components are envisaged, operating like any other Flownex component. These compound components will have built-in "intelligence" about how to model a certain turbine configuration, and do the necessary pre-processing to apply the correct model parameters, given a limited set of user inputs.

1.2 Purpose of the project

The purpose is therefore to develop thermo-hydraulic models for steam turbines (including their extraction lines) with various degrees of detail to predict steady state, transients (loading and de-loading) and secondary effects using data that are available to the end user.

1.3 Scope and limitation of the project

The models are limited to steam turbines and extraction lines, but include the appropriate volumes of the working fluids, predominantly on the piping connecting the various turbine sections. The electrical power developed by the steam turbines considered ranges from 200 MW to 686 MW. The models include reaction, impulse, reheat, non-reheat, wet-cooled and dry-cooled LPTs. The lowest steam quality considered during the modelling was 0.8723 at the LPT exhaust.

The models did not contain rotational inertia of the turbine rotors, IPT cooling steam (where applicable) and gland sealing. Also, the generator is not included; the power developed, therefore, is the thermal power.

The boundary of the model was on the inlets and outlets of the turbine, including a very short portion of the extraction lines. The characteristics of feed water heaters and other components connected to the turbine were simulated with boundary conditions.

1.4 Outline of dissertation

The remainder of this dissertation is structured as follows:

Chapter 2. Literature Review: Introduction of steam turbines, pressure drop correlations and efficiency methods. Flownex and the conversion of the various equations into an implementable format are discussed. A review of Eskom steam turbine architecture is also presented. The accuracy of acceptance test data is ascertained through a review of the ASME standard.

Chapter 3. Pressure Drop Correlations: description of the methodology used in the analytical solution as well as the Flownex solution of the various pressure drop correlations. A comparison is made between the various correlations and between the analytical and Flownex implementation.

Chapter 4. Efficiency Correlations: description of the methodology used in the analytical solution and Flownex solution of the various efficiency methods. A comparison is made between the various methods and between the analytical and Flownex implementation.

Chapter 5. Case Study Implementation of the Models: showing the steady state solution of turbine train models at various load conditions. A transient scenario is also modelled in Flownex and the results are compared to actual plant data.

Chapter 6. Compound Component: presenting the description of the compound component, together with the inputs required and results produced.

Chapter 7. Conclusions and Recommendations: concluding remarks based on the analysis conducted in Chapters 3, 4 and 5 as well as proposals for recommendations for future work.

2. Literature Review

2.1 Rankine cycle

Steam power plants are based on the Rankine cycle. The working fluid, water, is condensed at low pressure (line 7-1) so that the working fluid can be pumped. The pressure of the working fluid is raised in two stages (lines 1-2 and 3-4). The temperature of the working fluid is raised at constant pressure in the steam generator (line 4-5). The working fluid is expanded in the turbine in order to produce power (line 5-7).The ideal expansion of the working fluid in the turbine is represented by line 5-7*s*. Line 6-3 represents the extraction steam to the feed water heater in order to improve cycle efficiency as well as to reduce the temperature range in the steam generator.

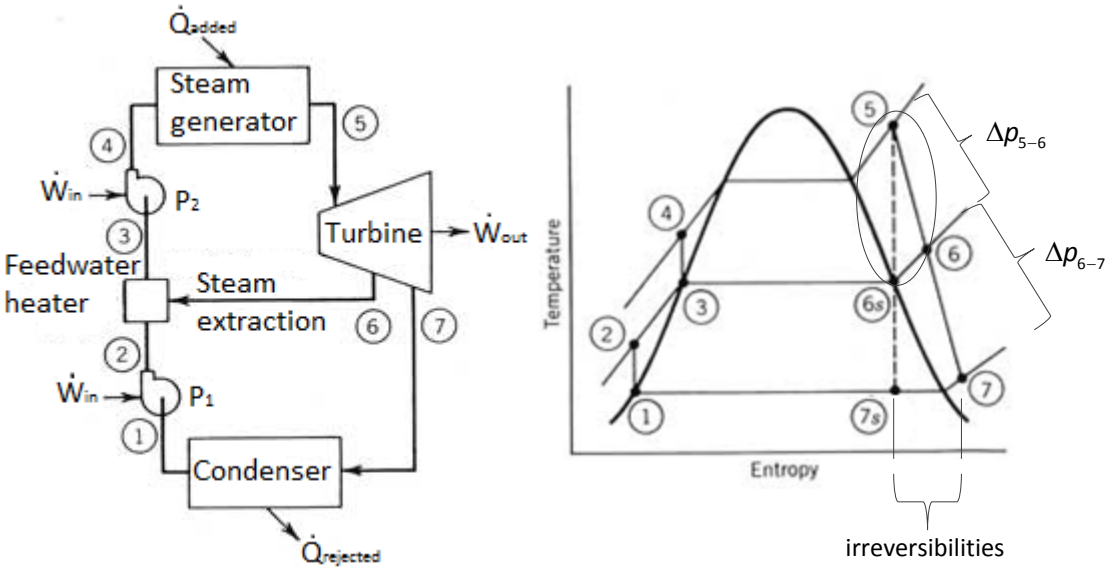

Source: Adapted from www.powerfromthesun.net/book/chapter12

Figure 1: Rankine cycle

The pressure difference from 5 to 6 (Δp_{5-6}) represents the pressure drop between the turbine inlet and the extraction point. The pressure drop Δp_{6-7} represents the pressure drop between the extraction point and the turbine exhaust. One aspect in this dissertation involves predicting these pressure drops using appropriate correlations. These correlations are discussed in section 2.4.

Turbines are not 100 % efficient, hence there is an increase in entropy due to the losses incurred. The result is that the actual expansion line from point 5 ends at point 7 and not 7*s*. Some of these

losses are discussed in section 2.5.1. The second focus of this study is to evaluate published models which would predict the isentropic efficiency of the turbine at different load cases.

2.2 Steam turbines

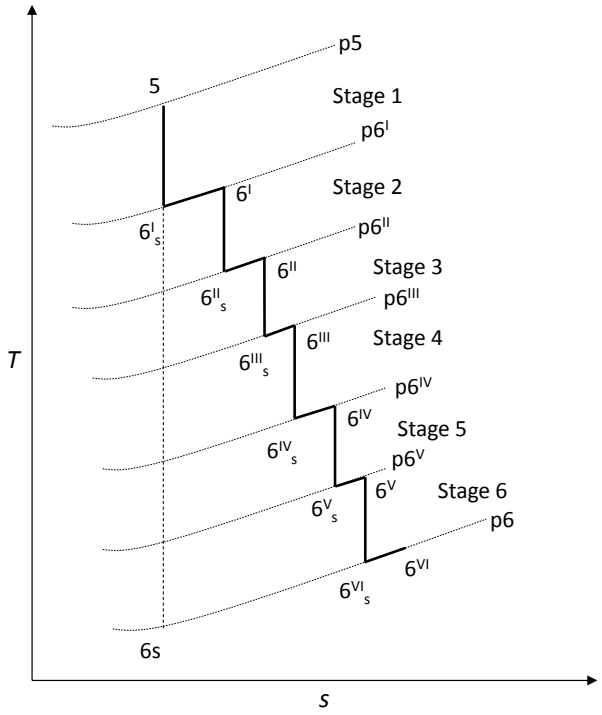

Source: Adapted from Zerban and Nye [2]

Figure 2: Representation of the expansion through each stage

The actual expansion line from 5 to 6 (and 6 to 7) is similar to one represented by Figure 2. This is the result of the stage-by-stage energy extraction in the turbine. This happens in two stages: first a portion of the thermal energy of the steam gets converted into kinetic energy through the fixed blades (or nozzles). Then the kinetic energy of the flow is extracted by the rotating blades, which transfers the work onto the turbine shaft. From a macro perspective, the flow exits at a lower density than the entrance, and it is said that the steam has expanded through the turbine, almost as-if it is expanding in a piston engine and doing work onto the shaft.

The vertical lines in Figure 2 represent the ideal flow expansion through the stage. It is generally assumed that the inlet velocity of the steam is negligible, and the flow through the nozzle is very close to isentropic [3]. The nozzle exit velocity V_{ai} can therefore be written as:

$$V_{ai} = \sqrt{2\left(h_a - h_b\right)} \tag{1}$$

The kinetic energy of the flow is then extracted by the rotating blades. Since the blades cannot extract all the kinetic energy of the steam, there is an exit velocity component. This exit velocity is then available for use in the next stage. This is called carry-over [3]. Wall friction, leaks and turbulence all result in losses, which in turn are converted to heat. The result is that the exit flow is also heated due to the losses. From a process-point of view, this appears like steam reheat, and is therefore called stage reheat [3].

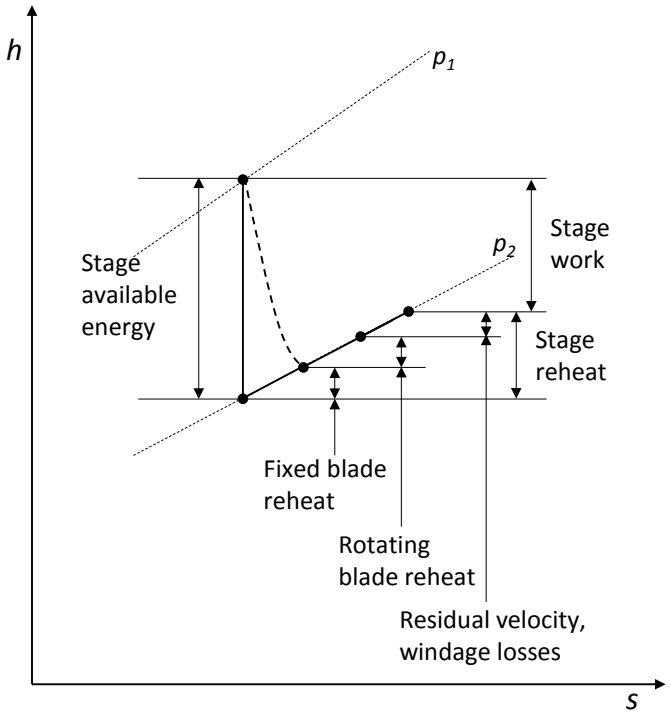

Source: Reproduced from Zerban and Nye [2]

Figure 3: Reheat losses of a single turbine stage

If one would follow the steam as it moves through the blade passages, the T-s diagram will have the saw-tooth shape shown in Figure 2. However, when studying a turbine as a single entity (using only inlet and outlet conditions), the exact expansion line through the turbine is irrelevant. The process through the turbine is therefore only described as was shown in Figure 1.

Steam turbines can be classified in several ways. One of the most important and common of these classifications is based on blade geometry and the energy conversion process. They are as follows:

- Impulse turbine.
- Reaction turbine.

2.2.1 Impulse turbine

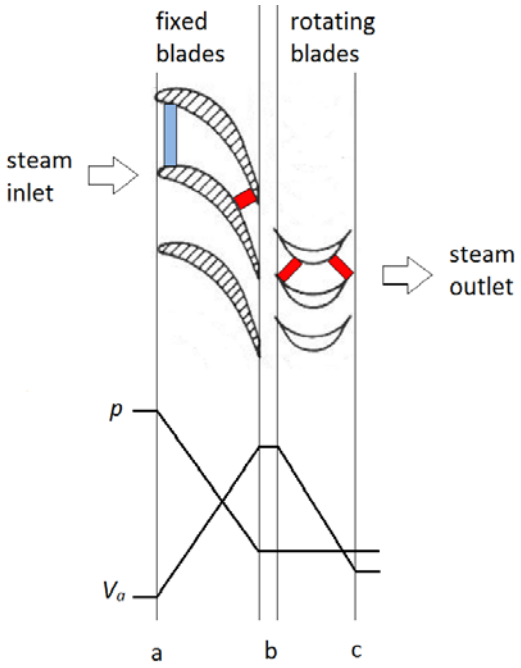

Source: Adapted from Eastop and McConkey [4]

Figure 4: Impulse turbine stage static pressure and absolute velocity variation

Figure 4 shows how the flow cross-sectional area changes from the fixed blade inlet to the rotating blade exit (coloured rectangles). The area significantly reduces along the fixed blades, causing a pressure drop and associated flow acceleration (see the bottom portion of the figure). The flow acceleration is denoted by the change in colour (blue to red) of the rectangles.

As the flow moves through the rotating blades, the static pressure remains constant because the flow cross-sectional area does not change. The relative velocity of the steam remains constant as denoted by the colour of the rectangles. However, the absolute velocity drops as the flow does work on the blades. The rotating blades change the direction (cause a change in momentum – i.e. an impulse) of the steam flow which contributes to the tangential force exerted on the blades by the steam which in turn produces the torque on the shaft.

The entire stage pressure drop therefore occurs in the fixed blades only. This suggests that one should be able to model the pressure drop using similar correlations used to model pressure drops in fixed geometry pipes. A typical model used to calculate secondary pressure drops in a pipe like bends or contractions is $\Delta p = k_L \tfrac{1}{2}\rho V^2$. This can be further expanded into a general empirical form as $\Delta p = C_k \rho^{\beta} Q^{\alpha}$, and is one of the correlations that will be considered in this study.

The actual energy extracted from the steam can be determined knowing the detail geometry of the blade passages and angles. With the aid of velocity triangles (shown in Figure 5), the relative and absolute flow velocities can be calculated graphically.

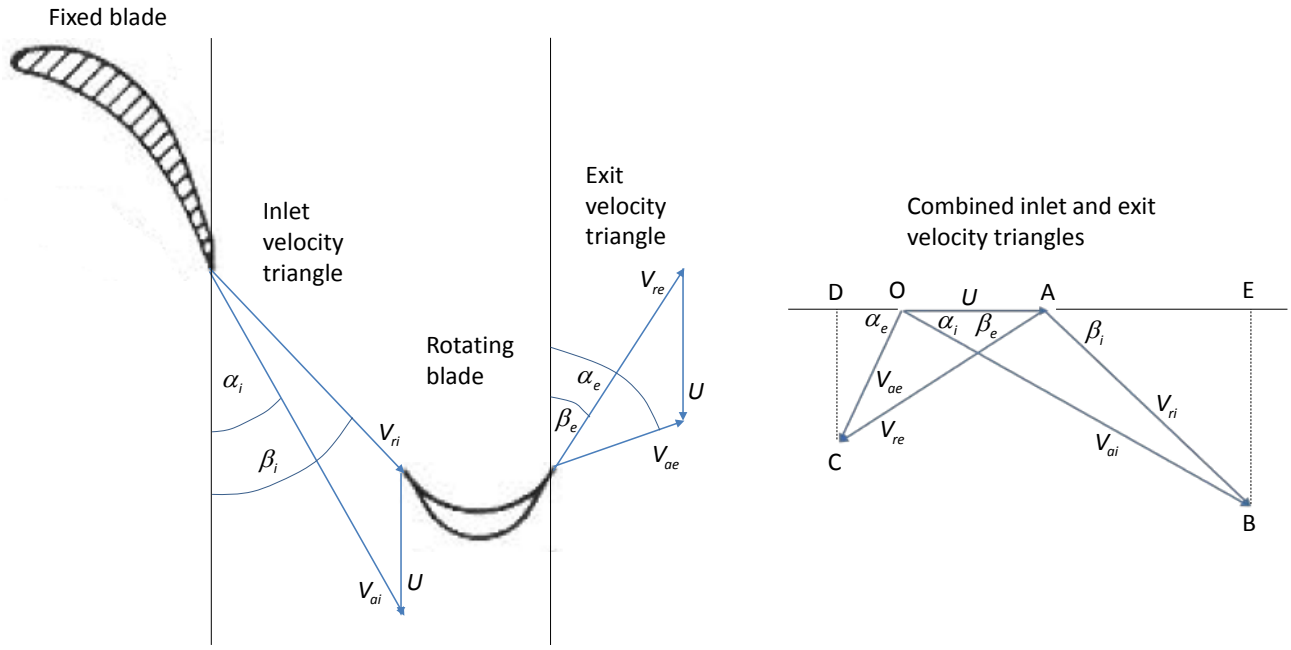

Source: Adapted from Eastop and McConkey [4]

Figure 5: Impulse turbine velocity triangles

Because the cross-sectional area in-between the rotating blade passages does not change for impulse blades, the relative velocity along the blade is the same, i.e. $V_{ri} = V_{re}$ (ignoring frictional losses along the blade passage). The power output per stage is then given by:

$$\dot{W} = \dot{m} V_{ri} U \left(\cos\beta_i + \cos\beta_e \right) \tag{2}$$

$$\text{where } V_{ri} = \frac{V_{ai}\cos\alpha_i - U}{\cos\beta_i}$$

The maximum amount of energy that can be extracted is when the absolute exit velocity V_{ae} is zero, i.e. all the kinetic energy of the incoming flow ($\frac{1}{2}V_{ai}^2$) is extracted. From inspecting the velocity triangles, one can see this means $\beta_e = 0$, which is physically impossible for an axial turbine. Additionally, to obtain maximum power output from equation (2), it means $\beta_i = 0$, or otherwise stated, $\alpha_i = 0$. This is also physically impossible to achieve in an axial flow turbine. In section 2.5.2 it will be shown that there is an optimum ratio of blade speed U versus fixed blade velocity V_{ai}, and that the efficiency is driven mostly by the fixed blade exit angle α_i.

2.2.2 Reaction turbine

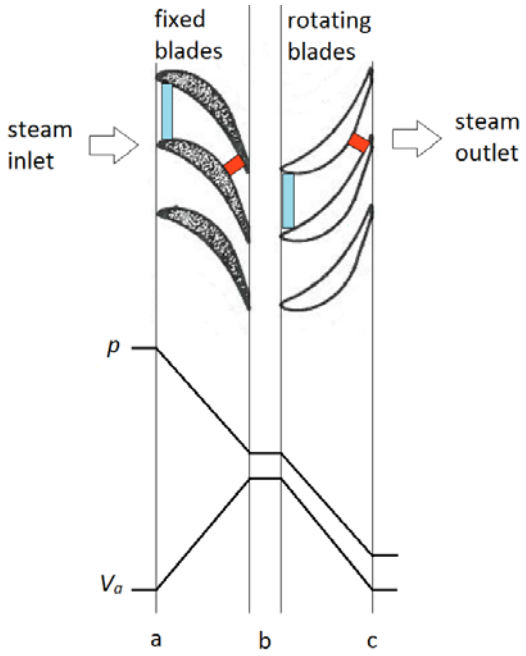

Source: Adapted from Eastop and McConkey [4]

Figure 6: Reaction turbine stage pressure and absolute velocity variation

Figure 6 shows how the flow cross-sectional area changes from the fixed blade inlet to the rotating blade exit for a reaction stage. The fixed blade flow cross-sectional area reduces similar to that of the impulse stages, but the cross-sectional area of the rotating blades flow passage is now not constant, but also reducing. The flow is therefore further accelerated in the rotating blade passages, giving rise to a reaction force, similar to the force one experiences when holding a high-flow water hose-pipe in the air. The flow acceleration (relative velocity) in both the fixed and rotating blades is denoted by the change in colour (blue to red) of the rectangles. A further pressure drop therefore occurs, but the absolute flow velocity still decreases as the kinetic energy is converted into shaft work. For practical purposes, there is always an element of impulse energy conversion because the flow needs to move generally in an axial direction through the turbine, hence requires a change in direction after the fixed blade exit.

In an impulse stage, the static enthalpy drop (and pressure drop) occurs only over the fixed blades, but for a reaction stage, a portion of the enthalpy drop (and pressure drop) occurs over the rotating blades as well. The degree of reaction is defined as the ratio of the enthalpy drop over the rotating blade to the overall enthalpy drop in the stage,

$$\Lambda = \frac{h_b - h_c}{h_a - h_c}$$

The degree of reaction in a pure reaction turbine is 100 % while the degree of reaction in a simple impulse turbine is 0 %. Most reaction turbines have a 50 % degree of reaction. For the typical pressure range of steam turbine stages, this also results in the ratio of about 0.5 for the pressure drop over the fixed blades to the overall pressure drop. The consequence of this fact for the current study is that a simple pressure drop correlation, as would be applicable for impulse stages, might not produce suitable results when applied to 50 % reaction stages. It is therefore important that the selection of turbines used to evaluate the various pressure drop correlations includes reaction as well as impulse machines.

The actual work extracted can again be determined using velocity triangles, as shown in Figure 7. For 50 % reaction stages the rotating blade is a mirror image of the fixed blade, resulting in a symmetrical velocity diagram [4]. Therefore $V_{re} = V_{ai}$, $V_{ri} = V_{ae}$ and $\beta_e = \alpha_i$.

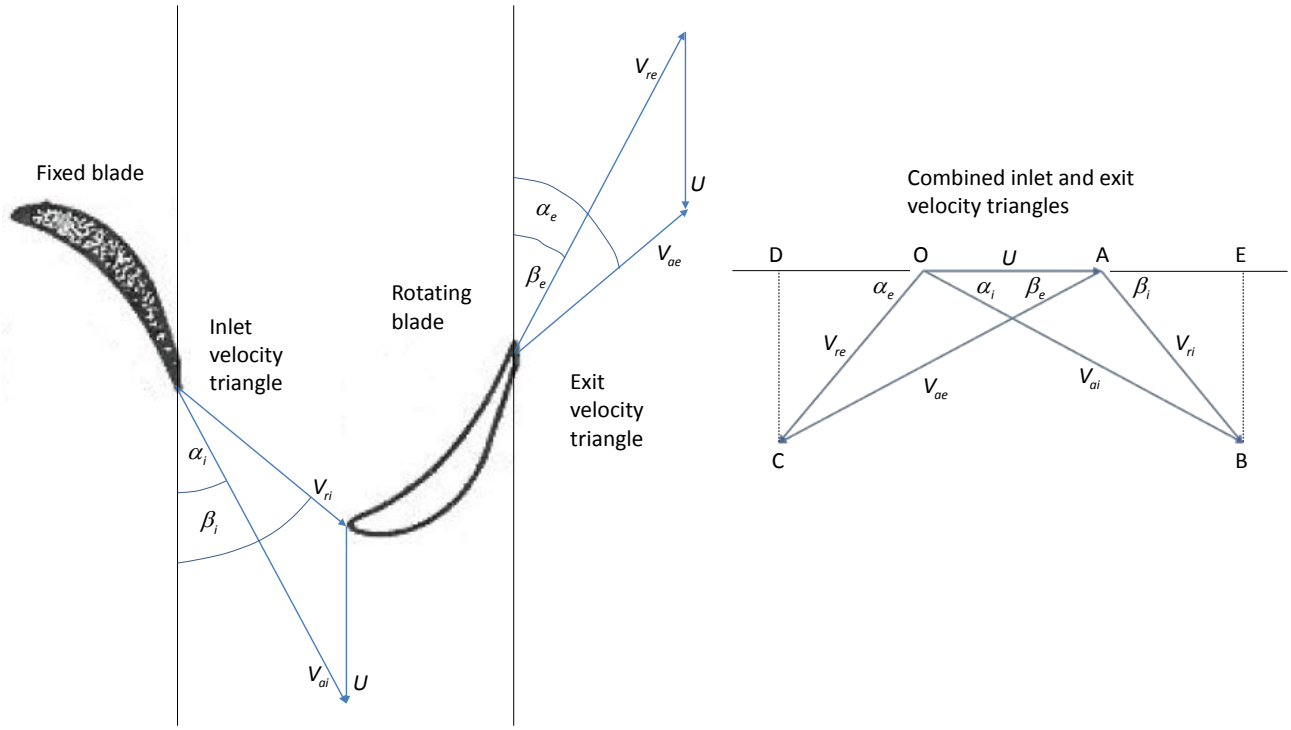

Source: Adapted from Eastop and McConkey [4]

Figure 7: Reaction turbine velocity triangles

The resulting power output of a stage (ignoring velocity changes due to wall friction), is then

$$\dot{W} = \dot{m}U\left(2V_{ai}\cos\alpha_i - U\right) \tag{3}$$

A similar conclusion can be made that the total incoming kinetic energy can only be extracted when both α_i and β_e is equal to zero, which is not physically possible. There is therefore also a carry-over component at the exit of the reaction stage for use in the next stage. However, the blade shapes allow for very small angles (10°-15°) [5], resulting in a smaller exit velocity V_{ae} than typically in the case of impulse blades.

Because this project focusses on modelling a turbine as a whole without internal geometry information, the application of velocity triangles and blade angles cannot be used. Instead, correlations will be studied which try to predict the efficiency of the turbine, given the design base efficiency is known. These correlations are built from analogies drawn from viewing the turbine on a macro-level as shown in Figure 1. These correlations will be elaborated in section 2.5.2

2.3 Steady state power plant modelling software

Below is a list of some software packages used in power plant modelling. They use different methods to predict efficiency and pressure drop across a steam turbine. However, the methods are based on similar research publications. All these software codes are applicable only to steady state simulations. The goal was to develop models with transient capabilities, therefore these software packages are not applicable. However, one may approximate reasonably slow transients in a quasi-steady state simulation, hence steady state methods may be applicable. It was therefore beneficial to have some insight into what methods the various software uses.

EBSILON® is steady state thermodynamic software developed by Staeg. The software is used in the engineering, design and optimisation of thermal power plants. The software solves the conservation of mass and energy equations. For more information on the software one is referred to https://www.steag-systemtechnologies.com/ebsilon_professional+M52087573ab0.html

PEPSE® is steady state energy balance software developed by Scientech. The program is used in the modelling, design, diagnostics and performance analysis of thermal power plants. For more information on PEPSE one is referred to http://famos.scientech.us/PEPSE.html

EtaPRO™ Virtual Plant™ is steady state thermodynamic software developed by GP Strategies. The software is used for assessing power plant performance. The software allows “what-if” mass and energy balances of the power plant cycle to be modelled. For more information on the software one is referred to http://powerplant.gpstrategies.com/prodVP.aspx

SteamPro is software used for the design of steam power plant cycles while SteamMaster is used for the off-design simulation of steam power plant cycles. Both SteamPro and SteamMaster are

developed by Thermoflow. For more information on SteamPro and SteamMaster one is referred to http://www.thermoflow.com/convsteamcycle_STM.html

2.4 Pressure drop correlations

The pressure drop characteristic of a component is used in solving the conservation of momentum equation. There are several correlations that have been developed over time to predict the pressure drop characteristic across a steam turbine. These correlations differ in accuracy, solving time and ease of implementation. Some of the most common of these are as follows:

- Stodola's law of ellipse.
- Schegliaiev's model.
- General empirical law.
- Constant flow co-efficient.

2.4.1 Stodola's law of ellipse

Stodola developed his law of ellipse experimentally using an eight-stage laboratory turbine [6]. It is valid for steam turbines operating with superheated or saturated steam, and when the flow is not choked. The law of ellipse establishes the relationship between three parameters:

1. Total inlet pressure.
2. Static outlet pressure.
3. Inlet mass flow rate.

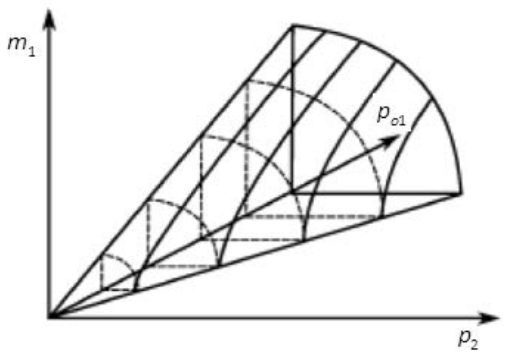

Source: Adapted from Wikipedia.org/wiki/Ellipse_Law

Figure 8: Graphical representation of Stodola's law of ellipse

In the above diagram, Stodola's "Cone of Steam Weights" represents the ellipses at various inlet pressures. The ellipse represents the "fundamental law for variation of steam mass flow with the outlet pressure for a given inlet pressure and constant speed" [7].

The law of ellipse relates the constant inlet flow co-efficient ϕ_1 with the pressure ratio (total inlet to static outlet pressure) in such a way that:

$$\phi_1 \propto \sqrt{1-\left(\frac{p_2}{p_{o1}}\right)^2} \tag{4}$$

The constant flow co-efficient is defined as:

$$\phi_1 = \frac{m_1}{\sqrt{\frac{p_{o1}}{v_1}}} \tag{5}$$

Substituting (5) into (4) results in:

$$\frac{m_1}{\sqrt{\frac{p_{o1}}{v_1}}} \propto \sqrt{1-\left(\frac{p_2}{p_{o1}}\right)^2} \tag{6}$$

To remove the proportionality sign, the mass flow rate and pressures need to be referenced to a design or nominal condition, giving:

$$\frac{\frac{m_1}{\sqrt{\frac{p_{o1}}{v_1}}}}{\frac{m_{1n}}{\sqrt{\frac{p_{o1n}}{v_{1n}}}}} = \frac{\sqrt{1-\left(\frac{p_2}{p_{o1}}\right)^2}}{\sqrt{1-\left(\frac{p_{2n}}{p_{o1n}}\right)^2}} \tag{7}$$

By algebraic manipulation the volume form of Stodola's law of ellipse is then:

$$\frac{m_1}{m_{1n}} = \sqrt{\frac{p_{o1} v_{1n}}{p_{o1n} v_1}} \sqrt{\frac{1 - \left(\frac{p_2}{p_{o1}}\right)^2}{1 - \left(\frac{p_{2n}}{p_{o1n}}\right)^2}} \tag{8}$$

Applying the Ideal Gas Law $pv = RT$ to (8) produces the temperature form of Stodola's law of ellipse:

$$\frac{m_1}{m_{1n}} = \frac{p_{o1}}{p_{o1n}} \sqrt{\frac{T_{o1n}}{T_{o1}}} \sqrt{\frac{1 - \left(\frac{p_2}{p_{o1}}\right)^2}{1 - \left(\frac{p_{2n}}{p_{o1n}}\right)^2}} \tag{9}$$

EBSILON®, SteamMaster and PEPSE® use Stodola's law of ellipse as the basis for some of their turbine calculations. PEPSE® specifically uses Stodola's law of ellipse in applications where expansion is to a controlled extraction and/ or high back pressure [8].

2.4.2 Schegliaiev's model

Like Stodola's law of ellipse, Schegliaiev's model proposes a relation between mass flow rate, pressure and temperature for partial load, knowing design or nominal conditions [9]. Schegliaiev's model is valid for steam turbines operating with superheated or saturated steam.

Based on the nozzle-flow analogy, Schegliaiev developed an expression for the partial load operation that relates the following:

1. Inlet mass flow rate.
2. Steam static pressures (inlet and outlet).
3. Inlet static temperature.

$$\frac{m_1}{m_{1n}} = \sqrt{\frac{T_{1n}}{T_1}} \sqrt{\frac{\left(p_1^{\,2} - p_2^{\,2}\right) - \sigma\left(p_1 - p_2\right)^2}{\left(p_{1n}^{\,2} - p_{2n}^{\,2}\right) - \sigma\left(p_{1n} - p_{2n}\right)^2}} \tag{10}$$

where $$\sigma = \frac{\varepsilon}{1 - \varepsilon} \text{ and } \varepsilon = \left(\frac{2}{k+1}\right)^{\frac{k}{k+1}} \tag{11}$$

2.4.3 General empirical law

The general empirical law can be used to predict the pressure drop across heat exchangers, valves and turbines (gas and steam). The correlation is valid for gases, liquids and two-phase flow. The general empirical pressure drop law relates total pressure drop to the following:

1. Inlet density.
2. Inlet volume flow rate.

$$p_{o1} - p_{o2} = \Delta p_0 = C_k \rho_1^{\beta} Q_1^{\alpha} \tag{12}$$

The simple turbine component of the transient thermo-hydraulic simulation package Flownex® uses the general empirical law as one of the methods of determining the pressure drop across a turbine.

2.4.4 Constant flow co-efficient

The constant flow co-efficient (5) is not a pressure drop correlation. However, it is used by PEPSE® and EtaPRO™ Virtual Plant™ as one of the options in their steam turbine components to predict pressure. The constant flow co-efficient method is invalid for expansion to a controlled extraction or high back pressure applications [8].

For the derivation of the constant flow co-efficient the reader is referred to Salisbury [10].

By algebraic manipulation it can be shown that the constant flow co-efficient is a special case of Stodola's law of ellipse [6] and the general empirical law when the outlet pressure is negligible compared to the inlet pressure.

The following demonstrates that the constant flow co-efficient is a special case of general empirical law:

Assuming $\alpha = 2$ and $\beta = 1$ (as per Flownex recommendation [11]), equation (12) becomes:

$$p_{o1} - p_{o2} = C_k \rho_1 Q_1^{2} \tag{13}$$

Assuming p_{o2} is negligible compared to p_{o1}:

$$p_{o1} = C_k \rho_1 Q_1^{2} \tag{14}$$

Substituting $Q_1 = \frac{m_1}{\rho_1}$ in (14) and re-arranging gives:

$$\frac{1}{C_k} = \frac{m_1}{\sqrt{\rho_1 p_{o1}}} \tag{15}$$

Since C_k is a constant, it follows that $\frac{1}{C_k} = \phi_1$, and knowing $\rho_1 = \frac{1}{\nu_1}$ we arrive again at the same form as equation (5):

$$\phi_1 = \frac{m_1}{\sqrt{\frac{p_{o1}}{\nu_1}}}$$

2.5 Steam turbine efficiency

There are two major components which define the total performance of a steam turbine, i.e. efficiency and availability [12]. The major component of interest in this dissertation is efficiency. The efficiency of a steam turbine is defined as the ratio of the actual enthalpy difference of the working fluid expanding between two pressures to the isentropic enthalpy difference between the same two pressures [12], [4].

Referring to Figure 1:

$$\eta = \frac{h_5 - h_7}{h_5 - h_{7s}} \tag{16}$$

In a power plant that works with a fixed boiler pressure, the HPT (without governing stage) efficiency decreases with an increase in flow throttling (with the governor valve closed to a greater degree). This is because the pressure ratio across the turbine increases and the velocity ratio decreases below the ideal design value. The efficiency of the HPT is therefore a function of the throttle flow ratio [13].

In a LPT, the efficiency is primarily a function of the exhaust velocity, and is termed “leaving losses” [13].

2.5.1 Factors influencing steam turbine efficiency

There are basically four major factors that influence steam turbine efficiency [12]. These four major factors are:

1. Stage leakage losses.
2. Stage moisture losses.
3. Leaving losses.
4. Basic aerodynamic losses associated with the stage structure.

- **Stage leakage losses** occur at the stationary and rotating blade tips (interstage seals) as well as at the gland seals. The interstage leakage loss represents steam that has not contributed to the expansion work and therefore results in a reduction in stage output. The interstage leakage loss is greater in a reaction turbine than an impulse turbine because of the pressure difference across the clearance passage in a reaction turbine. The stage leakage losses are influenced by:

1. Assembled clearance as compared to design clearance.
2. Increased clearance due to rubs at critical speeds when running up or running down the turbine.
3. Re-entry of the leakage steam into the main steam flow.

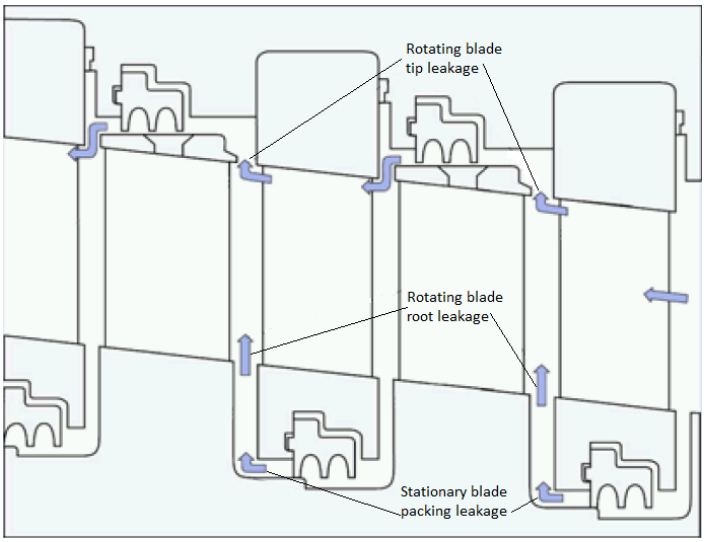

Source: Adapted from Hesler [14]

Figure 9: Stage leakage loss in a reaction turbine

- **Stage moisture losses**: When the working fluid expands into the moisture region, water particles are formed and transported in the steam. There is drag between the steam and the water particles because of the continual acceleration and retardation of the working fluid [12]. The moisture in the stage can also cause mechanical damage to the stage blades.
  The efficiency loss due to moisture ranges from 0.8 % to 1.2 % per 1 % average stage moisture content [12]. The stage moisture loss mainly affects the LPT of fossil plants and HPT and LPT of nuclear plants.

- **Leaving losses** are due to the following:
  1. Unused kinetic energy at the exhaust of the turbine.
  2. Hood losses.
  3. Turn-up losses.

  Kinetic energy losses in the HPT and IPT are relatively small when compared to the other losses and are usually ignored. In the LPT the exhaust velocity is significant and therefore cannot be ignored. Reducing the exhaust velocity below a critical value does not reduce the leaving losses, because of unfavourable blade velocity to steam velocity conditions [12].

  Hood losses are due to steam passage through the diffuser and exhaust hood. Hood losses for the LPT can be reduced by better design for the diffuser and better LP hood geometry selection.

  Turn-up losses are due to reduction in exhaust velocity at low load conditions. In these low load conditions recirculation occurs through the root section of the rotating blades. Turn-up losses can also occur during high back-pressure operation.

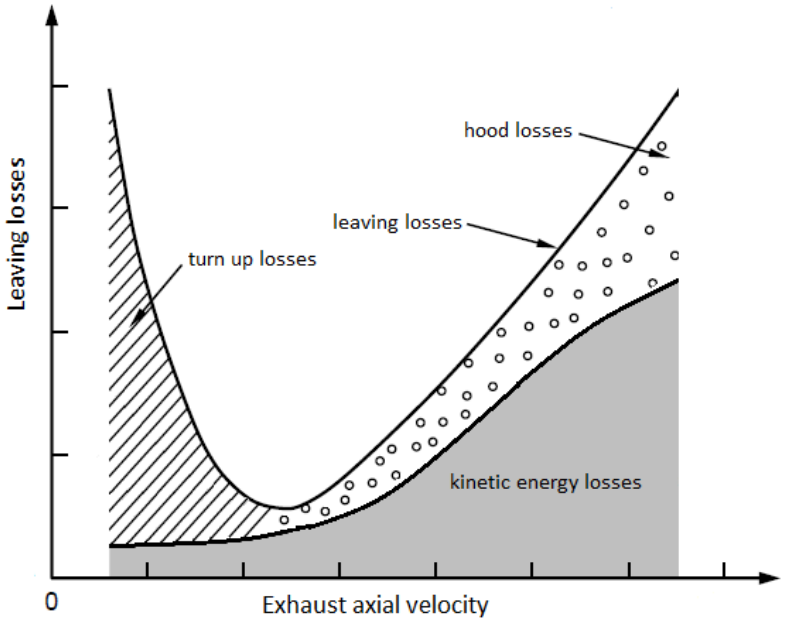

Source: produced with information from Sanders [12]

Figure 10: Typical leaving losses curve

- **Basic aerodynamic losses associated with stage structure** are influenced by profile and stage geometry, and are a function of the steam velocity and physical properties [12]. The following are major factors (greater than 2 %) which influence the basic aerodynamics:

  1. Fixed and rotating blade profile.
  2. Row aspect ratio.
  3. Wall-end and flare.
  4. Disc friction.

  Profile loss is defined as the ratio of total loss in stagnation pressure across the blade row to the difference between the stagnation and static pressures at the outlet. Profile losses are a result of boundary layer formation which steepens owing to adverse pressure gradients.

  The row aspect ratio is the ratio of the chord length to the blade length. The influence of the inner and outer casing wall of the first and second rows can be large because of secondary flow effects acting on a greater proportion of the discharge blade length. Secondary flow within the blade channel causes recirculation at the inner and outer side walls, so causing losses because of the introduction of vortices [12].

  Wall-end and flare losses occur at the inner and outer side walls. These losses are a result of wall friction and are influenced by discontinuities and direction changes which occur at

the wall. These losses are larger at the outer wall than the inner wall because of higher velocities and dramatic profile shape changes [12].

Disc friction loss occurs as a result of the disc rotating in the working fluid. The magnitude of the loss is influenced by the steam density and the amount of exposed area.

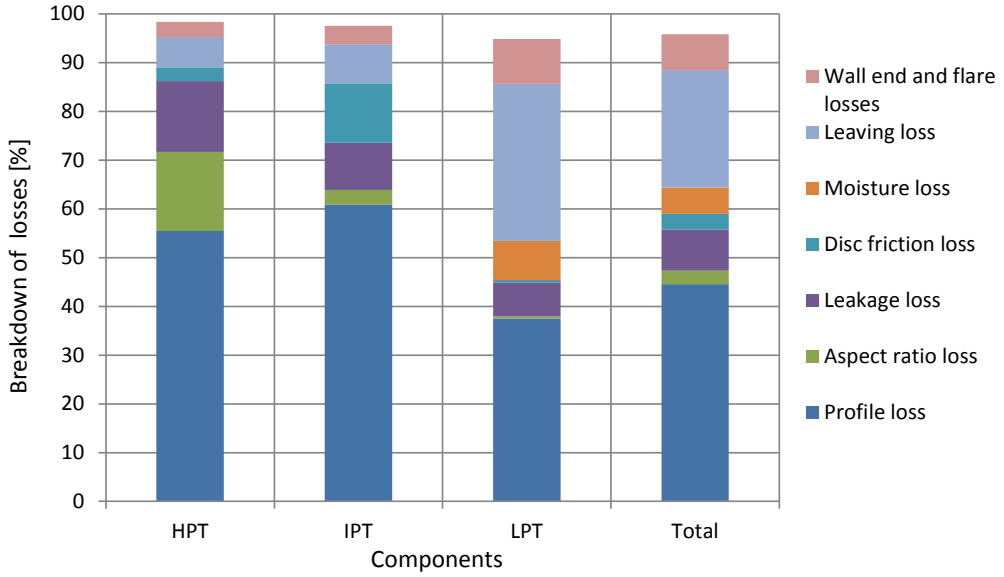

Figure 11: Typical percentage loss in a 500 MW impulse turbine

Figure 11 was compiled with data from Sanders [12]. Leaving losses and profile losses constitute the major losses in this particular type of steam turbine.

2.5.2 Methods of predicting steam turbine efficiency

There are various methods to determine the efficiency of new steam turbines and steam turbines operating at off-design conditions. The efficiency is specifically the static to static isentropic efficiency. Those considered are given below:

1. Stage by stage calculation method.
2. Spencer, Cotton and Cannon method.
3. Method employed in the PEPSE code.
4. Method employed in the EBSILON code.
5. Ray method.
6. Darie method.

- **Stage by stage calculation method:** A large steam turbine consists of a number of relatively independent components called stages [15]. The overall efficiency of a steam turbine can be determined from calculating the performance of the individual stages (i.e. stage by stage calculation) since overall performance depends on the efficiency of the individual stages [13]. This method is suitable for an existing steam turbine where the internal geometry of the steam path is known. It is not suitable for any steam turbine (new and existing) where the internal geometry of the steam path is unknown. For this project, it is assumed that the internal geometry of the steam path is unknown, therefore a stage by stage calculating method is not applicable.

Stage efficiency of impulse turbine: $\eta = 4\frac{U}{V_{ai}}\left(\cos\alpha_i - \frac{U}{V_{ai}}\right)$ (17)

Stage efficiency of reaction turbine: $\eta = \frac{2\frac{U}{V_{ai}}\left(2\cos\alpha_i - \frac{U}{V_{ai}}\right)}{1-\left(\frac{U}{V_{ai}}\right)^2 + 2\frac{U}{V_{ai}}\cos\alpha_i}$ (18)

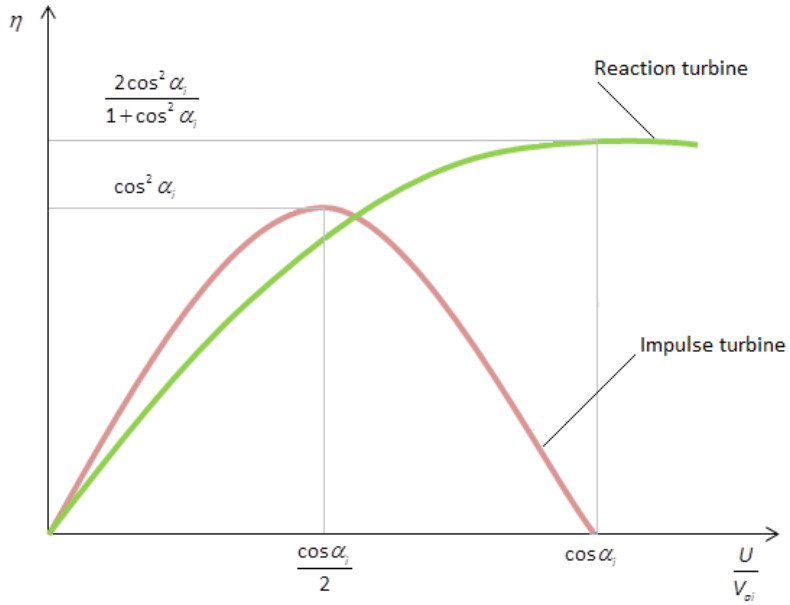

Source: Adapted from Wikipedia.org/wiki/Steam_turbine

Figure 12: Efficiency vs. ratio of blade speed to steam velocity for reaction and impulse turbine

Figure 12 shows that for a given inlet angle, the efficiency of a reaction turbine is better than an impulse turbine as the ratio of the blade speed to steam velocity increases.

- **Spencer, Cotton and Cannon method:** The method proposed by Spencer, Cotton and Cannon (SCC) uses a base efficiency and then applies corrections for various conditions. The authors developed efficiency correlations based on five factors:
  1. Expansion line efficiency, which can be determined from the following,
     a) Volumetric flow rate.
     b) Pressure ratio.
     c) Initial conditions (pressure and temperature).
     d) Configuration of the governing stage.
  2. Leaving losses.
  3. Gland seal and valve leakage losses.
  4. Mechanical losses.
  5. Generator losses.

  For a detailed description of the method, the reader is referred to Spencer, Cotton and Cannon [13].

Turbine type	Non-reheat	High pressure section		Intermediate pressure section	Reheat section		
	3600 rpm condensing 2 row governing stage	3600 rpm non-condensing 1 row governing stage	3600 rpm non-condensing 2 row governing stage	3600 rpm non-condensing without governing stage	3600 rpm condensing without governing stage	3600/ 1800 rpm condensing without governing stage	1800 rpm condensing without governing stage
Base efficiency	89.48	87	84	Fig.13	91.93	91.93	92.95
Correction for volume flow	$-\frac{430260}{Qv}N$	$-\frac{1005200}{Qv}N$	$-\frac{1350000}{Qv}N$		$-\frac{1270000}{Qv}N$	$-\frac{1270000}{Qv}N$	$-\frac{1270000}{Qv}N$
Correction for governing stage	Fig.2	Fig.7					
Correction for pressure ratio		Fig.6	Fig.10				
Correction for initial conditions	Fig.14				Fig.14	Fig.14	Fig.14
Correction for governiing stage at part load	Fig.4	Fig.8					
Correction for part load	Fig.3	Fig.9	Fig.11				
Correction for substitution of 1800 rpm LP section						$+1.25\left(\frac{AE_{1800}}{AE_{\text{reheat}}}\right)_{1.5}$	
Correction for mean of loops	Fig.5	Fig.12	Fig.12				

Figure 13: Extract of the SCC procedure [13]

- **PEPSE® method:** One of the methods that PEPSE software uses to determine the efficiency of an entire turbine is the SCC method. Once the efficiency of the turbine is determined the efficiency of the individual stages or groups of stages is determined by a set of expansion line curves built into PEPSE. These are enthalpy versus entropy curves on a Mollier chart. Specific points on the curve are determined from the individual group stage constant flow co-efficient since it relates to pressure and mass flow rate for the stage.

  From these curves, the curve for any load can be derived by making the slope of the chord of the new curve parallel with the chord of the original curve, but offset by the amount of change in entropy. The expansion line of the HPT section is a straight line while that of single reheat IPT and LPT sections are curved [8].

The PEPSE equation for fossil plant curved expansion line is given as

$$s = 10\frac{h_2 - (h + Y)}{371} + R_o(h - h_2) + s_2 - Z \tag{19}$$

where $R_o = \dfrac{(s_1 - s_2) + Z - \left(10\left(\dfrac{h_2 - (h_1 + Y)}{371}\right)\right)}{h_1 - h_2}$, $Z = 10^{-\frac{Y}{371}}$, and $Y = 650$

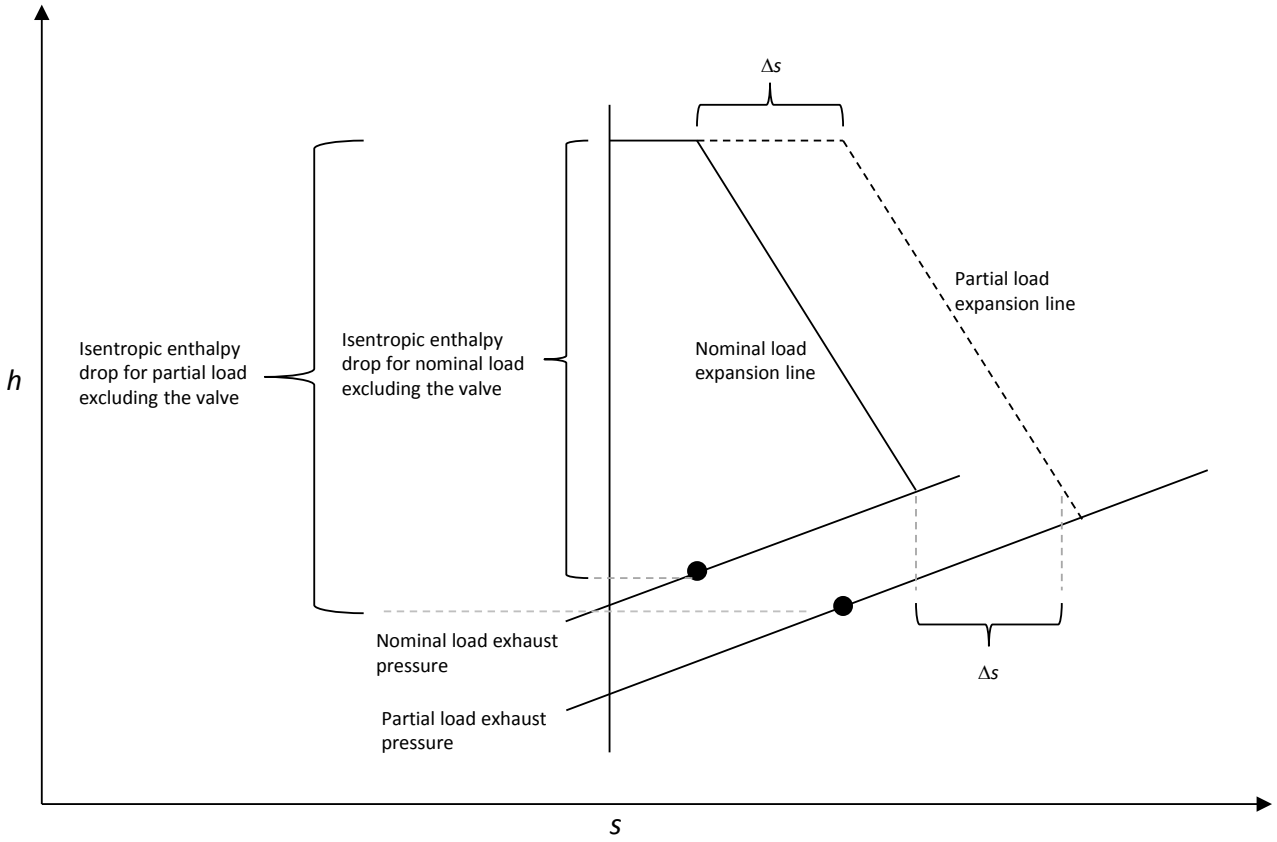

Source: Adapted from Minner [8]

Figure 14: HPT partial load expansion line developed from nominal load expansion line

- **EBSILON method:** In addition to using the SCC method as one of its options for determining the efficiency of steam turbines, EBSILON software uses normalized characteristic curves [16]. These curves use the nominal efficiency to determine efficiencies at other loads.

  These curves are functions of $\frac{m_1}{m_{1n}}$, $\frac{p_1}{p_2}\Big/\frac{p_{1n}}{p_{2n}}$, and $\frac{Q_1}{Q_{1n}}$.

- **Ray method:** Ray developed a semi-empirical relationship to predict the off-design efficiency of a steam turbine [17]. The assumption is that the efficiency is a function of the ratio of blade tip velocity to theoretical steam velocity. Blade tip velocity is proportional to turbine shaft speed and theoretical steam velocity is proportional to the square root of the isentropic enthalpy drop across the stage.

$$\eta = \eta_n - \kappa \left(\frac{\frac{N}{\sqrt{\Delta h_s}}}{\frac{N_n}{\sqrt{\Delta h_{sn}}}} - 1 \right)^2 \text{ with } \kappa = 2 \tag{20}$$

During normal operation the shaft speed is closely controlled to maintain it close to nominal speed. Therefore equation (20) reduces to:

$$\eta = \eta_n - 2 \left(\frac{\sqrt{\Delta h_{sn}}}{\sqrt{\Delta h_s}} - 1 \right)^2 \tag{21}$$

- **Darie method:** In their article, Darie et al [18] propose the following relationships to predict off-design steam turbine efficiency:

Pressure section $$\eta = \eta_n \sqrt{\frac{h_{2sn}}{h_{2s}}} \left(2 - \sqrt{\frac{h_{2sn}}{h_{2s}}} \right) \tag{22}$$

Governing stage $$\eta = \left(0.83 - \frac{0.15}{m_1 v_1} \right) \left(1 - 0.04 \left(1 - \sqrt{\frac{h_{2sn}}{h_{2s}}} \right) - 1.165 \left(1 - \sqrt{\frac{h_{2sn}}{h_{2s}}} \right)^2 \right) \tag{23}$$

2.6 Flownex

Flownex® is a one-dimensional thermo-hydraulic network simulation environment. Flownex is able to solve steady state as well as transient problems. The thermo-hydraulic system is solved numerically using an implicit pressure correction method. It solves the three conservation laws:

1. Conservation of mass.
2. Conservation of energy.
3. Conservation of momentum.

Flownex uses a state of the art pressure correction solution algorithm that results in fast and accurate simulations [19]. The following sequential steps are followed in the algorithm:

1. Guess the initial pressures at all nodes.
2. Calculate the mass flow rate using pressure-volume flow rate relationships.
3. Check for continuity at all the nodes.
4. Adjust the pressure to ensure continuity at all nodes.
5. Update mass flow rates using the new pressures.
6. Repeat steps 1-5 until the solution converges.
7. Solve the energy equation at all nodes.
8. Repeat steps 1-7 until the solution converges.
9. For transient problems, move to the next time step and repeat steps 1-8.

Flownex uses a segregated solution algorithm which sequentially solves the three governing equations and closure equations [19]. This enables the user to control various aspects of the solution procedure through relaxation parameters, adjusting the number of iterations and convergence criteria of the solution [19].

Flownex has a very useful designer function. The designer is used to calculate component parameters automatically to obtain a specific operating condition. The calculation is limited to one independent variable per equality constraint. Flownex uses the Newton-Raphson method to solve the set of non-linear equations.

2.6.1 Governing equations

The following are the governing equations solved in Flownex:

- Conservation of mass [20]

$$v\frac{\partial \rho}{\partial t} + m_2 - m_1 = 0 \tag{24}$$

- Conservation of energy [20]

$$\dot{Q} - \dot{W} = v\frac{\partial}{\partial t}\left(\rho h_o - p\right) + m_2 h_{o2} - m_1 h_{o1} + m_2 g z_2 - m_1 g z_1 \tag{25}$$

- Conservation of momentum [20]
    a) Incompressible flow

$$\rho L\frac{\partial V}{\partial t} + \left(p_{o2} - p_{o1}\right) + \rho g\left(z_2 - z_1\right) + \Delta p_o = 0 \tag{26}$$

    b) Compressible flow

$$\rho L\frac{\partial V}{\partial t} + \frac{p}{p_o}\left(p_{o2} - p_{o1}\right) + \frac{1}{2}\rho V^2\frac{1}{T_o}\left(T_{o2} - T_{o1}\right) + \rho g\left(z_2 - z_1\right) + \Delta p_o = 0 \tag{27}$$

2.6.2 Existing turbine components within Flownex

Flownex has two existing turbine components within its library, i.e. the normal turbine and simple turbine.

- **Turbine component:** The turbine component uses performance charts i.e. pressure ratio and efficiency, to determine the characteristics of the turbine. There is a library of standard charts available to the user or the user is able to input custom performance charts. The pressure ratio and efficiency charts are functions of corrected mass flow and corrected speed.

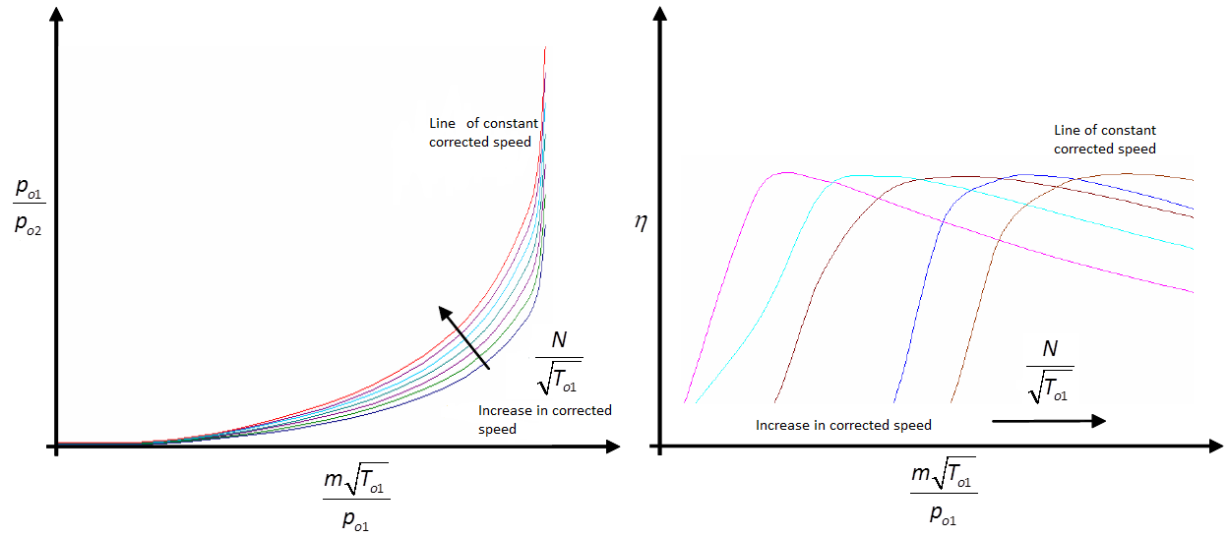

Figure 15: Example of pressure ratio and efficiency charts [11]

The user is able to construct composite turbo machines by adding compressors and generators via a shaft component to the turbine component. The model is also capable of calculating speed during transient simulations.

The turbine component is subject to following constraints:

1. Adiabatic turbine with compressible flow.
2. Negligible fluid mass and thermal inertia.
3. One dimensional flow at turbine inlet and outlet.

The turbine component requires the following inputs

1. Performance chart.
2. Rotational speed.
3. Inlet guide vane angle.
4. Geometric scaling factor.
5. Power supplied to the grid.
6. House load.
7. Generator efficiency.
8. Switch gear efficiency.

Turbine performance charts are very rarely available to the user therefore the use of this component is not applicable to this dissertation.

- **Simple turbine component:** The simple turbine component is a turbine with one working point, i.e. constant isentropic efficiency and total pressure drop [11]. The component can handle two-phase flow and choking in the throat of the element. The component is capable of calculating power developed but does not include rotational inertia, nor does it have the capacity to calculate speed during transient simulation.

  The pressure drop across a steam turbine can be input by the user in three formats for the simple turbine component:

  1. The restrictor with discharge co-efficient.

$$\Delta p_o = p_{o1}\left(1-\frac{p_s}{p_{o1}}\right) \tag{28}$$

  2. The restrictor with loss co-efficient.

$$\Delta p_o = C_\ell p_{o1}\left(1-\frac{p_s}{p_{o1}}\right) \tag{29}$$

  3. The general empirical law which was described in section 2.4.3 and equation (12).

  The simple turbine component requires the following input in order to operate:

  1. Isentropic efficiency.
  2. Pressure drop input method with additional information:
     a. Restrictor with discharge co-efficient.
        i. Throat diameter or area.
        ii. Discharge co-efficient.
     b. Restrictor with loss co-efficient.
        i. Throat diameter or area.
        ii. Loss co-efficient.
        iii. Contraction co-efficient.
     c. General empirical law.
        i. Turbine loss constant.
        ii. The index for density and volume flow rate.

  This component can be used without knowledge of the details of the steam path which makes it most suitable for this project.

2.6.3 Compound component

In a flow network model, parts of that network may be repeated a number of times. It can become laborious creating the same sub-network repeatedly so to alleviate this problem Flownex provides the compound component functionality [21].

From the user's perspective the compound component represents a single component which can be used like all other components. However, in reality the compound component contains all the details of the sub-network which can be used repeatedly in the same project or copied to the global environment where it can be used in other projects.

It is also possible to include scripting elements inside the compound component which would handle the pre-processing or conversion of user inputs into the appropriate parameters of the internal components. This is particularly useful for the development of the steam turbine.

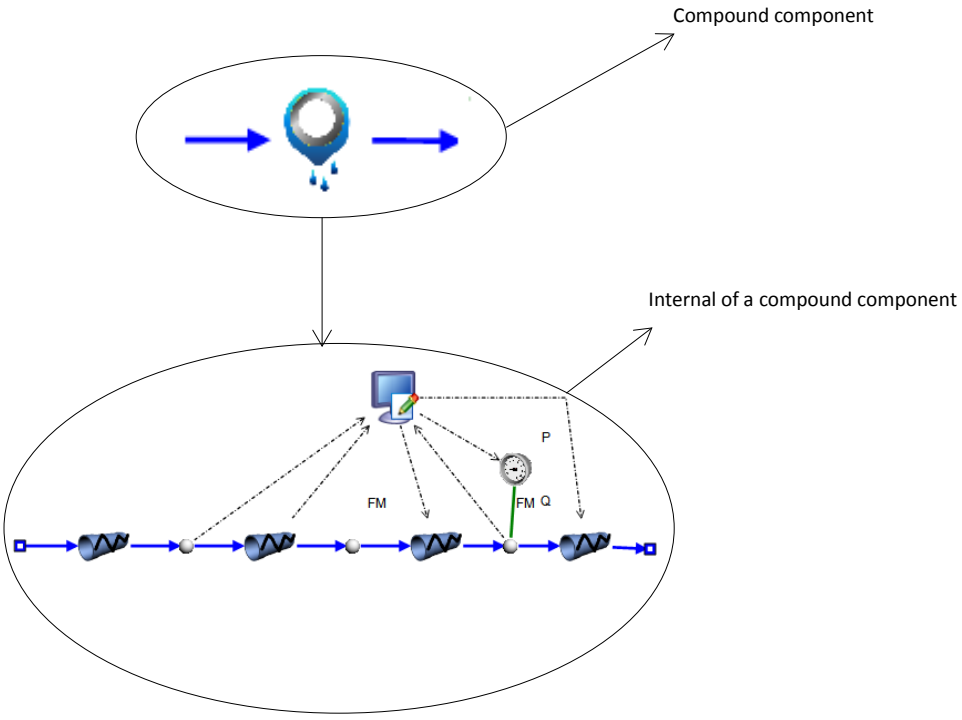

Source: Dr WF Fuls

Figure 16: Example of a compound component

2.7 Architecture of steam turbines used in Eskom

The aim of this exercise was to study the steam turbine architecture and functionality of the various power plants in the Eskom fleet in order to determine whether certain turbines and power plants could be grouped together. The grouping of turbines and power plants could assist in developing compound models of complete turbine trains, i.e. HPT+IPT+LPT in one component with multiple extraction points.

Eskom has 16 power plants that employ steam turbines as a prime mover to drive their generators in order to produce electricity. The power plants constructed prior to 1971 do not have reheat systems. These turbine trains consist of two cylinders, an HPT and a LPT. The power output of these turbines ranges from 95 MW to 200 MW per unit.

The power plants constructed after 1971 have reheat systems. These turbine trains consist of four cylinders, HPT, IPT and 2xLPT pairs. The power output of these turbines ranges from 400 MW to 800 MW per unit. In addition, Eskom has one nuclear power plant with an output of 965 MW per unit. The nuclear power plant turbine train consists of four cylinders.

Eskom has 38 units with reaction machines and 63 units with impulse machines. All the steam turbines used by Eskom are axial flow machines, therefore this dissertation is concerned only with this type of turbine.

The OEMs of these turbines vary but the turbine OEM for a particular power plant is usually the same for all the turbine trains at that plant. Eskom made a conscious decision not to be reliant on one turbine OEM, therefore the Eskom turbine fleet consists of turbines from various turbine OEMs.

As can be expected when using different turbine OEMs the turbine hardware across the Eskom fleet is not homogenous. The turbines vary in terms of whether they are reaction or impulse machines, in the number of cylinders, the number of stages per cylinder, the number of flows per cylinder, the number of extractions per flow etc.

Even though the turbine hardware might be different across the Eskom fleet it can be grouped by considering the following criteria:

1. Whether the power plant employs reheating.
2. The number of flows[1] on the HPT, IPT and LPT.
3. The number of extraction points per HPT, IPT and LPT flow.
4. Whether the HPT has any governing stages.

[1]Flows are the number of parallel streams of steam exhausting (normally one or two) from the turbine cylinder from a single entry

5. Whether the IPT requires cooling steam.

Based on the above criteria the heat balance diagrams and acceptance test reports for the various power plants were analysed to determine whether the turbines and power plants could be categorised into groups. One will note that from the above criteria, no distinction is made between impulse and reaction blades because the models developed need to be applicable to both types of blades.

From the analysis it was determined that all the steam turbines in the Eskom fleet could be clustered into 10 groups. The number of groups required was reduced through the following:

- The turbine with the largest number of sections is defined as the a base model
- Allowance is made for whether the extraction points are symmetrical or asymmetrical
- The physical inlet, extraction and exhaust pipes are ignored and considered as simple nodes.

The result is that only two generic groups are sufficient to model all the steam turbines in the Eskom fleet. They are shown below:

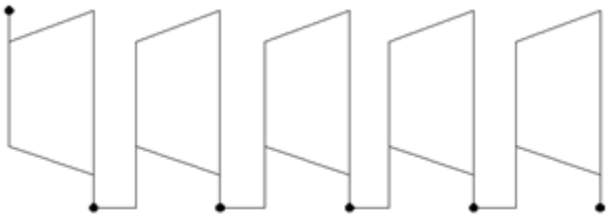

Figure 17: Generic group 1

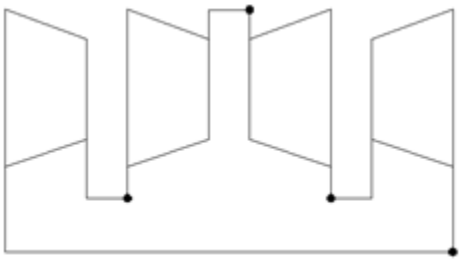

Figure 18: Generic group 2

Turbines with fewer number sections than the number in the Generic group 1 can be modelled by "blanking off" the extractions of the extra sections. Generic group 2 is used for modelling double

flow turbines with asymmetrical extractions. The generic groups enable the addition of the required inlet, cooling steam, extraction and exhaust pipes at the nodes.

For the details of these groupings reference should be made to Appendix A.

2.8 Confidence/ accuracy of acceptance test data

This study relied on acceptance test data to judge the accuracy of the various methods. To establish confidence in the acceptance test data and thus the model results, the ASME Performance Test Code [22] was reviewed. Section 4 of the code recommends the instrumentation to be used, its accuracy, installation, location and calibration requirements to ensure a low degree of uncertainty in the heat rate calculation. By following the guidelines of the code, the results for a full scale heat rate test for a typical reheat fossil fuelled unit have an uncertainty level of approximately 0.25 %.

The following sections are summaries of the code to support the confidence of the data used.

2.8.1 Duplication of instrumentation

The ASME standard requires duplicate instrumentation to measure certain critical data such as flow nozzle pressure difference, steam temperature and exhaust pressure. The use of duplicate instrumentation reduces the uncertainty of the average duplicating instruments relative to a single instrument.

2.8.2 Calibration

An accuracy ratio of less than 10:1 is required for calibrated instrumentation. Accuracy ratio refers to the ratio of the accuracy of the measuring standard to the accuracy of the instrument being calibrated [22]. Extremely accurate instrumentation has an accuracy ratio of 4:1. The calibration of the instrumentation has to cover the range in which it is used. The increment between calibration points and the method of interpolation between the points is selected to achieve the lowest possible calibration uncertainty.

2.8.3 Measurement of electrical power

The power output of an AC generator must be measured with adequate instrumentation that ensures accurate measurements under all load power factors and unbalance, i.e. no uncertainty is introduced due to measuring method.

In order to achieve accurate metering of a three-phase system ASME recommends that three single meters be used for four wire generator connections and two single meters be used for three wire generator connections. This recommendation is based on Blondel's theorem, which states that in an electrical system of N conductors, N - 1 measuring instruments are required to measure the true electrical power or energy of the system [22].

For AC generator tests the active power must be measured with instrumentation with an uncertainty of ±0.1 % of the reading for power factor ≥ 0.8. Reactive power should be measured with instrumentation with an uncertainty of ±0.2 % of the range.

The instrumentations used to measure the gross electrical output of the generator must be calibrated to a secondary standard that is traceable to a recognised national standard laboratory. Calibration must occur before and after each test.

ASME provides guidelines and diagrams for connecting of the instrumentation in order to ensure that significant error is not introduced to measured power. The test instruments must be connected on the lines from the generator as close as possible to the generator terminals and on the generator side of any external connections by which power can enter or leave the circuit [22]. The influence of inductance on measurement should be minimised by the use of twisted and shielded pairs of instrumentation leads. The arrangement of the instrumentation has to be checked for stray fields. The selection of the wire gauge on the voltage circuit is based on the wiring length and a given load of the potential transformers, with consideration of resistance of safety fuses.

2.8.4 Primary flow measurement

Accurate primary flow measurement is essential in determining heat rate if the results are to be considered the basis for acceptance test [22]. All known errors are required to be reduced so that the individual effect is less than 0.05 % of the primary flow measured.

The ASME standard recommends the use of low beta ratio throat tap nozzles because of the excellent results achieved by these nozzles. Figure 19 shows the layout and basic requirements to install the flow meter in order maintain the accuracy of the measurement system. The beta ratio

(d/D) is limited to the range of 0.25 to 0.5. The instrument is required to be installed at least 20 diameters downstream of any obstruction on straight piping and at least 16 diameters downstream of a flow straightener.

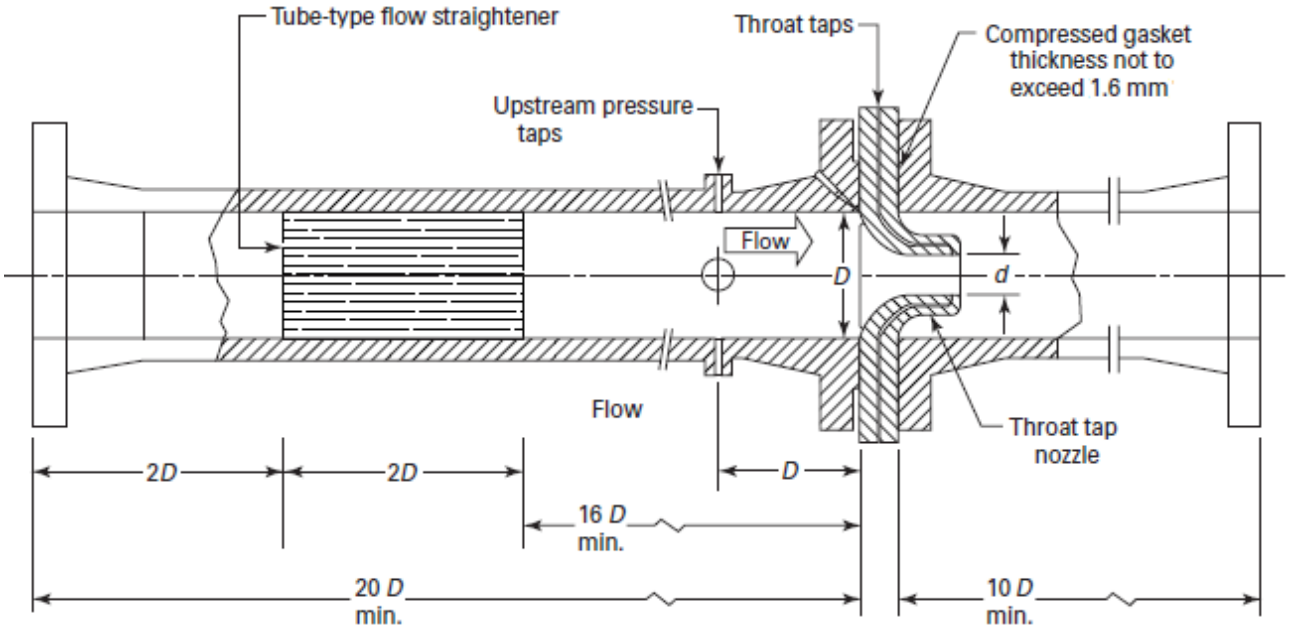

Figure 19: Schematic of primary flow section [22]

2.8.5 Differential pressure measurements

For measuring primary flow, differential pressure transducers with an accuracy class of 0.05 % or better (0.1 % maximum uncertainty) must be used. The differential pressure transducers should not introduce an uncertainty greater than ±0.1 % of the minimum flow measured. The transducers have to be calibrated before and after each test. The before and after calibration curves should not differ by more than 0.05 % of the mass flow rate. The temperature of the two lines connecting the primary element and each instrument should not exceed 2 K.

The change in zero reading before and after each test run should not deviate by more than 0.1 % of the differential observed during the test run. At any time during the test run, the corrected instantaneous reading of the two instruments must agree with one another within 0.2 % after correction for any calibration difference between two tap sets [22].

2.8.6 Additional flow measurements

The instrument and method used to measure flow other than primary flow should not affect the heat rate by more than ±0.1 %.

The boiler feed pump turbine steam flow rate must be determined with instruments whose combined uncertainty is not greater than ±2 % so as to limit the influence on the heat rate to not more than ±0.5 %.

2.8.7 Absolute pressure measurement

Calibrated pressure transducers of 0.1 % accuracy class have to be used to measure all critical pressures.

Calibrated pressure transducers of 0.25 % accuracy class must be used to measure all non-critical pressures.

To ensure reliable and accurate measurements the pressure transducers should be installed in positions that are free of vibration, dirt and large variations of ambient temperature. The pressure taps have to be installed on straight pipe sections as far away as possible from upstream obstructions such as elbows.

The pressure taps at the turbine side of the extraction pipes have to be installed as close as possible to the turbine connections but not so close that flow disturbances affect the pressure reading. Errors caused by pressure taps are a function of the type of fluid, tap diameter and configuration of the tap holes at the wall of the pipe, therefore the ASME standard requires the use of certain tap diameters and configurations. The holes need to be at right angles to the surface of the wall adjacent to fluid and the innermost part holes have to be de-burred. In order to prevent air or water pockets, the connecting pipes must be continuously sloped from the level of the tap to level of the instrument. For measurement of pressure below atmospheric, provision has to be made for bleeding off of the air.

The zero reading should not vary by more than 0.1 % of the reading during the test.

The exhaust pressure of a condensing turbine has to be measured at, or on either side of and adjacent to the exhaust joint. The exhaust joint is where the turbine exhaust connects to the condenser neck.

2.8.8 Temperature measurement

The temperature measurement systems should have an uncertainty of ±0.5 K. Thermocouples and resistance thermometers must be calibrated before and after each test run. The before and after calibration values of the instrument should not deviate by more than 1 K.

The ASME standard recommends the following temperature measurement systems:

- Platinum resistance type thermometers, including leads calibrated and used in conjunction with random bridge (0.03 % accuracy) measuring instruments.
- Thermocouples with continuous thermocouple wires and integral cold junctions calibrated and used in conjunction with a random high quality digital voltmeter (±0.03 % accuracy or better).
- Calibrated thermocouples or random thermometers with an uncertainty not exceeding 0.5 K for cold junction ambient temperature reference measurements.

When the temperature is used to determine enthalpy, the temperature measurement device is required to be installed as close as possible to the corresponding pressure measurement point. The thermowells must be located downstream of the pressure taps. If the thermowells are located upstream of the pressure taps, then they should not be located on the same longitude. Temperature sensors must be located sufficiently downstream of an elbow or extraction nozzle to minimise temperature difference caused by flow stratification. Thermocouple leads should not be subjected to large temperature gradients. To avoid high electric fields, the thermocouple and its lead wires should not be run in the same cable trays as power lines.

2.8.9 Instrument location

To ensure reliable and accurate acceptance test results the proper location of the instrumentation is important. The ASME standard recommends instrumentation locations to achieve reliable and accurate results. Figure 20 below is an example of an ASME recommendation. Note that all the plants used in this study had surface condensers connected to cooling towers. In other words the condenser is integrated right below the LPT exhaust hood. This makes it virtually impossible to measure the LPT exit flow velocity, and thus it is not possible to determine the actual total outlet pressure of the LPT. The static pressure inside the condenser is the only measurement available.

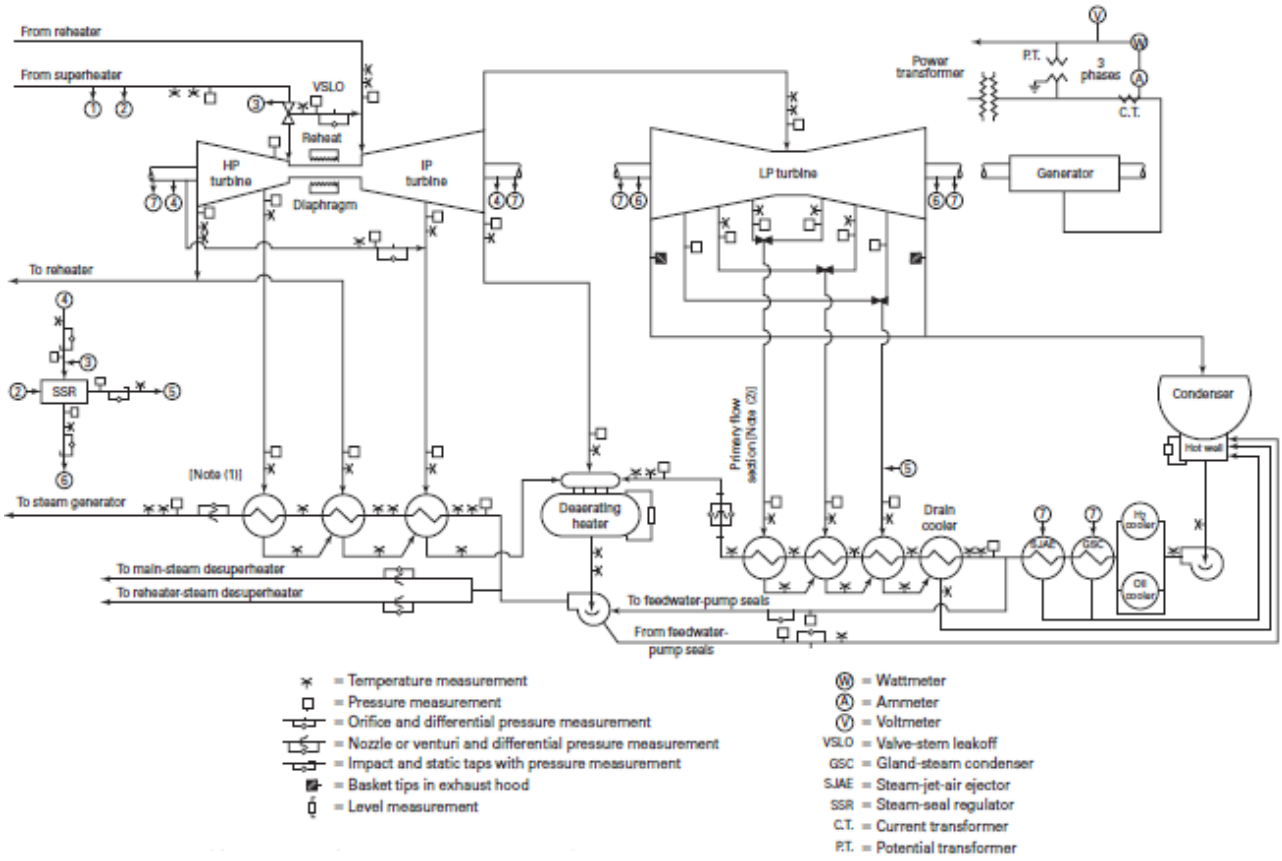

Figure 20: Location of test instrumentation [22]

2.8.10 Conclusion on accuracy of acceptance test data

Eskom normally specifies the ASME code for plant acceptance tests. However, there is no guarantee that the code was followed in its entirety, nor that some procedural or installation error could have happened. Some of the acceptance test data are old and there is no proof that the tests were carried out as required. However, most of the acceptance test reports do contain mass and energy balance checks as method of verifying the accuracy of the data. These reports have been used for the life of the plant as reference data whenever upgrades or re-commissioning is done. It is therefore generally seen as the most reliable and accurate process conditions for the plant.

Acceptance test data usually is much more reliable and trustworthy, since there is more stringent control of the accuracy of the instruments, their calibration and their installation. Acceptance test data provides a regulated set of data to which the accuracy of the models developed can be tested and therefore more desirable in modelling process flow than plant data collected from the Distributed Control System.

From the information gathered from the ASME standard one can conclude the following about model results:

- Critical pressure and non-critical pressure errors within ±0.1 % and ±0.25 % respectively are considered negligible.
- Main steam flow and extraction line flow errors within ±0.05 % and ±2 % respectively are considered negligible.
- Temperatures within ±0.5 K are considered negligible.

Finally, it must be noted that regardless of the precision of the actual measurement, the data given in the acceptance test results have a certain truncation, i.e. only 3-4 significant digits are reported. This truncation (or round-off) might in some cases result in a value which is less accurate than the original measurement, especially in the case of pressures where there is quite a large range from HPT inlet to LPT outlet.

3. Pressure Drop Correlations

Section 2.3 introduced various pressure drop correlations. Stodola's law of ellipse, Schegliaiev's model and general empirical law are the correlations of interest for this project. As mentioned in section 2.6, the pressure drop in the simple turbine component used in Flownex can be input in three formats. The general empirical law format is the chosen format for this project since it does not require any details of the steam path to be known.

The general empirical law correlation can be directly implemented in Flownex. However, Stodola's law of ellipse and Schegliaiev's model need to be converted to the general empirical law format before they can be implemented.

The steam velocity at the inlet to and outlet from the turbine is unknown therefore it is difficult to determine accurately the total inlet and outlet pressure. When the Stodola and Schegliaiev correlations are converted to general empirical law format it is assumed that the total pressure is equal to the static pressure. The velocity effect on pressure is small in most instances except for the LPT exhaust pressure.

In the case where the LPT is modelled separately in Flownex, an unavoidable error is introduced when specifying the outlet boundary condition, as Flownex can only apply total pressure to the boundary, while the actual exhaust pressure is the static pressure in the condenser.

Also note that the units for the turbine loss constant, C_k, depend on the value of the indexes α and β. It is therefore different for the different models used. When applying C_k in Flownex, base SI units must be used to achieve a consistent result, since Flownex performs all calculations in base SI units, despite the fact that the user has the option to specify inputs in different units.

After algebraically manipulating equation (8), the volume form of Stodola's law of ellipse in general empirical law format is:

$$\Delta p_o = \underbrace{\left(\left(\frac{\nu_1}{\nu_{1n}}\right)\left(\frac{p_{o1}}{p_{o1n}}\right)\left(\frac{1}{m_{1n}}\right)^2 \frac{\left(p_{o1n}{}^2 - p_{o2n}{}^2\right)}{\left(p_{o1} + p_{o2}\right)}\right)}_{C_k\ [\mathrm{kg^{-1}m^{-1}}]} \rho_1{}^2 Q_1{}^2 \tag{30}$$

The volume form of Stodola's law of ellipse in general empirical law format using the ideal gas law and assuming average density for equation (30) is:

$$\Delta p_o = \underbrace{\left(\left(\frac{\nu_1}{\nu_{1n}}\right)\left(\frac{p_{o1}}{p_{o1n}}\right)\left(\frac{1}{m_{1n}}\right)^2 \frac{\left(p_{o1n}{}^2 - p_{o2n}{}^2\right)}{R_{steam}\left(T_{o1}+T_{o2}\right)}\right)}_{C_k\ [\mathrm{m}^{-4}]} \rho_{ave} Q_{ave}{}^2 \tag{31}$$

The temperature form of Stodola's law of ellipse, equation (9), in general empirical law format is:

$$\Delta p_o = \underbrace{\left(\left(\frac{T_{o1}}{T_{o1n}}\right)\left(\frac{1}{m_{1n}}\right)^2 \frac{\left(p_{o1n}{}^2 - p_{o2n}{}^2\right)}{\left(p_{o1}+p_{o2}\right)}\right)}_{C_k\ [\mathrm{kg}^{-1}\mathrm{m}^{-1}]} \rho_1{}^2 Q_1{}^2 \tag{32}$$

The temperature form of Stodola's law of ellipse in general empirical law format using the ideal gas law and assuming average density for equation (32) is:

$$\Delta p_o = \underbrace{\left(\left(\frac{T_{o1}}{T_{o1n}}\right)\left(\frac{1}{m_{1n}}\right)^2 \frac{\left(p_{o1n}{}^2 - p_{o2n}{}^2\right)}{R_{steam}\left(T_{o1}+T_{o2}\right)}\right)}_{C_k\ [\mathrm{m}^{-4}]} \rho_{ave} Q_{ave}{}^2 \tag{33}$$

Schegliaiev's model, equation (10), in general empirical law format is:

$$\Delta p_o = \underbrace{\left(\left(\frac{T_1}{T_{1n}}\right)\left(\frac{1}{m_{1n}}\right)^2 \frac{\left(p_{o1n}{}^2 - p_{o2n}{}^2\right) - \sigma\left(p_{o1n}-p_{o2n}\right)^2}{p_{o1}\left(1-\sigma\right)+p_{o2}\left(1+\sigma\right)}\right)}_{C_k\ [\mathrm{kg}^{-1}\mathrm{m}^{-1}]} \rho_1{}^2 Q_1{}^2 \tag{34}$$

The general empirical law, equation (12), using inlet conditions and assuming $\alpha = 2$ and $\beta = 1$ as per reference [11] is simply:

$$\Delta p_o = C_k \rho_1 Q_1{}^2 \tag{35}$$

With C_k [m^{-4}] in equation (35).

The general empirical law using average conditions is:

$$\Delta p_o = C_k \rho_{ave} Q_{ave}{}^2 \text{ with } Q_{ave} = \frac{m}{\rho_{ave}} \text{ and } \rho_{ave} = \frac{\rho_1 + \rho_2}{2} \quad (36)$$

With C_k [m^{-4}] in equation (36).

In equations (30) to (34), C_k, is a function of the unknown outlet pressure therefore the C_k value is not constant. In order to solve for the outlet pressure an iterative solution is required for C_k for each off-design condition.

The average density in equations (31), (33) and (36) is a function of the unknown outlet pressure and outlet enthalpy, therefore to solve for the outlet pressure an iterative solution is required for each load case with an assumption of isentropic expansion (or nominal condition efficiency). In equation (36) C_k is constant.

Equation (35) is explicit therefore it does not require an iterative solution.

3.1 Analytical solution of pressure drop correlations

3.1.1 Methodology

The first step was to evaluate the various pressure drop correlations analytically. This was done using Mathcad. The correlations, equations (30) to (36), were manipulated to solve two scenarios:

1. The inlet mass flow rate, given inlet pressure, inlet temperature (and, if needed, inlet quality) and outlet pressure.
2. The outlet pressure, given the inlet pressure, inlet temperature (and, if needed, inlet quality) and inlet mass flow rate.

All the correlations were tested on the HPT of three reference power plants i.e. PP-A (618 MW reheat impulse machine), PP-B (200 MW non-reheat impulse machine) and PP-C (500 MW reheat reaction machine). In this first evaluation phase all the correlations were tested on both impulse and reaction turbines.

The HPT of PP-C and PP-A do not have any extraction points. The model developed for these two power plants considered the whole HPT.

PP-B's HPT has four extraction points. The HPT is actually a combined HPT (from inlet to redirection chamber) and IPT (from redirection chamber to IPT exhaust). The HPT model developed considers only the inlet to the redirection chamber.

Nominal load conditions (100 % load) from the acceptance test data for the three reference plants were used to model the HPTs. The off-design conditions (80 %, 60 % and 46 % load) were then predicted and compared to the acceptance test results.

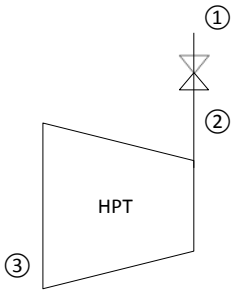

Figure 21: Schematic of the HPT

Table 1: PP-C HPT acceptance test data

Position	Property	100 % load	80 % load	60 % load	46 % load
1	Pressure (MPa)	16.12	16.35	16.42	16.42
	Temperature (°C)	510.8	510.8	510.5	510.6
	Mass flow (kg/s)	403.43	323.56	248.11	197.41
2	Pressure (MPa)	14.19	11.39	8.725	6.932
3	Pressure (kPa)	3374	2669	2014	1607
	Temperature (°C)	295.2	283.5	272.6	266.1

Table 2: PP-A HPT acceptance data

Position	Property	100 % load	80 % load	60 % load
1	Pressure (MPa)	15.965	15.936	15.934
	Temperature (°C)	535.74	533.87	534.98
	Mass flow (kg/s)	482.67	393.13	304.4
2	Pressure (MPa)	15.115	12.297	9.5372
3	Pressure (kPa)	3873.4	3167.4	2452.7
	Temperature (°C)	330.87	321.93	314.59

Table 3: PP-B HPT acceptance test data

Position	Property	100 % load	80 % load	60 % load
1	Pressure (MPa)	10.4	10.529	10.527
	Temperature (°C)	539.8	541.1	539.7
	Mass flow (kg/s)	202	158.89	125.11
2	Pressure (MPa)	9.257	7.031	5.537
3	Pressure (kPa)	3970	3111	2400

3.1.2 Evaluation of results

The detailed results for all cases can be found in Appendix B. Only a summary of the results will be presented here, with the focus on drawing certain conclusions.

To compare all the results, a percentage error is defined as:

$$error = \frac{calculated\ value - acceptance\ test\ value}{acceptance\ test\ value} \cdot 100 \tag{37}$$

With the above definition in mind, it follows that a negative error implies an under-prediction, and a positive error an over-prediction.

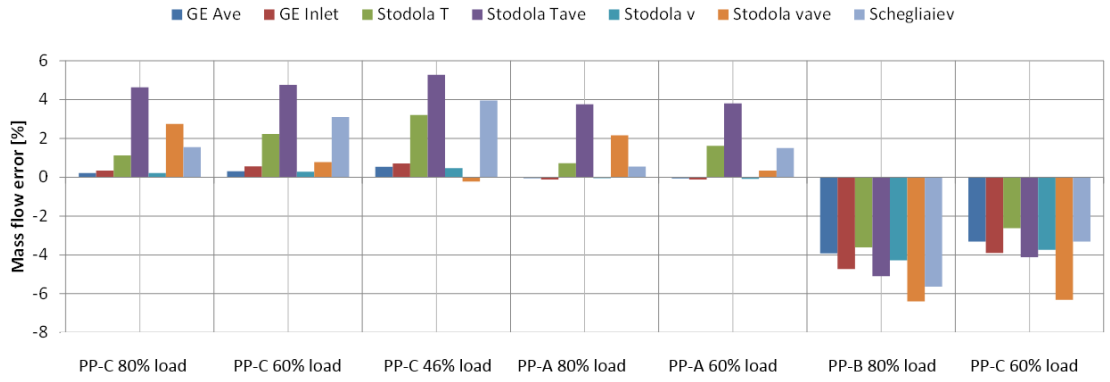

Figure 22: Analytical mass flow error of the HPT of the various plants at different loads

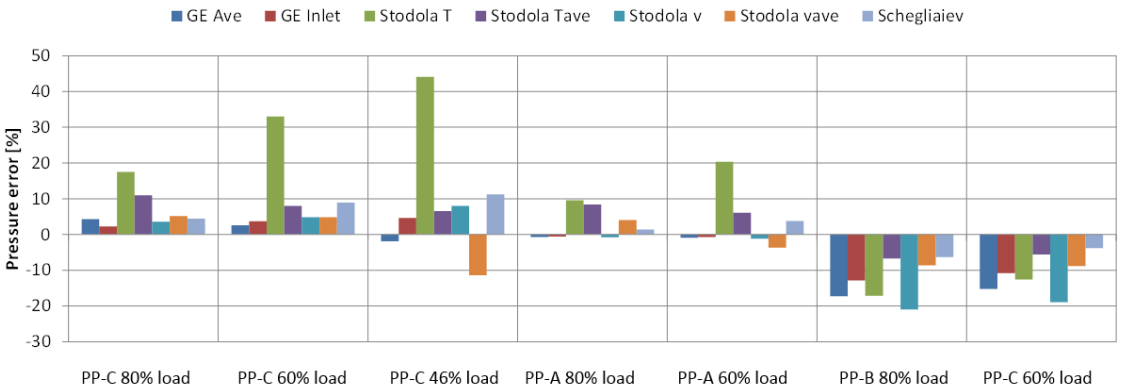

Figure 23: Analytical pressure error of the HPT of the various plants at different loads

The errors from the various models for the plants considered are shown in Figure 22 for predicting the mass flow rate, and Figure 23 for predicting the outlet pressure. Both follow a similar trend. Most of the correlations for PP-C and PP-A tend to overestimate the mass flow rate and outlet pressure, while for PP-B the correlations tend to underestimate the mass flow rate and outlet pressure.

From Figure 22 and Figure 23 it is difficult to see which correlations are more accurate. The chosen correlations need to be accurate and consistent in predicting mass flow rate and pressure. To have a better understanding of which is more accurate, the absolute pressure error is plotted against the absolute mass flow error.

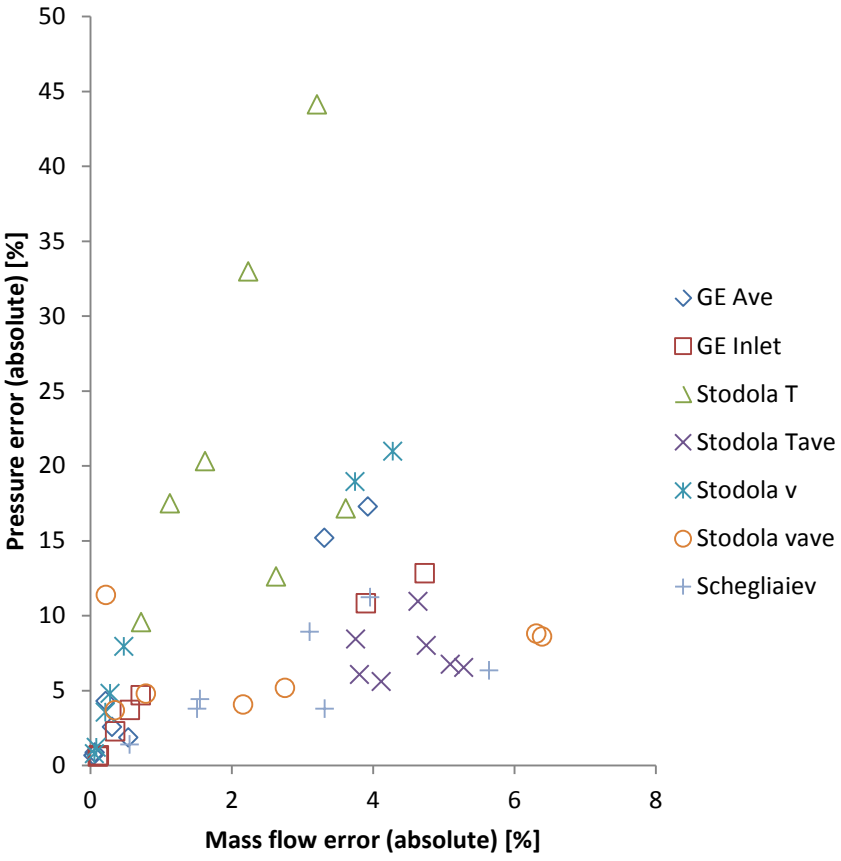

Figure 24: Absolute pressure error vs. absolute mass flow error

The points closest to the origin are the most accurate while those further away are less accurate. Correlation data points grouped in a cluster indicate that the correlations are consistent in predicting results, despite being less accurate, while those correlations that are widely dispersed are less consistent.

From Figure 24, one will note that correlations "GE Ave" and "GE Inlet" appear to be the most accurate and consistent. "Stodola Tave" is consistent but less accurate. "Stodola T" is inconsistent and less accurate.

As a further step in determining which correlations to implement, the magnitude of each point was determined (distance from origin to each data point in Figure 24). From this the mean error and standard deviation of the magnitude for each correlation were determined and plotted on a bubble plot shown in Figure 25. The Y-axis represents the mean error, hence the lower the centre of the bubble, the more accurate the method. The diameter of the bubbles represents the standard deviation. A larger diameter implies a greater standard deviation, or a low degree of consistency. The best solution is the smallest bubble at the lowest position.

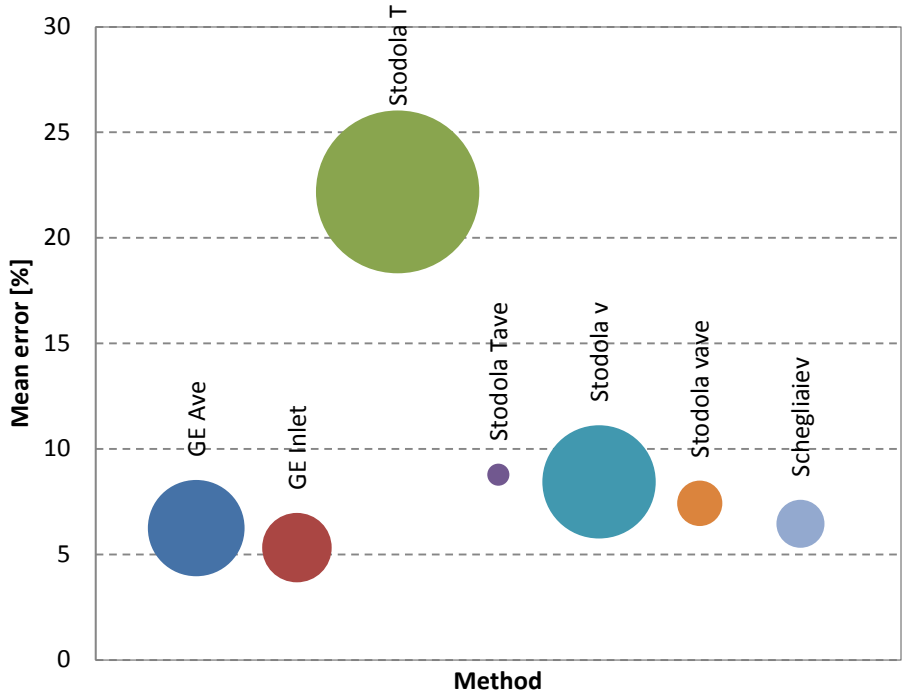

Figure 25: Mean error and standard deviation for each pressure drop correlation

From Figure 25, one will note that "Stodola T" has the highest mean error and standard deviation. Correlation "Stodola Tave" has the lowest standard deviation but the second highest mean error. Correlations "GE Inlet" and "GE Ave" have the lowest and second lowest mean error respectively but their standard deviation is larger than "Schegliaiev".

Based on results for the HPT, correlations "GE Ave" and "GE Inlet" were the chosen correlations to be implemented. However, the Stodola correlation is a popular correlation used by many

simulation packages. This suggests that the Stodola correlation might have some advantages not uncovered by this study. For this reason, "Stodola v" was also chosen for implementation.

It is interesting to note that Figure 25 is highly influenced by PP-B's HPT. If the results of PP-B were removed, the result would be as presented in Figure 26. One notices a large improvement in the mean error (between 2.9 % and 4.77 % absolute difference improvement) and standard deviation (between 3.19 % and 5.38 % absolute difference improvement) of correlations "GE Ave", "GE Inlet" and "Stodola v" when compared to Figure 25.

PP-B's turbine employs partial arc admission. In the evaluation of PP-B's HPT, the "first stage pressure" (refer to Appendix B Figure B. 3 p 86) values were used. From the figure one notes the large difference (±1000 kPa) between "first stage pressure" and the pressure after the governor valves during off-nominal load conditions. The "first stage pressure" is measured at the first stage inlet for the arc of blades supplied by "governor valve 4". During nominal load conditions the "first stage pressure" is more representative of the overall first stage pressure since all the governor valves are fully open. During off-nominal load conditions the "first stage pressure", is less representative of the overall first stage pressure since three governor valves are throttled and the fourth valve is closed. It is believed that this discrepancy in the first stage pressure causes the results (outlet pressures and mass flow rates) obtained using the "first stage pressure" produced larger errors than those achieved for PP-C and PP-A. The use of the average pressures after the governor valves (average of valves 1, 2, 3, and 4 and 1, 2, and 3) instead of the "first stage pressure" in the model was considered. This produced results with even larger errors, hence "first stage pressure" values (as per acceptance test data) were used in the evaluation.

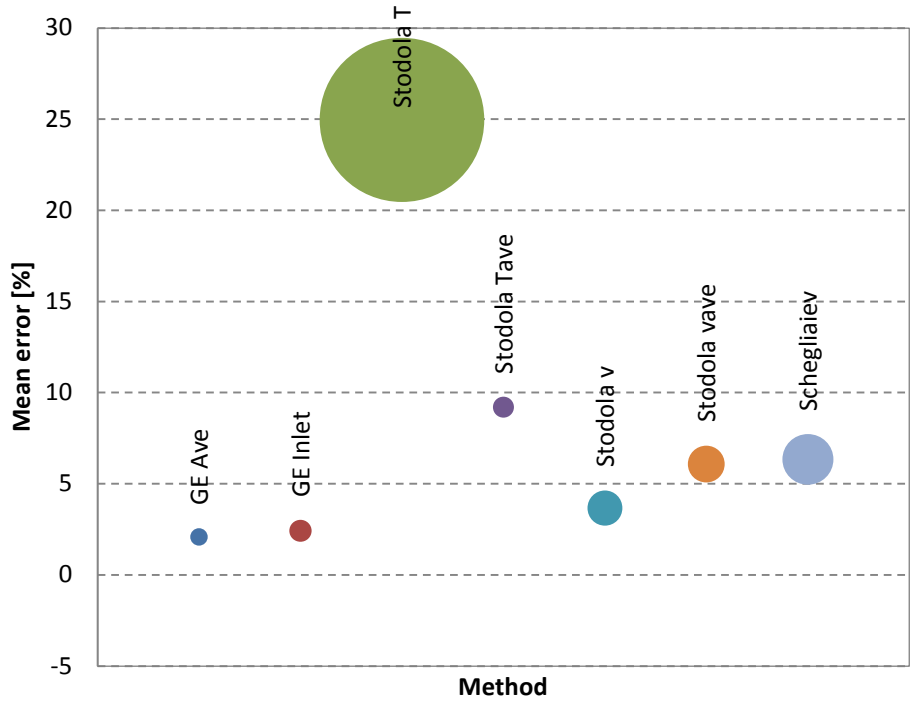

Figure 26: Mean error and standard deviation excluding PP-B

To further verify the three chosen correlations (especially at lower pressures), they were tested analytically for all the remaining turbine sections of the reference plants.

In additional to the HPT, PP-C has one double flow IPT and two double flow LPTs. The LPTs are not identical in terms of their extraction.

PP-A has one single flow IPT and two double flow LPTs in additional to the HPT. The condenser is in series i.e. the cooling water first cools the exhaust steam from one LPT before cooling the exhaust steam of the other LPT. In a series condenser the LPTs exhaust to different condenser pressures.

PP-B has one double flow LPT in additional to the HPT.

All the sections of the turbines were analysed individually, i.e. not connected to each other. It is also important to note that the turbine was "split" into individual turbines at each steam extraction point. The result is that the correlations were effectively tested on a total of 23 turbine sections i.e. 14 impulse sections and 9 reaction sections.

A similar approach was followed to analyse the errors, except that the mass flow error vs. pressure error was not taken as absolute. This was done to visualise the level of over- or under-estimation.

NB: In the derivation of equation (31), "Stodola vave", and equation (33), "Stodola Tave", an assumption of average density was made as mentioned in section 3. During the analytical solution it was noted that a mass flow rate and pressure error resulted under nominal conditions. Therefore the assumption of average density for these specific equations is invalid.

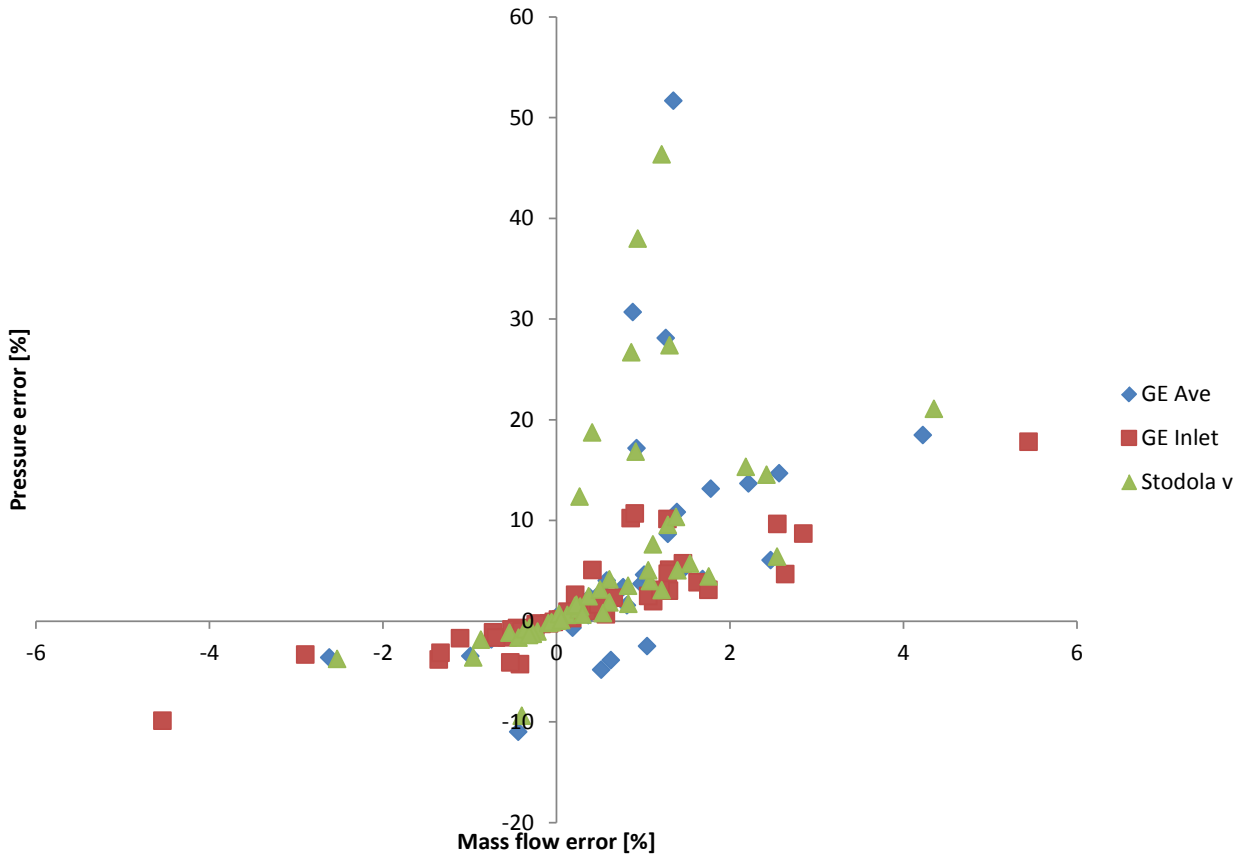

Figure 27: Pressure error vs. mass flow error for the three correlations

From Figure 27, one will notice that "Stodola v" is less accurate and less consistent than "GE Ave" and "GE Inlet". "GE Inlet" seems to be more accurate and consistent than "GE Ave". The correlations tend to over-estimate the results in most occasions.

To determine definitively the best correlation to use, another bubble plot was generated with the mean error and standard deviations, but this time the mass flow errors and pressure errors were considered separately. One notes, from Figure 28, that when determining mass flow, the mean error and standard deviation for all three correlations are very small. When the correlations are used to calculate pressure, "Stodola v" has the largest mean error and standard deviation.

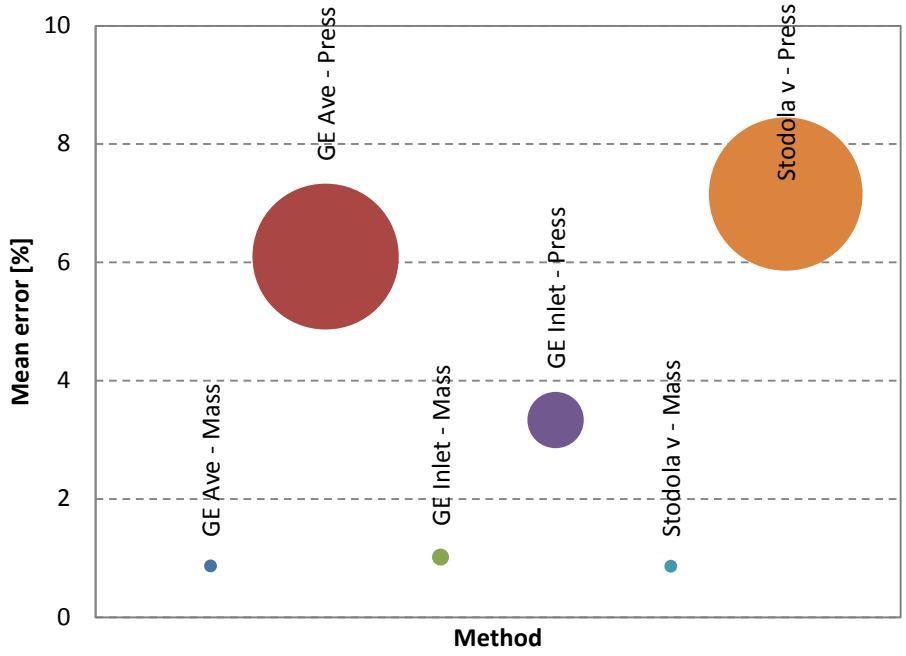

Figure 28: Mean and standard deviation for pressure and mass flow error

In Figure 29 the mass flow and pressure errors were combined in a similar manner as for Figure 25. One will note that "GE Inlet" has the lowest mean error and standard deviation while "Stodola v" has the largest mean error and standard deviation.

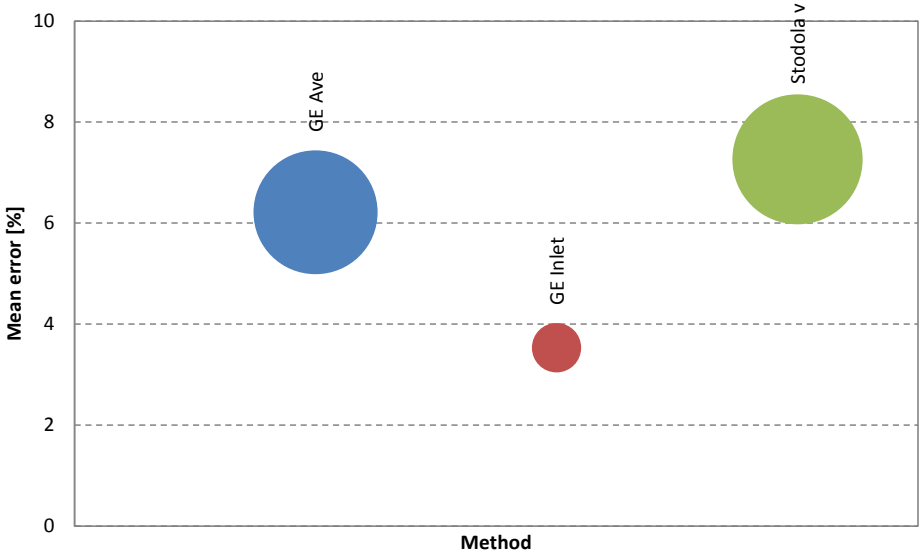

Figure 29: Mean error and standard deviation of the three correlations

From the various pressure error plots for the all the turbine sections in Appendix B one notices that the error is larger towards the LPT section. This could be attributed to the larger uncertainty of the acceptance test data at the low pressures (as indicated in section 2.8.10). Also, for some turbines the exit conditions are in the two-phase region, which could create additional inaccuracies.

Fortunately an error at low pressures has a small effect on the error predicted on the enthalpy of the steam. The error made in the energy conservation equation (25) is therefore also small.

For example:

Actual pressure = 5 kPa, assume x = 0.9 then actual enthalpy = 2318.4 kJ/kg

Calculated pressure = 6 kPa, assume x = 0.9 then calculated enthalpy = 2325.1 kJ/kg

% pressure error $= \frac{6-5}{5} \cdot 100 = 20\%$

but

% enthalpy error $= \frac{2325.1-2318.4}{2318.4} \cdot 100 = 0.289\%$

3.2 Flownex implementation of the pressure drop correlations

3.2.1 Methodology

The various pressure drop correlations were also implemented in Flownex to determine which would be the most appropriate method to use. In this Flownex model the velocity of the steam is zero therefore the total pressure is equal to the static pressure. All the correlations were tested on the HPT of PP-C. As in the analytical case, the Flownex models were set up to solve two scenarios:

1. The inlet mass flow rate, given inlet pressure, inlet temperature and outlet pressure.
2. The outlet pressure, given the inlet pressure, inlet temperature and inlet mass flow rate.

Nominal load conditions (100 % load) were used to model the HPT. The off-design conditions (80 %, 60 % and 46 % load) were then predicted and compared to the analytical solution results. The off-design conditions were predicted by changing the boundary conditions i.e. the given values from points 1 and 2 above.

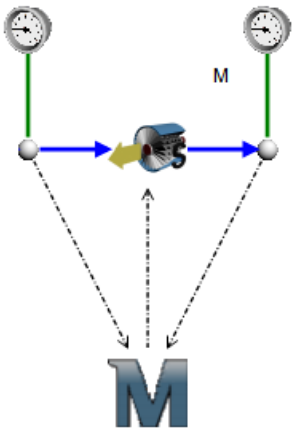

Figure 30: Flownex pressure drop correlation model

Figure 30 shows how a Mathcad component was added to the Simple Turbine in Flownex to implement correlations (30) to (34). For the two general empirical law correlations the Mathcad component is not necessary, as this is a built-in form used in Flownex.

One of the major obstacles in implementing equations (30) to (34) was that they are implicit in terms of the outlet pressure or temperature. Being implicit, they can only be solved iteratively. The Mathcad component was used to calculate the C_k value. Because the C_k co-efficient is dependent on the off-design condition inlet and outlet pressures, it varies for every load condition for the implicit models. The Mathcad component in the Flownex model uses the steam property values in their base units to calculate C_k therefore units for C_k are compatible with the correlations used.

In the 2013 version of Flownex (which was used in this study) the Mathcad component is called only once before the solution algorithm starts. To "force" Flownex to run the Mathcad component iteratively, the model was first run in steady state and then in transient mode. The transient mode calls the Mathcad component at each time step, and even though the problem being analysed is a steady state condition, the Mathcad component gets called iteratively, and eventually converges. Consequently this increases the solving time.

Flownex has an iterative script component that calls the script during each iteration step. The next logical step would have been to convert the Mathcad calculations into an iterative script. Since it was only required to test the models at this stage, there was no need to do this conversion. If, however, one of the explicit models proved to be the most accurate, the final compound component would need to contain an iterative script instead of the Mathcad component.

Some of the correlations required certain fluid properties to be accessed, such as the nominal density. The nominal density could not be calculated without making the model complicated. It

would be unreasonable to complicate the model for only one value. The nominal density is constant for the model, therefore nominal density was input into the model instead of being calculated. However, the density for each load case was calculated.

In general empirical law correlations C_k is constant for all load conditions, therefore the Mathcad component is not required. As a result the general empirical law requires less effort to implement, and runs the fastest.

3.2.2 Evaluation of results

The detailed results can be found in Appendix B, Table B. 5. The results were compared to the analytical solution results (Table B. 4), and the difference between the two in % error is presented in Figure 31.

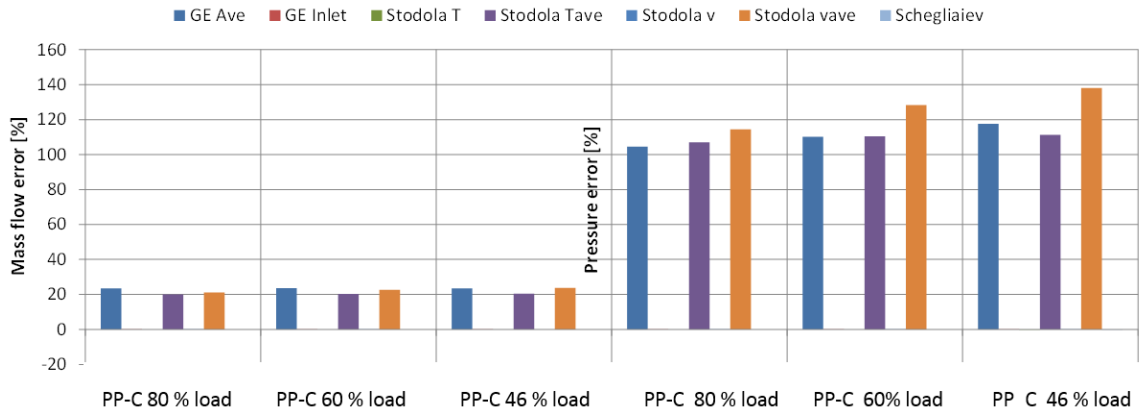

Figure 31: Flownex vs. analytical solution error for mass flow and pressure

It may appear that only the correlations using average conditions are presented in Figure 31. In fact, these models produced such large errors compared to the others, that one cannot see the errors of the other models errors on the figure. These large errors are due to the simple turbine component being based on the upwind differencing scheme, which implies that it uses the inlet conditions in its solution instead of the average conditions.

Figure 32 is the same as Figure 31 except that it excludes the correlations using average conditions. This was done to get a better visualization of the magnitude of the errors of the other correlations.

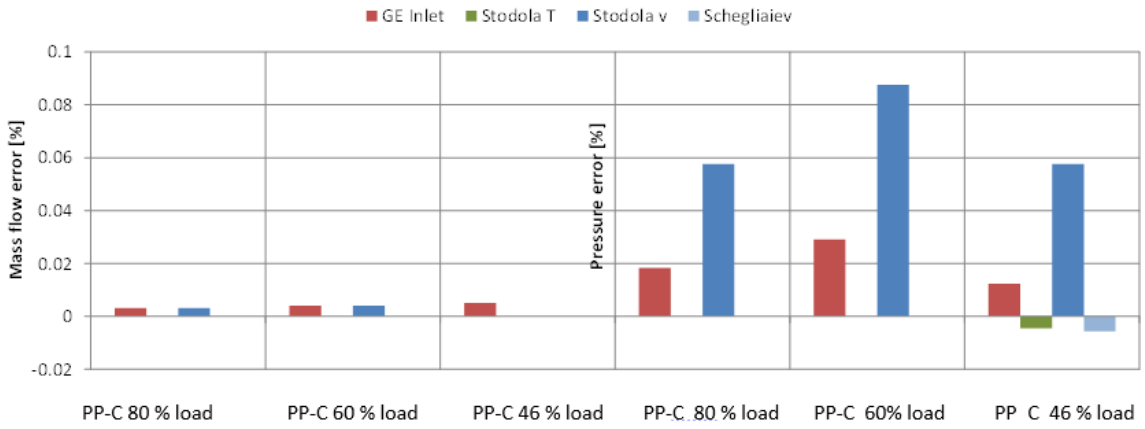

Figure 32: Flownex vs. analytical solution error for mass flow and pressure excluding correlations using average conditions

The differences in results achieved between Flownex and analytical solution are very small. This verifies that the correlations were correctly implemented in Flownex. The reason for the differences is mainly due to the fact that there were slight differences in the fluid properties (specifically density) used in the analytical solution and Flownex. To a lesser extent, rounding off error and convergence criteria also contribute to the difference.

Based on the error analysis of the analytical solution and Flownex results, correlations "GE Inlet" and "Stodola v" were chosen for implementation. "GE Ave" had to be eliminated since it could not be implemented in Flownex. (Recall from Figure 26 that "Stodola T" produced the worst accuracy, despite its accurate implementation in Flownex.)

4. Efficiency Correlations

4.1 Analytical solution of efficiency correlations

4.1.1 Methodology

The various methods to predict efficiency were evaluated analytically using Mathcad. The methods tested were SCC, PEPSE, Ray and Darie.

All of the above-mentioned methods were tested on all the turbines of the three reference power plants: PP-A, PP-B and PP-C.

Nominal load efficiency (100 % load) from the acceptance test data for the three reference plants was used to predict the off-design efficiency (80 %, 60 % and 46 % load) and was then compared to the acceptance test results.

Below is a brief description of how the methods were implemented. No attempt is made to explain the complete process of the individual methods, the focus rather being on the assumptions or simplifications that were made.

- **SCC method**: An extract of the SCC procedure was given in Figure 13. A variation of the procedure was used in this study. In the variation, the SCC method was followed in reverse order to calculate the new base efficiency from nominal efficiency. Once the new base efficiency was determined the normal SCC procedure was followed to determine the off-design efficiency. The SCC procedure has methods for HPT with governing stages; however, none of the reference plants have a governing stage on the HPT. Therefore, for the HPT an assumption was made to correct only for initial conditions.

- **PEPSE method**: The expansion line of the HPT is a straight line. Even though the actual expansion line of a single reheat IPT and LPT is curved, it was also assumed to be straight. The slope of the nominal efficiency expansion line was determined using the inlet and outlet enthalpy and entropy. This slope is the same for off-design efficiency calculation. The Y-intercept was calculated for each off-design case using the off-design inlet enthalpy and entropy. This resulted in an equation where enthalpy is a function of entropy for the expansion line. From the steam properties formulation (IAPWS97), the enthalpy can be determined as a function of pressure and entropy. The off-design outlet enthalpy was determined by a simple Mathcad algorithm to solve the two enthalpy functions since only outlet pressure was known. The algorithm is shown in Appendix C (p 104).

- **EBSILON method**: The exact characteristic curves used by EBSILON could not be obtained. This, together with the fact that the curves need to be calibrated for each turbine, resulted in this method not being evaluated.

- For the **Darie method** only the pressure stage efficiency correlation was evaluated since data for turbines without governing stage was available and that for turbines with governing stages was not available.

4.1.2 Evaluation of results

The detailed results can be found in Appendix C. For the error analysis, the error was determined as

$$\Delta\eta = calculated\ \eta - actual\ \eta \tag{38}$$

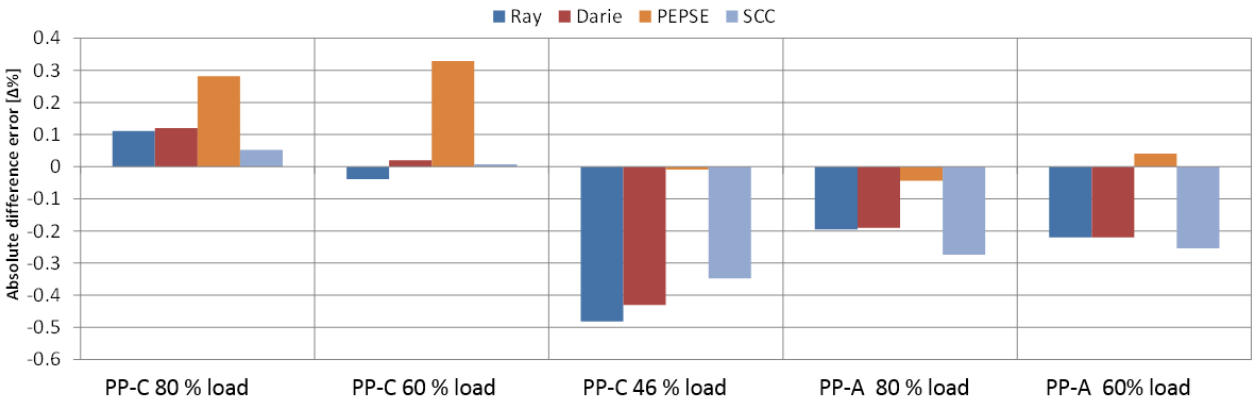

Figure 33: Efficiency error for various methods for HPT

The HPT efficiency of PP-B is not shown here because there is an abnormality in the acceptance test data. The efficiency increases significantly with a decrease in load, which is contrary to what normally happens. This is further explained in Appendix C, p 103.

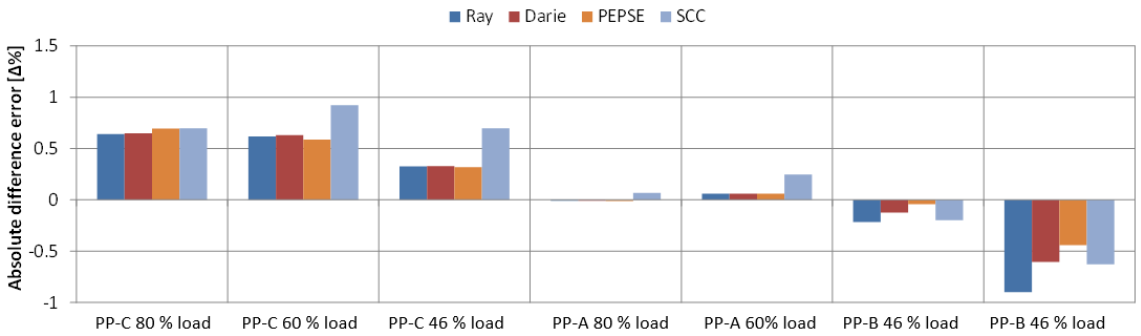

Figure 34: Efficiency error for various methods for IPT

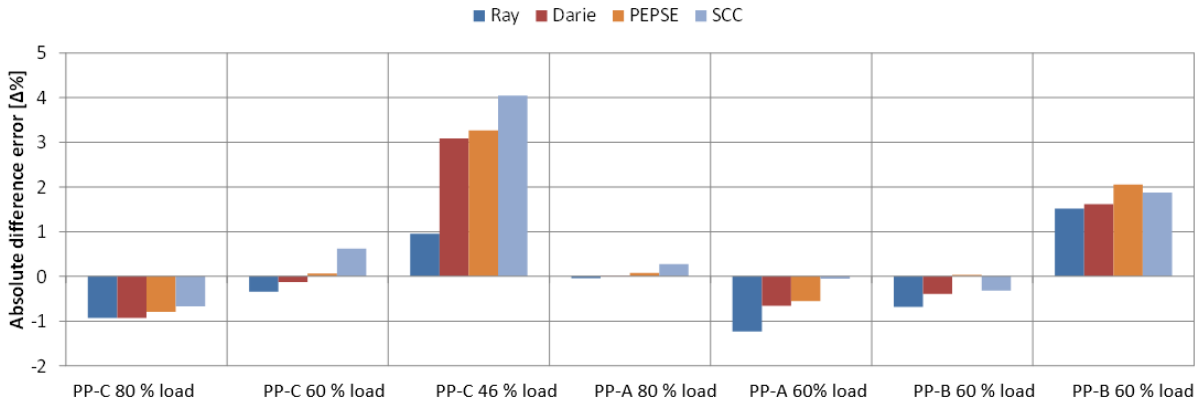

Figure 35: Efficiency error for various methods for LPT

In Figure 33, Figure 34 and Figure 35, one notices that errors tend to increase from HPT to LPT. The errors for estimating the off-design efficiency for LPT are much larger than for HPT and IPT. This might be due to the fact that the efficiency of LPT cannot be measured directly because of the wet steam at the LPT exhaust. The other possibility is that some the efficiency methods might not be capturing all the effects for the LPT (e.g. the high exhaust velocity).

To identify definitively the efficiency method to implement, the mean error and the standard deviation of the absolute error were determined for all the turbines of the various reference plants.

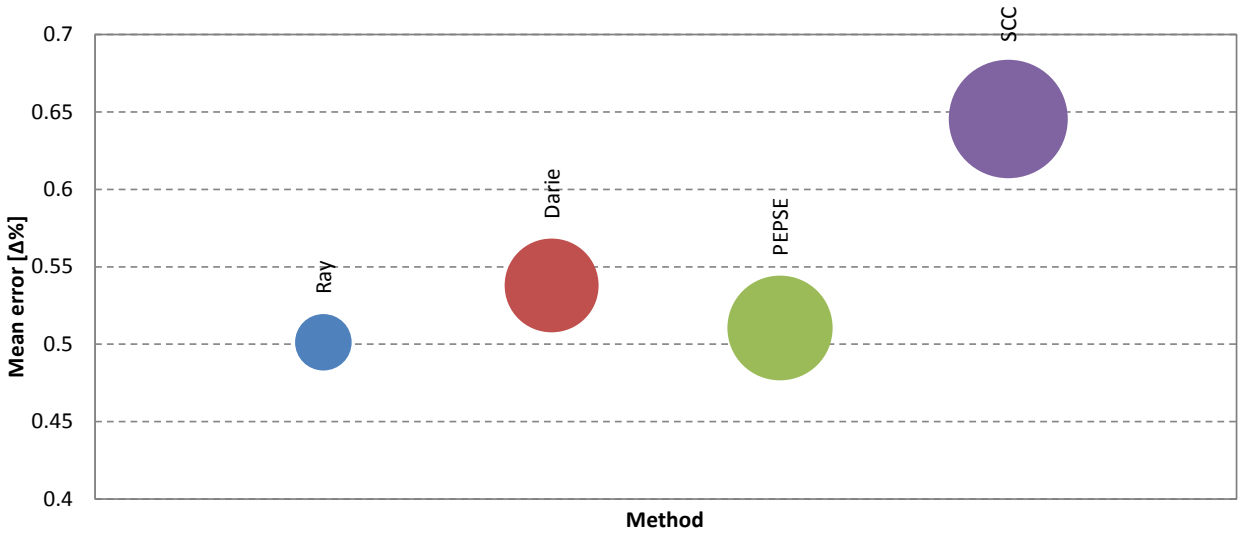

Figure 36: Mean error and standard deviation for various efficiency methods

From Figure 36, one notices that the mean error given by methods “Ray”, “Darie”, “PEPSE” and “SCC” is similar and minimal. “Ray” has the smallest standard deviation followed by “Darie” and “PEPSE”.

4.2 Flownex implementation of efficiency correlations

4.2.1 Methodology

As with the pressure drop models, various methods to predict efficiency were implemented in Flownex. The methods tested were SCC, Ray and Darie. The PEPSE method could not be implemented in Flownex since certain fluid properties could not be accessed.

All the above-mentioned methods were tested on the HPT of PP-C.

Referring to Figure 37, the Mathcad component was used to determine the efficiency of the turbine given the boundary conditions. The calculated efficiency was then input to the simple turbine 1.

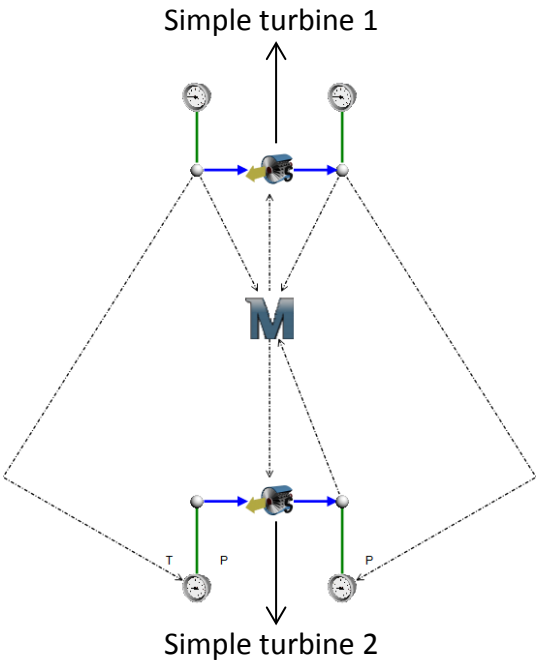

Figure 37: Flownex efficiency method model

Most of the efficiency methods were difficult to implement. One of the major problems was that certain fluid properties could not be accessed in the 2013 version of Flownex. The “Ray” and “Darie” methods required the isentropic enthalpy drop and isentropic outlet enthalpy respectively

in their calculation. To obtain the isentropic outlet enthalpies it was necessary to model the simple turbine 2, operating under isentropic conditions.

The "PEPSE" method required the outlet enthalpy to be determined as a function of pressure and entropy but since this was not possible using the 2013 version of Flownex, this method could not be implemented.

4.2.2 Evaluation of results

The detailed results can be found in Appendix C, Table C. 5. The results were compared to the analytical solution results, Table C. 4, and the difference between the two, in % error, is presented in Figure 38.

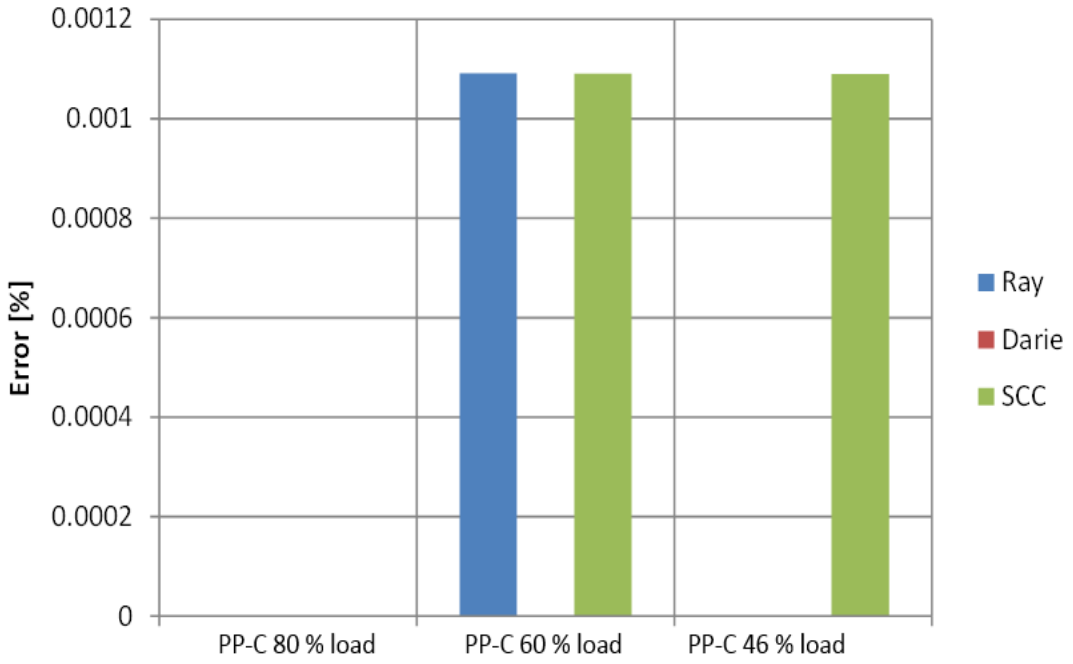

Figure 38: Flownex vs. analytical solution errors for the efficiency methods.

Figure 38 shows the comparative analytical and Flownex errors for the efficiency methods. The differences in results achieved between Flownex and analytical solution are very small. This verifies that the methods were correctly implemented in Flownex. The reason for the differences in results is errors due to rounding off.

Based on the error analysis of analytical solution and Flownex results, the "Ray" method was selected for implementation.

5. Case Study Implementation of the Models

5.1 Complete model

5.1.1 Methodology

The steam turbine train of PP-A, PP-B, PP-C and PP-F was modelled in steady state using “GE inlet” and “Stodola v” pressure drop correlations. The models were calibrated at 100 % load. The models were then used to predict off-design conditions (80 %, 60 % and 46 % load). For PP-F, the model was used to predict conditions at various back pressures. The results from the model were then compared to acceptance test data.

The following paragraphs describe some modelling blocks that were used in Flownex to develop the complete turbine train.

- **Turbine valves:** The turbine valves were modelled as a pipe with an orifice. The flow through the valve was adjusted by varying the orifice diameter ratio inside the pipe element.

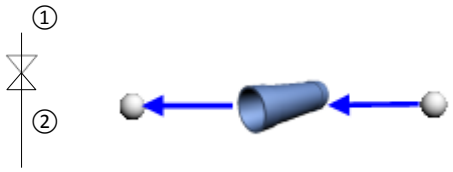

Figure 39: Schematic and Flownex representation respectively of a simulated valve

- **Reheater:** The reheater was modelled as a node with volume that is connected to the inlet and outlet pipes. The heat and spray water added to the reheater was modelled as a boundary condition with a temperature and mass source specified.

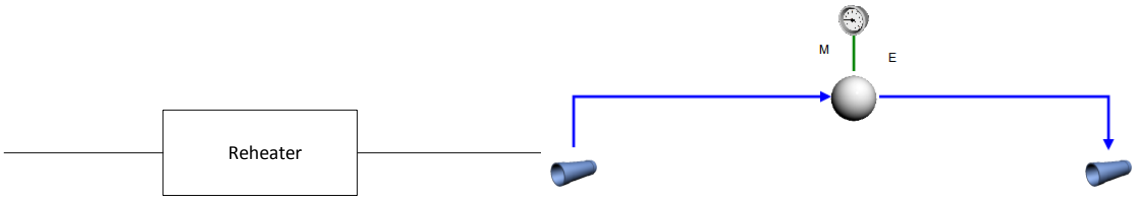

Figure 40: Schematic and Flownex representation respectively of the reheater

- **Multi extraction steam turbine:** The multi extraction steam turbine like IPT and LPT were modelled by splitting the turbine into sections. The sections were defined as inlet to extraction,

extraction to extraction and extraction to exhaust. Each turbine section was modelled with a simple turbine component. The extraction flow was accounted for by using a condensing surface component which is a compound component developed by Dr WF Fuls that extracts the steam for a feed water heater by specifying (user input) the energy required by the feed water heater.

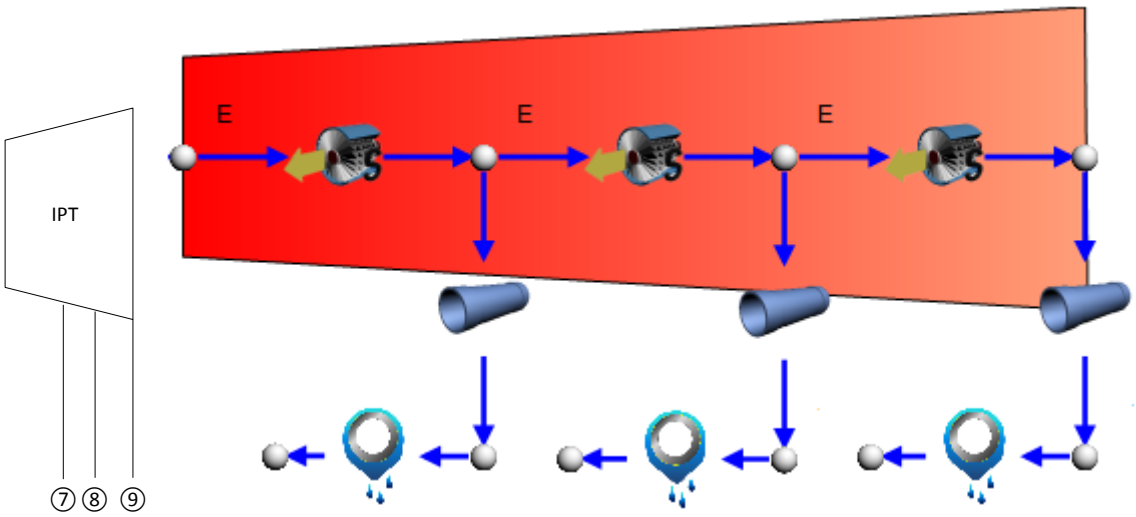

Figure 41: Schematic and Flownex representation respectively of a multi extraction steam turbine

- **General modelling considerations:** The models in this study did not have any auxiliary components connected to them. To accommodate for the auxiliary components, the heat extracted by the feed water heaters was specified on the condensing surface component and for BFPT a pressure boundary condition was specified on the extraction pipe. These heat extractions and pressure were adjusted for each load case to correspond to the acceptance test data. The upstream and downstream nodes of each turbine section were given a volume. This was done to make the static properties of the steam equal to the total properties of the steam at these nodes. The only other boundary conditions specified were the pressure and temperature in front of the HPT valves, reheater temperature, spray water flow rate and condenser pressure.

  The turbine loss factor, C_k, for each turbine section was calculated from nominal load conditions acceptance test data using the chosen pressure drop correlation.

  The IPT cooling steam (where applicable) and gland sealing system were not modelled as their mass flow rate is minimal compared to the main steam mass flow rate. Also, most of the acceptance test data do not supply information on IPT cooling steam and gland sealing system mass flow rates.

- **Model calibration:** The models were calibrated at nominal load conditions employing the Flownex designer function, which was used to calculate the following:
    1. Orifice diameter ratio of the pipe representing the HPT governor valves to ensure the correct inlet mass flow rate.
    2. The pipe (representing the HPT and IPT valves) loss factor to ensure the correct drop across the valves.
    3. The reheater inlet and outlet pipe loss factor to ensure the correct pressure drop across the reheater.

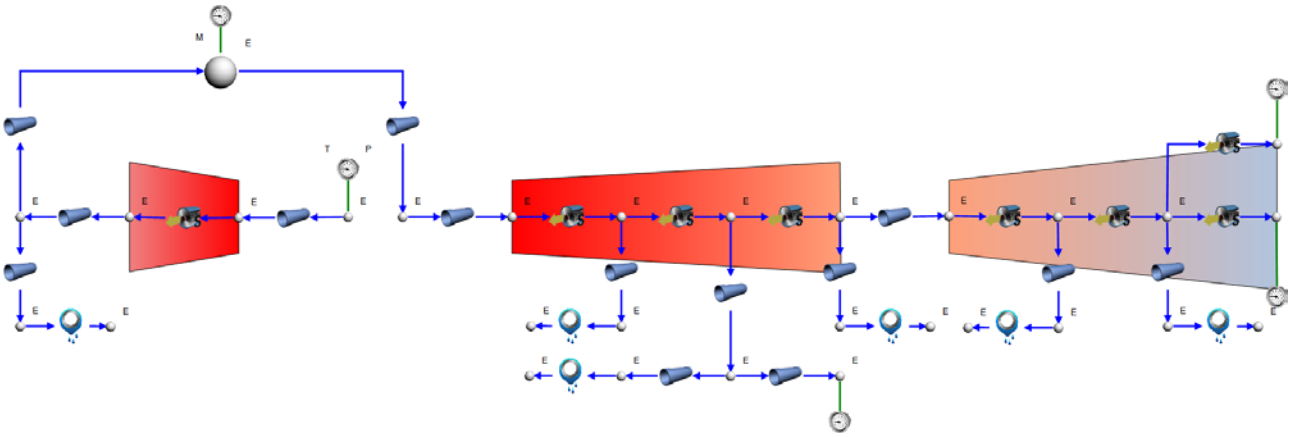

Figure 42: Model of PP-A Turbines

5.1.2 Evaluation of results

The results for PP-A are discussed in this section. The detailed results for the different plants at the various load cases can be found in Appendix D.

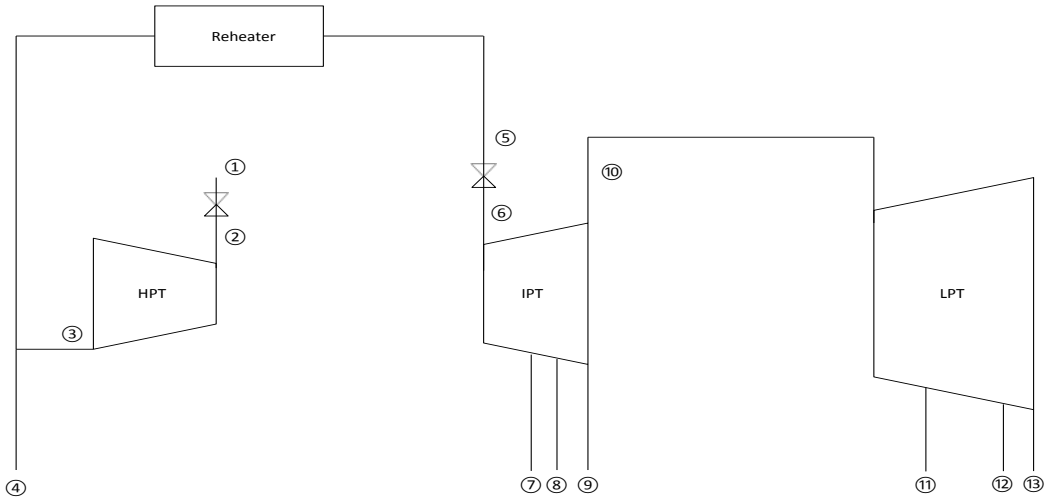

Figure 43: Schematic of PP-A

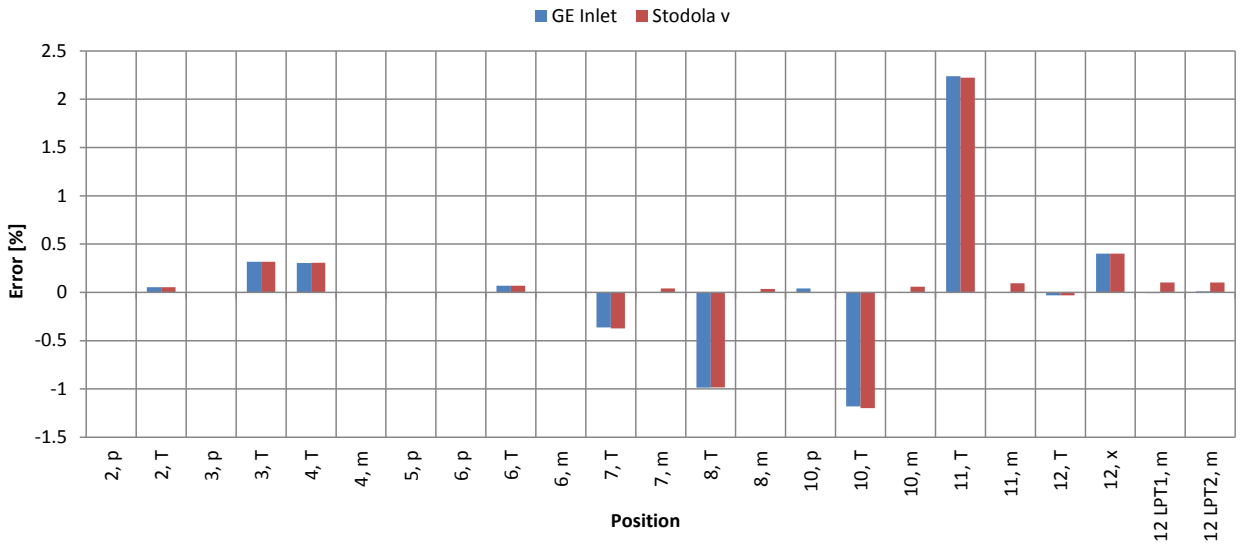

Figure 44: Error for PP-A at calibration (m – mass flow rate, p – static pressure and T – static temperature)

Figure 44 shows the error at calibration. The error at calibration for the remaining reference plants can be found in Appendix D. One notes that the errors are small. The larger errors are temperatures at the extractions and these are due to applying the overall efficiency of the IPT and LPT to individual turbine sections instead of applying the individual efficiency of each turbine section. This was done because acceptance test data provide the overall efficiency, not the

individual turbine section efficiency. This error can be improved on by applying the PEPSE method to find the efficiencies of each turbine section.

The small errors in pressure and mass flow rate could be due to truncation errors in the acceptance test data or inaccuracies in the model. The mass flow error could also be ascribed to the simplification of ignoring the IPT cooling steam and gland sealing mass flow rates. Whatever the reason for their existence, these errors are negligible as they fall within the ASME standard.

Figure 45: Error for PP-A at 80 % load

Figure 46: Error for PP-A at 60 % load

From Figure 45 and Figure 46, one notices that the errors for the off-design cases are quite small. In some instances "GE Inlet" performs better while at other times "Stodola v" performs better. As in Figure 44, the temperature errors are larger for the same reason i.e. the overall efficiency of the IPT and LPT was applied to individual turbine sections instead of applying the individual efficiency of each turbine section. The errors at off-design conditions for the remaining reference plants can be found in Appendix D.

The mean error and standard deviation of the absolute errors for off-design conditions for all reference plants was calculated. Figure 47 shows that the errors are very small for both pressure drop correlations. Therefore, for the reference plants operating with high vacuum, either of the two correlations could be used.

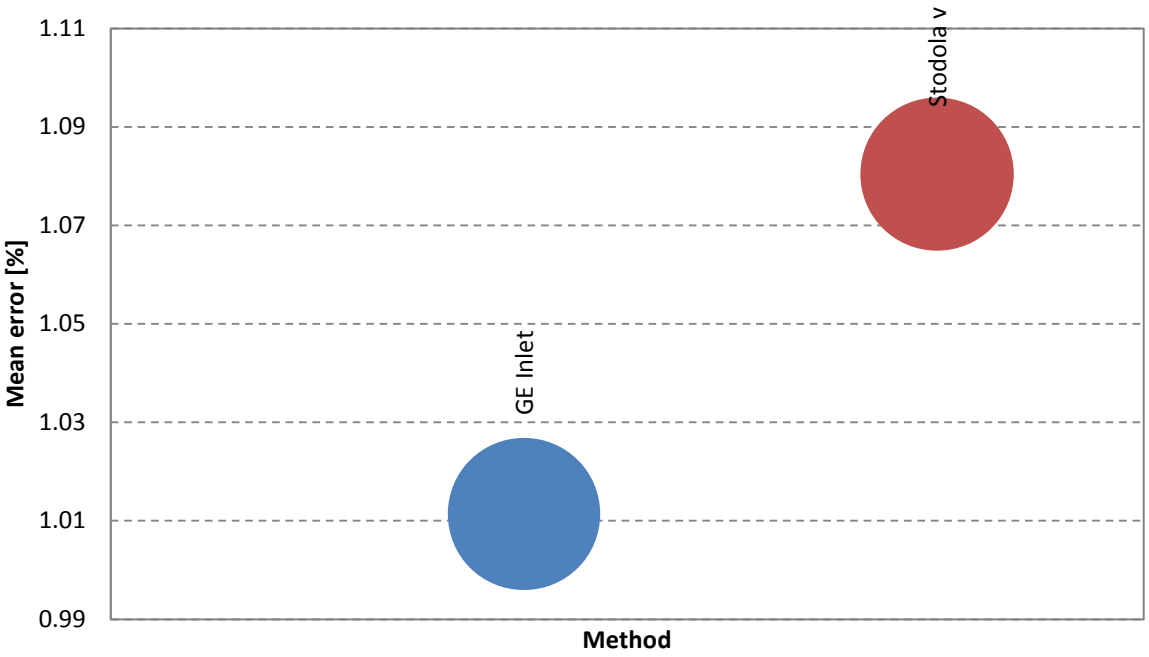

Figure 47: Mean error and standard deviation for all the reference plants

For the transient scenario model of PP-C, it was decided to use "GE Inlet" since it is easier to implement than "Stodola v".

5.2 Transient model of plant situation

The steam turbine models developed were required to have transient capabilities. To verify these capabilities, a transient scenario was modelled. The model results were compared to actual plant data in an attempt to validate the model.

Eskom specifies that the plant instrumentation supplied should have an accuracy of 0.02 % of the full range of the instrument. The loop accuracy of the property being measured is based on all equipment in the loop including transportation of the signals by cables (e.g. volt drops). The loop accuracy is 0.05 % of the full range of the instrument. Eskom specifies that the accuracy of the instrumentation should not drift by more than 0.02 % over a period of six years. Unlike the stringent control of acceptance test instrumentation and techniques, plant instrumentation set up lacks this control. Therefore even though the accuracy specifications for the instruments and set up are high, there is no guarantee that all requirements were met.

PP-C underwent a control and instrumentation upgrade in 2008. The transient test was conducted in 2012. Theoretically, the accuracy of the instrumentation should still be within specification if all the requirements were fulfilled. In addition, the power generated is measured at the power plant and at National Control, providing double assurance that this measurement is within the accuracy specified i.e. 0.02 %.

It must be noted though that this exercise was more to verify that the turbine models can be connected together and simulate a transient which then produces reasonable agreement with plant data. There may have been some transient characteristics of the complete system which was not fully incorporated.

5.2.1 Scenario description

The transient scenario that was selected for modelling was a governor valve step. This is one of the standard tests performed to determine the mechanical characteristics of the unit.

The test required the unit to operate with the turbine load control and boiler pressure support on manual. The valve admission set point was also on manual. The valve admission point gradient rate limiter was set to 600 % per min of the normal valve opening rate. The boiler controls and the rest of the unit controls were all on automatic.

From a stable load, the HPT governor valves were stepped up by approximately 2.5 % of the valve stroke. The transient response of the unit was recorded for the following three to four minutes.

5.2.2 Scenario conditions

The test was conducted on Unit 1 of PP-C on the 13 October 2012 between 9:45 am and 10 am.

The unit was generating approximately 444 MW at that time. Both banks for the HP feed water heaters were out of service, therefore the extracted steam mass flow rates were set to 0 kg/s at these extraction boundary conditions i.e. at HP heater 7 and HP heater 6.

The governor valve step took approximately two seconds.

5.2.3 Flownex model

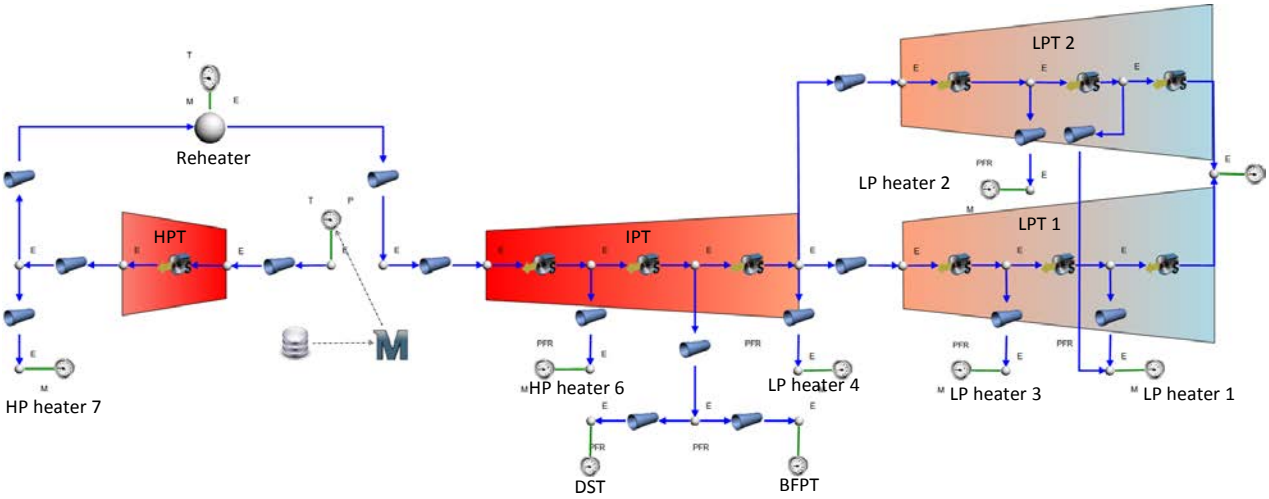

Figure 48: Flownex representation of PP-C

- Simplifications and assumptions:

  During the transient scenario the following assumptions were made:

  1. The mass flow rates in the extraction line to the auxiliary components stays constant.
  2. Constant efficiencies. During the evaluation of the various efficiency correlations in section 4 it was noted that the efficiencies do not change significantly over the operating range considered. Calculating the efficiencies during the transient scenario would have resulted in a more complex model. This was a small transient scenario, therefore the efficiencies were assumed to be constant.
  3. The condenser vacuum is constant.
  4. The reheater spray water flow rate and temperature are constant.
  5. The boiler temperature is constant.

The boiler was not modelled as it was outside the scope of this dissertation. To account for the boiler pressure change during the transient, the pressure was input via the Mathcad component. When the model was run, the boiler pressure was calculated via linear interpolation and input into the model boundary condition.

The acceptance test model developed for PP-C was used to evaluate the transient scenario. The internal clearances of PP-C's IPT increased over time due to deformation and ageing. Even after overhauling the IPT, the clearances were not brought back to design values. The increase in clearances caused the pressure drop across the turbine to decrease. To compensate for deformation and ageing, the turbine loss constant, C_k, of the first IPT section was adjusted. The new IPT loss constant, C_k, was calculated based on IPT inlet data at nominal plant conditions.

5.2.4 Plant vs. Flownex results

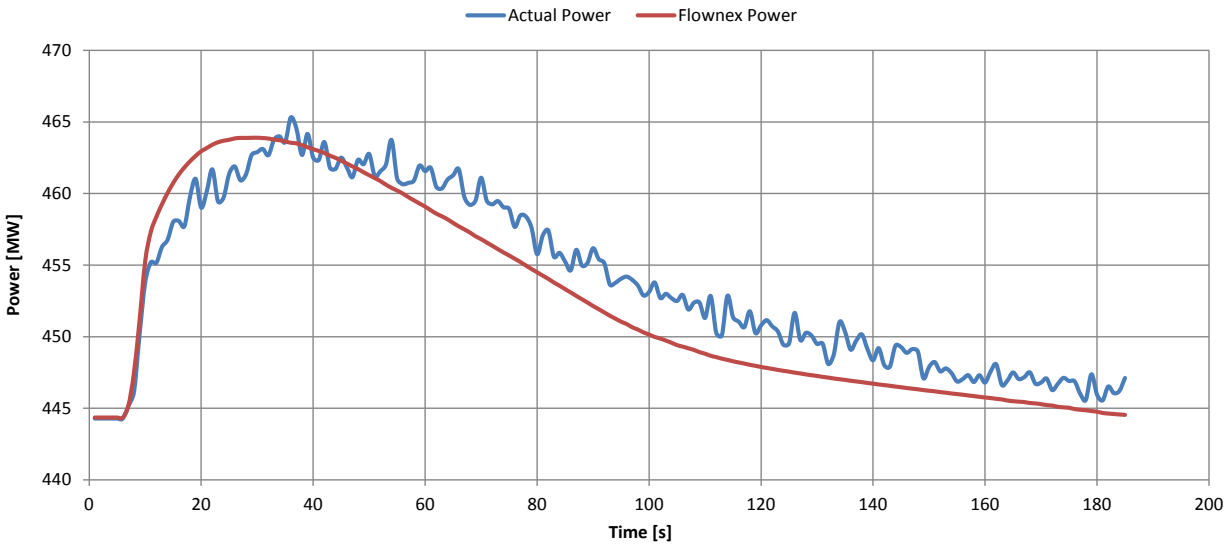

Figure 49: Actual power vs. Flownex power for PP-C

The transient scenario was initiated after five seconds. From Figure 49, one notices that there is good correlation between power predicted by Flownex and the measured power at the beginning of the transient. The variations noted after 10 seconds as indicated on the graph might be due to the simplifications and the assumptions explained below.

The over-estimation of the power by the model from approximately 10 seconds to 40 seconds might be the result of exclusion from the model of the thermal mass of the piping and reheater.

This means that all the energy from the steam is transferred to the turbine instead of some of the energy being transferred to the piping and reheater.

Stepping the governor valves open will cause the steam to the reheater to increase in temperature and mass flow rate. Therefore, to control the temperature of the reheater steam more spray water is required. This means that the steam mass flow rate to the IPT will increase. By assuming the reheat spray water mass flow rate is constant, the steam mass flow rate to the IPT and LPT is under-estimated after some time period. Power is proportional to the steam mass flow rate, therefore the model will under-estimate the power after some time period.

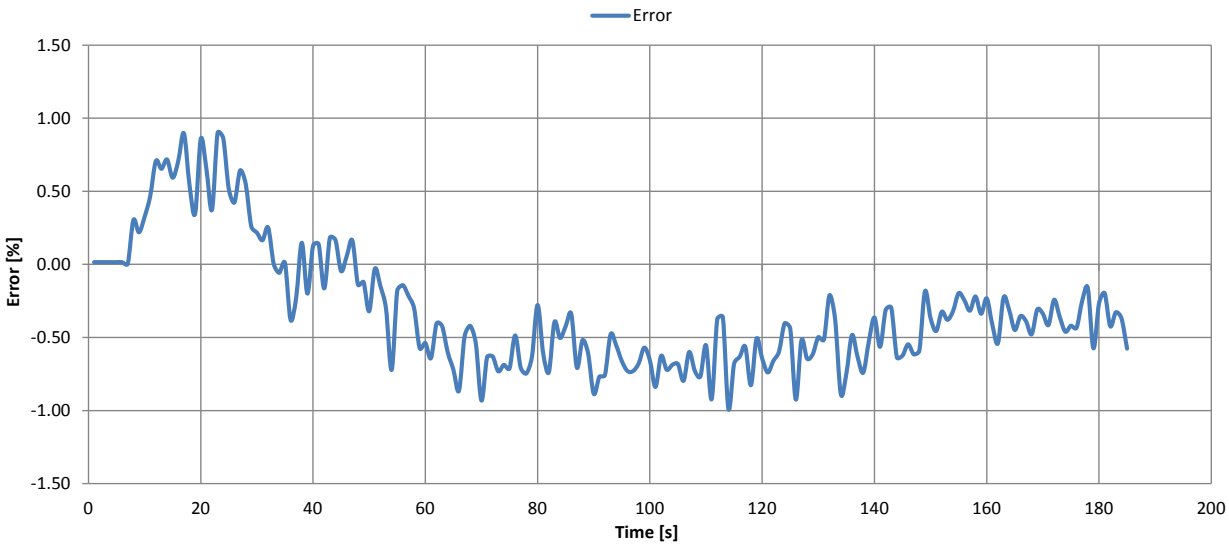

Figure 50: Error for power

Figure 50 shows that even with simplifications and assumptions the error is within ±1 %. Flownex tends to over-estimate the power at start, and then under-estimates the power.

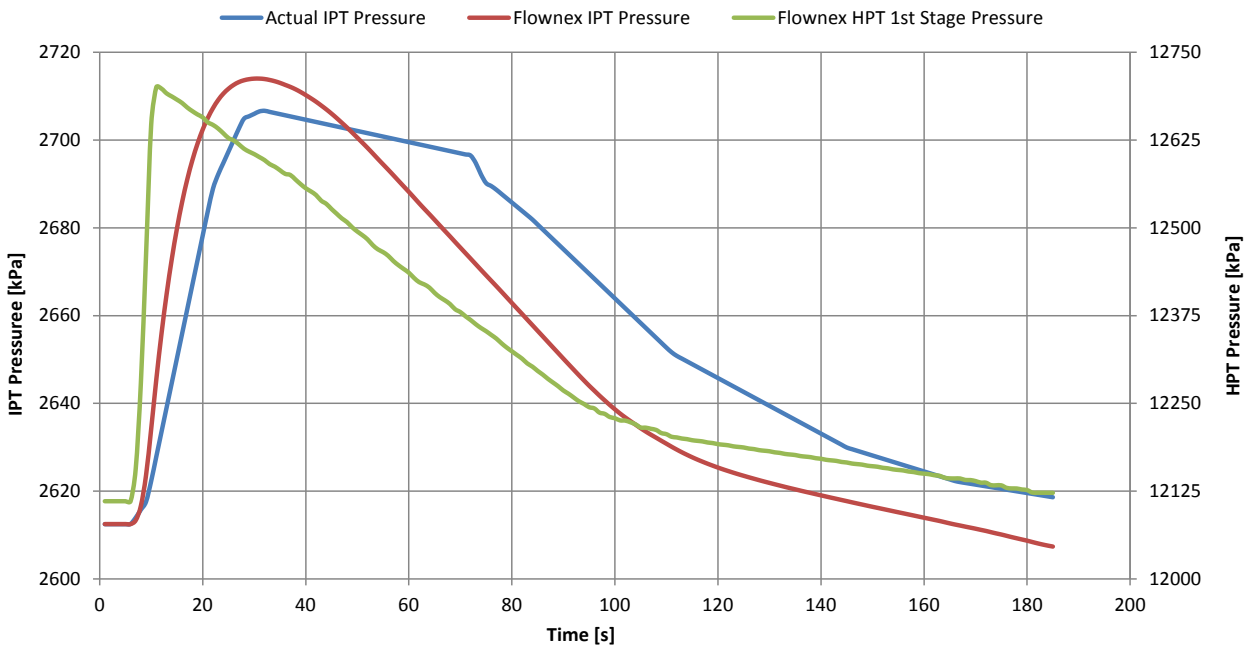

Figure 51: Actual IPT pressure vs. Flownex IPT pressure for PP-C

Due to the reheater volume between the HPT and the IPT, one would expect a delay in the pressure at the IPT inlet. This delay can be seen in Figure 51. Unfortunately, there are not enough sample points for the actual IPT pressure to allow for a good visual assessment on the variation in the results. The shape of both trends is similar, but it appears that the actual pressure delay is longer than that predicted by Flownex. This may be because of inaccurate incorporation of the flow resistance in the reheater section, or the omission of thermal mass contribution of the reheater. Despite this difference, maximum error is just above 1 % as can be seen in Figure 52.

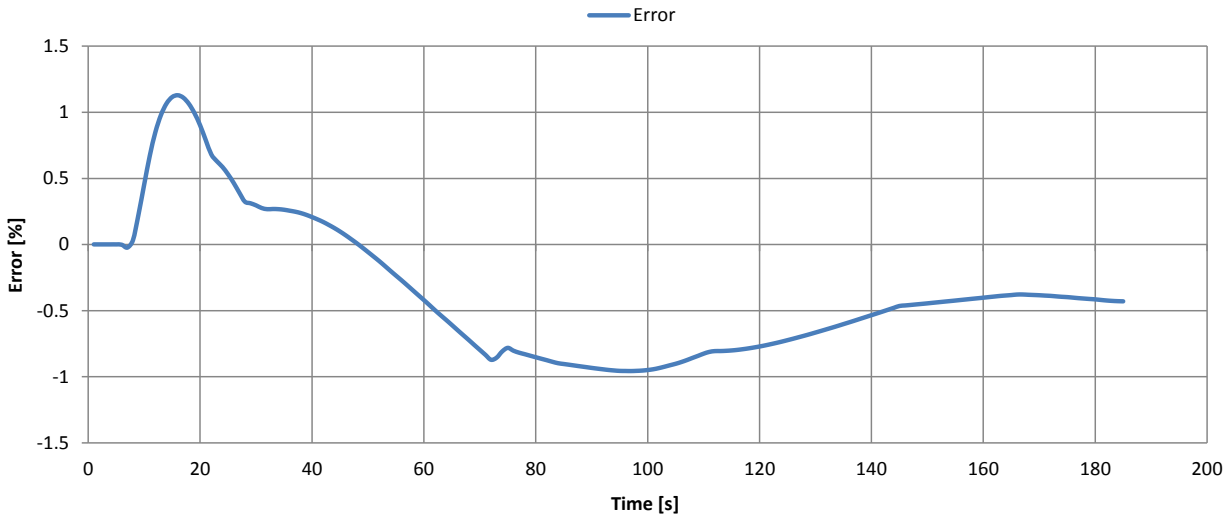

Figure 52: Error for IPT pressure

6. Compound Component

Modelling of turbine systems can be laborious. A compound component was developed for a turbine section to ease the modelling process and to perform pre-processing of user inputs. This chapter describes the compound component, the inputs required, results obtained and also explains how the compound component operates.

6.1 Description of the component

The compound turbine component makes use of the simple turbine component and the script component. The compound component represents a turbine section, i.e. inlet to exhaust (no extractions) or inlet to extraction or extraction to extraction or extraction to exhaust. The compound component uses the general empirical law, equation (35), to calculate the pressure drop through the turbine. The "Ray" method, equation (21), is used to determine off-design efficiency.

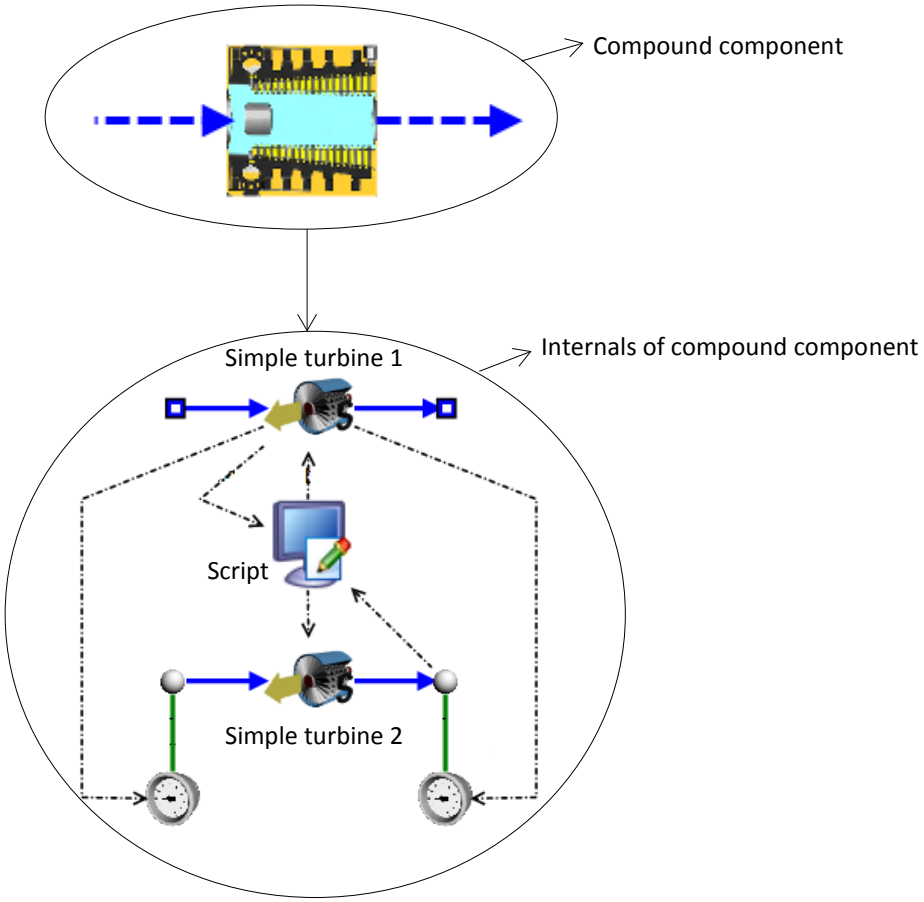

Figure 53: Compound turbine component

Simple turbine 1 represents the actual turbine section.

The script is used to calculate the turbine loss constant, C_k, and the off-design efficiency given certain inputs. The turbine loss constant is used for simple turbine 1 and 2. The off-design efficiency is used only for simple turbine 1. Refer to Appendix E for details of the script.

Simple turbine 2 uses the upstream pressure, upstream enthalpy and downstream pressure from simple turbine 1 to determine the outlet isentropic enthalpy (100 % efficient). The outlet isentropic enthalpy is used in the script for off-design efficiency calculations. This was found to be the easiest way to determine the isentropic enthalpy for any given input condition. Perhaps in future versions of Flownex, one would be able to interrogate the built-in fluid properties table using pressure and entropy to obtain the desired enthalpy. Then this second turbine component would not be necessary.

6.2 How to operate

The compound component operates like any other Flownex component. Simple turbine 2 uses properties from simple turbine 1, therefore to solve for efficiency the model is required to be run twice to achieve a correct steady state solution. If the isentropic enthalpy could be calculated inside the script, then the second turbine would not be necessary, nor the second call to the solver.

6.2.1 Inputs

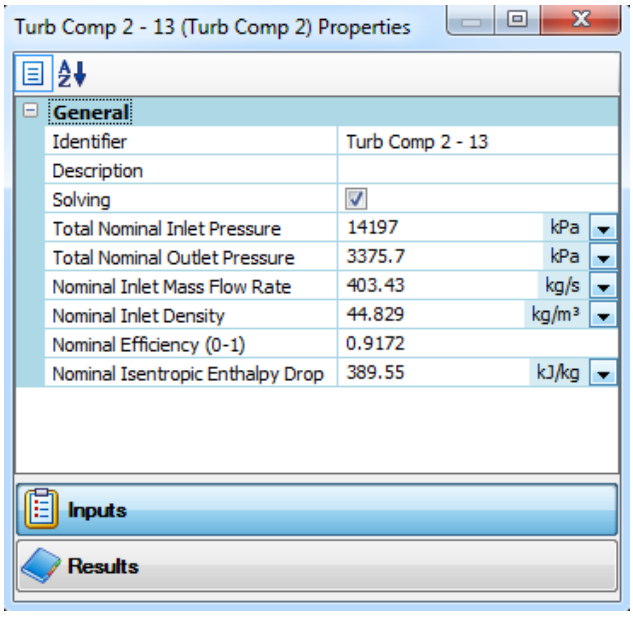

Figure 54: Compound turbine component inputs

In addition to the standard Flownex inputs (fluid assign and boundary conditions) the compound component requires the inputs shown in Figure 54. These inputs are used by the script for internal calculations. They are all process conditions for the **nominal** case, which can be found from the 100 % load case acceptance test data. For an aged turbine, ideally one need to produce more updated process data from a dedicated test, instead of using acceptance test data as-is.

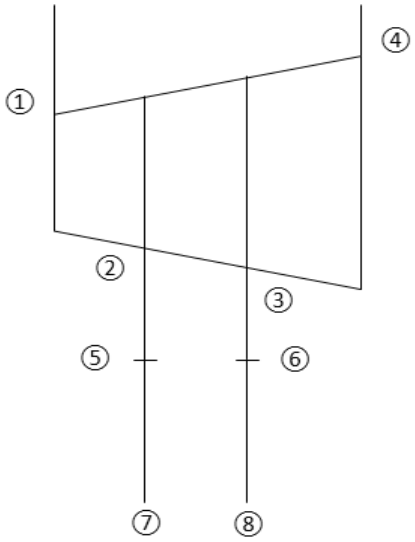

Figure 55: Schematic showing different turbine sections

- **Total nominal inlet pressure:** This is the total inlet pressure under nominal conditions of the turbine section considered. With reference to Figure 55, if the turbine section is inlet to exhaust (1-4) or inlet to extraction (1-2), then this pressure is simply the total inlet pressure at (1). The pressure at the extraction point inside the turbine (2) or (3) is normally unavailable, but rather the pressures at the turbine extraction flanges (5) or (6), or at the auxiliary components (7) or (8). If the turbine section is extraction to extraction (2-3) or extraction to exhaust (3-4) then this pressure is the total pressure at the extraction flange (5) or (6) plus some losses. These losses are usually 1-3 % of the pressure inside the turbine (2) or (3) [13]. If only the total pressure at the auxiliary component (7) or (8) is known then the pressure drop in the extraction piping (5-7) or (6-8) must be factored in as well.
- **Total nominal outlet pressure:** This is the total outlet pressure under nominal conditions of the turbine section considered. With reference to Figure 55, if the turbine section is inlet to exhaust (1-4) or extraction to exhaust (3-4) then this pressure is simply the total exhaust pressure (4). If the turbine section is inlet to extraction (1-2) or extraction to extraction (2-3) then this pressure is the total pressure at the extraction flange (5) or (6) plus some losses. These losses are usually 1-3 % of the pressure inside the turbine (2) or (3) [13]. If only the total

pressure at the auxiliary component (7) or (8) is known then the pressure drop in the extraction piping (5-7) or (6-8) must be factored in as well.

- **Nominal inlet mass flow rate:** the inlet mass flow rate under nominal conditions through the turbine section considered. Care must be taken to subtract the preceding extraction flows for all turbine sections that are not inlet to extraction (1-2) or inlet to exhaust (1-4).
- **Nominal inlet density:** the inlet density under nominal conditions to the turbine section considered. This is obtained from the temperature (or quality) at the specific inlet location, and the inlet pressure as defined above. Note that the inlet velocity is assumed to be negligible, hence the total inlet pressure can also be used as the static pressure for the density calculation.
- **Nominal efficiency:** the efficiency under nominal conditions. Normally it is the efficiency of the complete HPT, IPT or LPT. However, if the efficiency of the individual turbine section is available then it should be used, as it provides a more accurate representation.
- **Nominal isentropic enthalpy drop:** the difference between the inlet enthalpy and the outlet isentropic enthalpy of the individual turbine section under nominal conditions. With reference to equation (21), the nominal isentropic enthalpy drop is constant for all load conditions. The isentropic enthalpy drop for each load condition is determined by the compound component. The nominal isentropic enthalpy drop is needed for the off-design efficiency calculation. Having this value as a user input simplifies the model. If it was possible to calculate the isentropic exit enthalpy using the script, then this user input could be eliminated.

6.2.2 Results

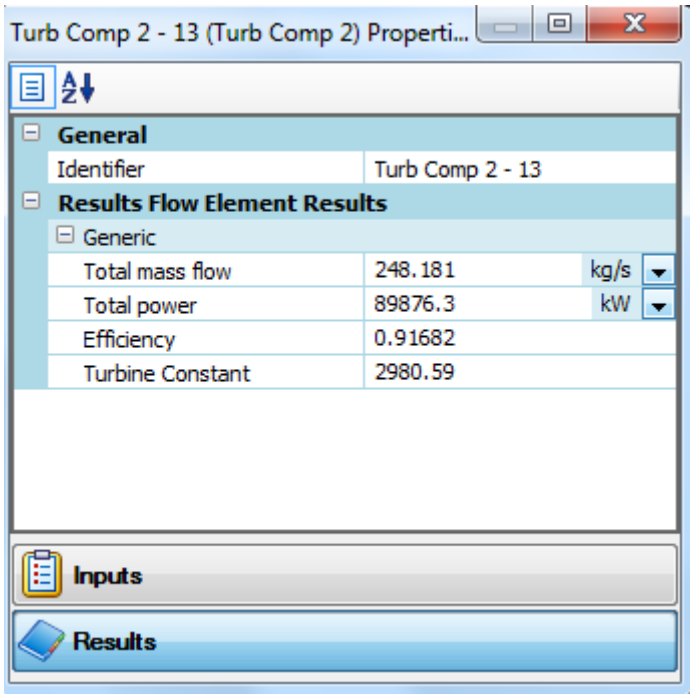

Figure 56: Compound turbine component results

Figure 56 shows the selection of results exposed by the compound component. Most of the other results like inlet or exit conditions can be obtained from the joining nodes.

- **Total mass flow:** the calculated off-design mass flow rate through the complete turbine or the individual turbine section.
- **Total power:** the calculated thermal power developed by the complete turbine or the individual turbine section.
- **Efficiency:** the calculated off-design efficiency of the complete turbine or the individual turbine section.
- **Turbine Constant:** the calculated turbine constant used by the general empirical law.

7. Conclusions and Recommendations

7.1 Conclusions regarding the pressure drop correlations

Various pressure drop correlations that describe the pressure drop across a steam turbine were introduced in section 2.3. These correlations were tested analytically on the HPT of PP-A, PP-B and PP-C. From the results and error analysis it was established that correlations "GE Inlet", "GE Ave" and "Stodola v" respectively were accurate and consistent in predicting the mass flow rate and pressure.

These three correlations were then analytically tested on the remaining individual turbine sections of the three reference plants. The results and error analysis confirmed that the correlations were valid for the complete range of turbine sections tested (HPT, IPT and LPT).

All the correlations were implemented in Flownex and tested on the HPT of PP-C. This was done to determine whether the correlations could be successfully implemented in Flownex. There was good correlation between the analytical and Flownex results except for the pressure drop correlations using average conditions. This is because Flownex uses only inlet conditions for the turbine model.

From the analytical and Flownex results as well as the error analysis it was concluded that correlations "GE Inlet" equation (35) and "Stodola v" equation (30) are the most accurate and consistent in predicting pressure and mass flow rate. The "GE Inlet" correlation achieved a mean error of 3.53 % with a standard deviation of 3.76 % while the "Stodola v" correlation achieved a mean error of 7.26 % with a standard deviation of 9.93 %.

7.2 Conclusions regarding the efficiency correlations

Various methods to predict off-design steam turbine efficiency were discussed in section 2.5.2. All the methods used nominal efficiency to predict off-design efficiency. The various methods were analytically tested on all the turbines of the reference power plants. All the methods provided good results. These methods were not tested on turbines with governing stages as acceptance test data for steam turbines with governing stages was unavailable.

For the PEPSE method it was assumed that the expansion line is straight for IPT and LPT sections even though in reality it is curved. Even with this assumption, the results were fairly accurate. If the equation for a curved expansion line could be implemented, the results might improve.

All the various methods, except the PEPSE method, were successfully implemented in Flownex. There was good correlation between the analytical and Flownex results for the implemented methods. The PEPSE method could not be implemented in Flownex since it required certain fluid properties that could not be extracted from Flownex. It was also difficult to implement the other methods because they all required additional fluid properties which are not readily available to the Flownex user.

From the analytical and Flownex results it was concluded that the Ray method equation (21) is the most accurate and one of the least complicated methods to implement. The Ray method achieved a mean error of 0.5 % with a standard deviation of 0.43 %.

7.3 Conclusions regarding complete turbine train implementation

The steady state models of the turbine train of four power plants were successfully implemented in Flownex using “GE Inlet” and “Stodola v”. The mean absolute errors achieved for both correlations were approximately 1 %. This shows that for high vacuum steam turbine trains either “GE Inlet” or “Stodola v” will provide good results. The mean absolute error for the turbine train was much lower than the mean absolute error for the individual turbine sections, i.e. some turbine sections do produce larger errors, but this does not affect the overall result significantly.

The “GE Inlet” correlation was also successfully used to predict a transient scenario where the governor valves were stepped approximately 2.5 %. The power predicted by the model was within ±1 % of the measured power from the plant data. This accuracy was achieved despite some assumptions and simplifications since only the turbine train was modelled.

7.4 Limitations of this study

The models developed in Flownex did not account for rotational inertia or a generator because the simple turbine component does not have this functionality. Therefore load rejection, islanding, run up and run down of the turbine train could not be tested.

The models also did not consider gland sealing and IPT cooling steam since data was not available in the acceptance test of some of the reference plants; also, these flow rates are much smaller than the main flow rate.

The valves were modelled simply as pipes with an orifice. The exact valve curves were not input into the model. Therefore there is not a clear relationship between “valve position” and “orifice ratio”.

7.5 Recommendations

It is recommended that a component using “GE Ave” be developed in Flownex.

Equation (19), recommended by PEPSE for a curved expansion line (for single reheat IPT and LPT), should be analytically implemented and compared to the results using a straight expansion line.

When the problem of extracting fluid properties from Flownex is resolved the PEPSE method should also be evaluated in Flownex.

For a complete turbine train model it is recommended that:

1. The effect of gland sealing and IPT cooling steam on the accuracy of the model be investigated.
2. To enable more accurate transient analysis, the models should include rotational inertia, generator, valve curves and control loops. This will enable load rejection, islanding, run ups and run downs to be tested.

The compound component described in Chapter 6 should be incorporated into another compound component that contains the various options to define the generic turbine train configurations. The summary of section 2.7 can be used as a basis for developing such compound components.

8. List of References

[1] A. S. Leyzerovich, Steam Turbines for Modern Fossil-Fuel Power Plants, Lilburn: The Fairmont Press, Inc, 2008.

[2] A. H. Zerban and E. P. Nye, Steam Power Plants, Scranton: International Textbook Company, 1952.

[3] E. F. Church, Steam Turbines, New York: McGraw-Hill Book Company, Inc, 1928.

[4] T. D. Eastop and A. McConkey, Applied Thermodynamics for Engineering Technologists: S.I. Units, London: Longman, 1993.

[5] P. K. Nag, Power Plant Engineering, New Delhi: Tata McGraw Hill Publishing Company Limited, 2008.

[6] D. H. Cooke, "On Prediction of Off Design Multistage Turbine Pressure by Stodola's Ellipse," *Journal of Engineering for Gas Turbines and Power,* vol. 107, no. 3, pp. 596-606, 1985.

[7] A. Stodola, Steam and Gas Turbines Volume 1, New York: Peter Smith, 1945.

[8] Minner, G. L. et al, "Turbine Calculations," in *PEPSE Volume 2 Manual: Engineering Input Description*, Idaho Falls, Scientech, Inc., 2004, pp. 8-1 to 8-34.

[9] Bresolin, C. S. et al, "Application of Steam Turbines Simulation Models in Power Generation Systems," *Engenharia Termica (Thermal Engineering),* vol. 5, no. 01, pp. 73-77, 2006.

[10] J. K. Salisbury, Steam Turbines and Their Cycles, New York: John Wiley & Sons, Inc., 1950.

[11] M-Tech Industrial, *Flownex Library Manual,* Potchefstroom: M-Tech Industrial, 2013.

[12] W. P. Sanders, Turbine Steam Path Engineering for Operations and Maintenance Staff, Ballston Spa: TPL Turbo Parts, LLC, 2008.

[13] R. C. Spencer, K. C. Cotton and C. N. Cannon, "A Method for Predicting the Performance of Steam Turbine-Generators.... 16,500kW and Larger," *Journal of Engineering for Gas Turbines and Power,* vol. 85, no. 4, pp. 249-298, 1963.

[14] S. Hesler, *EPRI Web Cast: Steam Turbine Thoery and Design Tutorial,* Charlotte: EPRI, 2009.

[15] R. L. Bartlett, Steam Turbine Performance and Economics, New York: McGraw Hill Book Company, Inc., 1958.

[16] STEAG Energy Services, *Ebsilon Professional Documentation,* Zwingenberg: STEAG, 2011.

[17] A. Ray, "Dynamic modelling of power plant turbines for controller design," *Applied Mathematical Modelling,* vol. 4, no. April, pp. 109-112, 1980.

[18] G. Darie and H. I. Petcu, "Methodology and software for prediction of cogeneration steam turbines performances," in *17th European Symposium on Computer Aided Process Engineering*, 2007.

[19] M-Tech Industrial, *Flownex Library Theory Manual,* Potchefstroom: M-Tech Industrial, 2013.

[20] P. G. Rousseau and B. du Toit, Practical Thermal-Fluid System Simulation Short Course, M-Tech Industrial, 2013.

[21] M-Tech Industrial, *Flownex General User Manual,* Potchefstroom: M-Tech Industrial, 2013.

[22] ASME, ASME PTC 6: Steam Turbine Performance Codes, New York: ASME, 2004.

Appendix A. Turbine Architecture

Group	Description	Drawing	Diagram
1	• All reheat power plant HPT. • Single flow. • No extractions. • No governing stage.	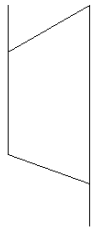	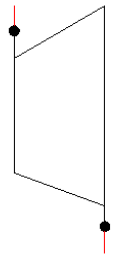
2	• All (except PP-D and PP-B) Non-reheat power plant HPT. • Single flow. • 4 extractions. • No governing stage or redirection chamber.	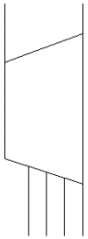	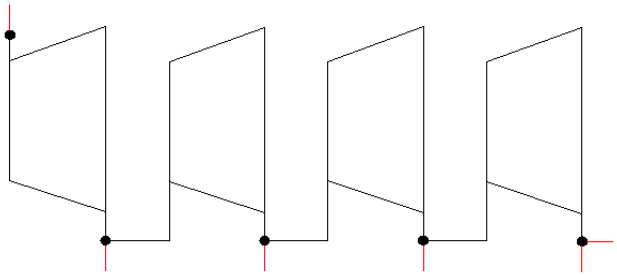
3	• Non-symmetrical extraction IPT (PP-E, PP-G and PP-F). • Double flow. • 2 extractions per flow. • No cooling steam.	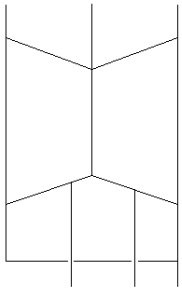	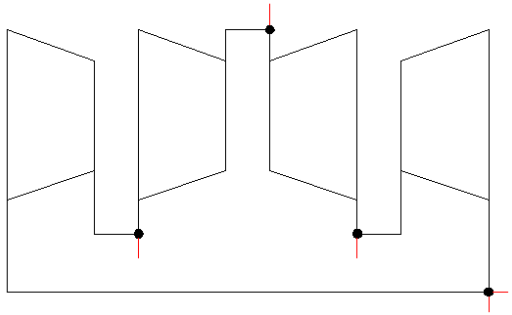

Group	Description	Drawing	Diagram
4	• Symmetrical extraction IPT (PP-H, PP-I and PP-P) • Double flow. • 2 extractions per flow. • Cooling steam.	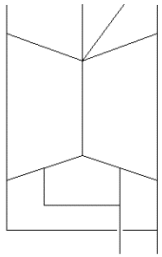	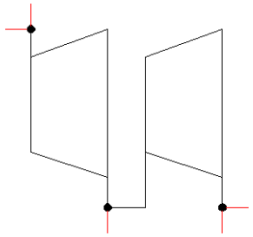
5	• IPT (PP-L, PP-A, PP-M and PP-C) • Single or double flow. • 3 extractions per flow. • Cooling steam.	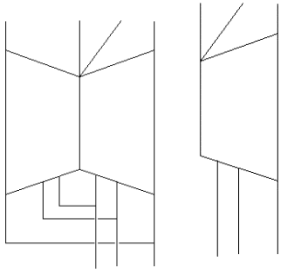	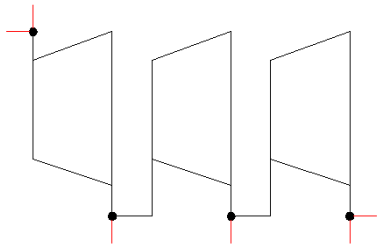
6	• LPT (PP-E, PP-G, PP-H units 1-3, PP-F, PP-L, PP-A, PP-M, PP-C, PP-B, PP-N and PP-O units 1-7) • Double flow. • 2 extractions per flow.	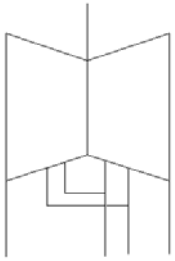	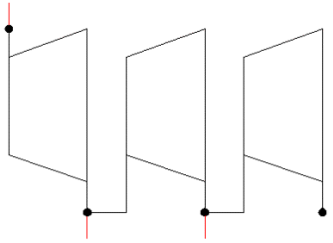

Group	Description	Drawing	Diagram
7	• LPT (PP-H 4-6, PP-I, PP-P, PP-D, PP-O 8-9 and PP-K) • Double flow. • 3 extractions per flow.	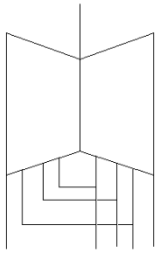	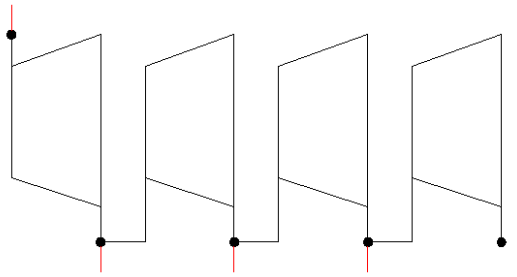
8	• PP-J IPT and LPT • Double flow. • 1 extraction per flow.	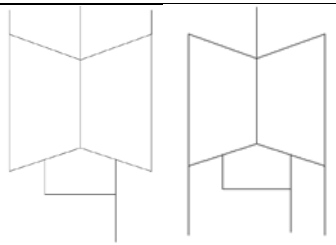	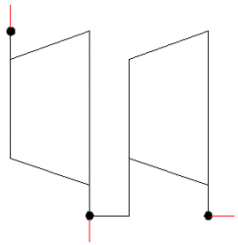
9	• PP-D and PP-B HPT. • Single flow. • 4 extractions. • One governing stage or redirection chamber.	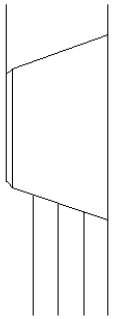	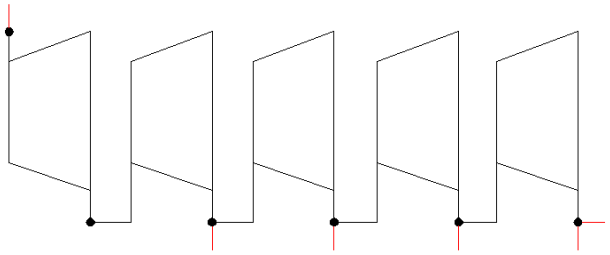

Group	Description	Drawing	Diagram
10	• PP-K HPT. • Double flow. • 3 extractions per flow. • One governing stage per flow.	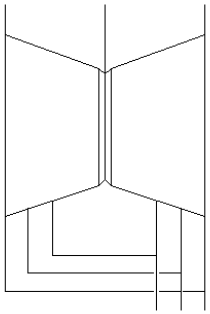	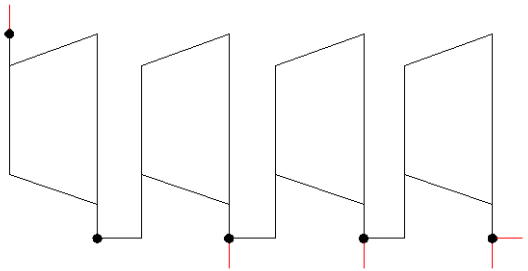
Generic 1	• Symmetrical extraction turbine. • Single or double flow. • 4 extractions per flow. • One or no governing stage or redirection chamber. • With or without cooling steam.		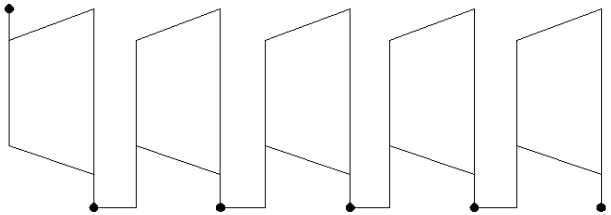
Generic 2	• Unsymmetrical extraction turbine. • Double flow. • 2 extractions per flow. • No governing stage. • With or without cooling steam.		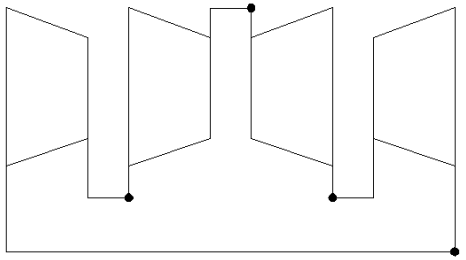

Appendix B. Pressure Drop Correlations

B.1: Remaining acceptance test/ heat balance data

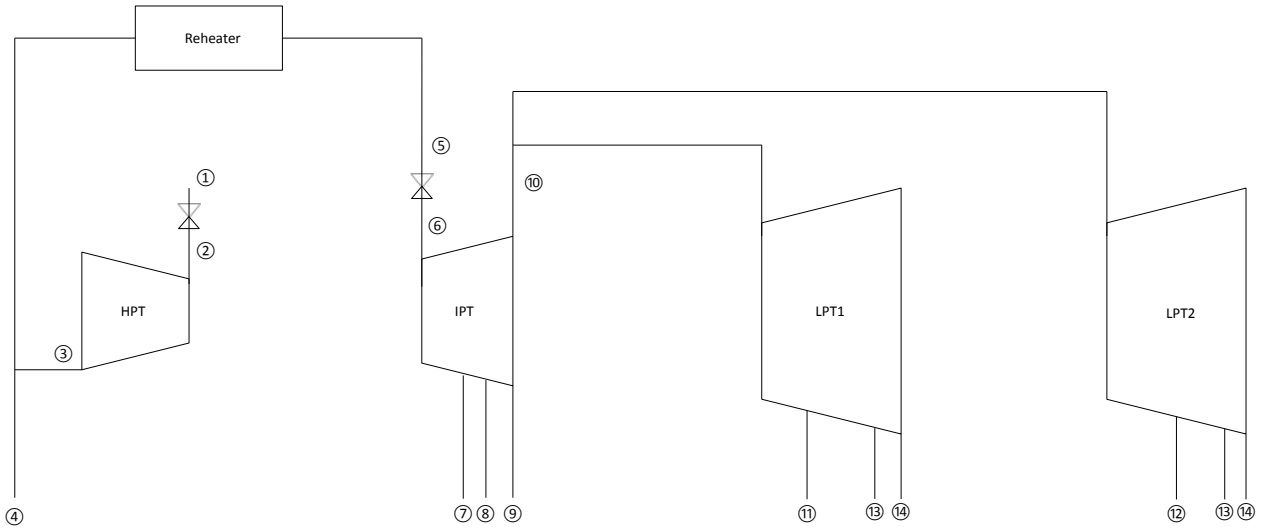

Figure B. 1: Schematic of PP-C

Table B. 1: Remaining acceptance test data for PP-C

Position	Property	100 % load	80 % load	60 % load	46 % load
5	Pressure (kPa)	3125	2465.5	1853.1	1470.3
	Temperature (°C)	515	509.6	516.8	513.2
	Mass flow (kg/s)	393.79	310.85	232.26	184.83
6	Pressure (kPa)	Not mentioned.			
7	Pressure (kPa)	1760.4	1400.2	1054.9	839.4
	Temperature (°C)	431.8	427.1	432.05	427.6
	Mass flow to next section (kg/s)	376.24	295.48	220.63	174.93
8	Pressure (kPa)	920.5	736.3	551.7	436.6
	Temperature (°C)	342.5	340.3	345.5	341.6
	Mass flow to next section (kg/s)	340.77	268.86	200.78	158.53
9	Pressure (kPa)	418.6	333	251.2	199.8
	Temperature (°C)	246.6	246.3	252.4	249.6
10	Pressure (kPa)	418.6	333	251.2	199.8
	Temperature (°C)	246.6	246.3	252.4	249.6
	Mass flow to LPT1 (kg/s)	162.79	128.8	96.553	76.42
	Mass flow to LPT2 (kg/s)	160.2	126.76	95.021	75.207
11	Pressure (kPa)	170.9	137.9	105.1	84.4
	Temperature (°C)	157.6	157.5	164.6	166.1
	Mass flow to next section (kg/s)	143.68	114.33	86.334	68.691

12	Pressure (kPa)	58.5	46.5	35.4	28.3
	Temperature (°C)/ Quality	0.9841	0.9886	0.9949	79.6
	Mass flow to next section (kg/s)	148.47	117.96	88.998	70.766
13	Pressure (kPa)	22.8	18.4	14.5	11.9
	Quality	0.9502	0.9559	0.9625	0.971
	Total mass flow to next section (kg/s)	280.56	223.2	169.38	135.95
14	Pressure (kPa)	7.9	6.2	5.6	5.9
	Quality	0.9202	0.9227	0.9392	0.9618

Refer to Figure 43.

Table B. 2: Remaining acceptance test data for PP-A

Position	Property	100 % load	80 % load	60 % load
5	Pressure (kPa)	3588.6	2933.2	2267.5
	Temperature (°C)	536.38	534.72	533.85
	Mass flow (kg/s)	456.73	372.1	287.25
6	Pressure (kPa)	3505.7	2862	2211.6
7	Pressure (kPa)	1935.3	1586.9	1231.9
	Temperature (°C)	447.44	446.57	446.57
	Mass flow to next section (kg/s)	424.97	347.15	269.15
8	Pressure (kPa)	674.1	554.7	428.3
	Temperature (°C)	303.81	303.68	303.23
	Mass flow to next section (kg/s)	386.08	317.04	245.15
9	Pressure (kPa)	290.78	239.92	185.79
	Temperature (°C)	202.53	202.85	203.29
10	Pressure (kPa)	289.32	238.56	184.73
	Temperature (°C)	203.17	203.42	203.99
	Mass flow to LPT (kg/s)	368.68	303.49	235.29
11	Pressure (kPa)	131.08	109.91	85.75
	Temperature (°C)	129.18	130.79	131.77
	Mass flow to next section (kg/s)	347.88	287.12	223.35
12	Pressure (kPa)	43.84	36.7	28.5
	Quality	0.97	0.98	0.98
	Total mass flow to next section (kg/s)	327.4	270.66	211.84
13 (LPT1/ LPT2)	Pressure (kPa)	8.683/ 5.964	7.288/ 5.249	6.18/4.718
	Quality	0.9286/ 0.8964	0.9331/ 0.9034	0.9434/ 0.9128

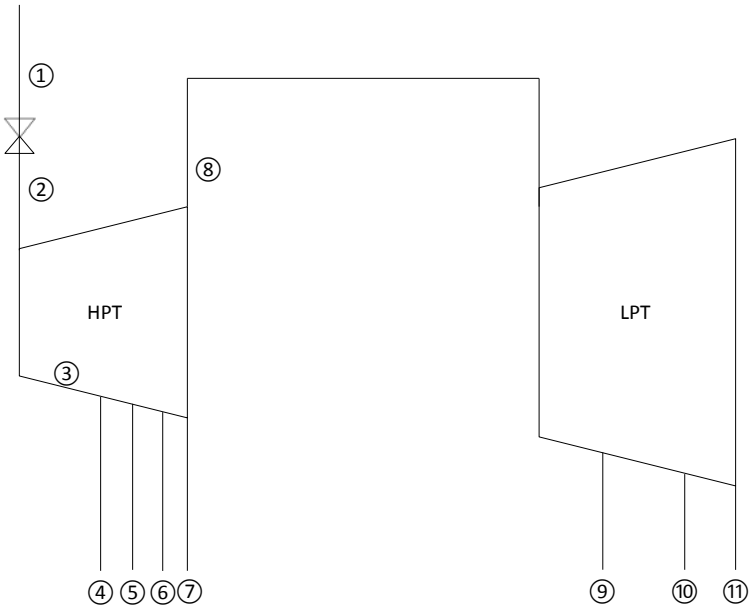

Figure B. 2: Schematic of PP-B

TEST NO.		1	2	3	4
NOMINAL LOAD	MW	190	160	200	125
GOVERNOR VALVES					
Position of governor valve 1		60mm OPEN	25mm OPEN	FULL OPEN	16mm OPEN
Position of governor valve 2		59mm OPEN	23mm OPEN	FULL OPEN	10mm OPEN
Position of governor valve 3		58mm OPEN	22mm OPEN	FULL OPEN	13mm OPEN
Position of governor valve 4		2mm OPEN	SHUT	FULL OPEN	SHUT
Steam pressure after governor valve 1	kPa	9 449	8 064	9 657	6 361
Steam pressure after governor valve 2	kPa	9 521	8 095	9 687	6 398
Steam pressure after governor valve 3	kPa	9 405	8 015	9 609	6 330
H.P. CYLINDER					
First stage pressure (governor valve 4) ...	kPa	8 232	7 031	9 257	5 537
Redirection chamber	kPa	3 636	3 111	3 970	2 400

Figure B. 3: Extract of PP-B acceptance test results

Table B. 3: Remaining data for PP-B from acceptance test and heat balance

Position	Property	100 % load	80 % load	60 % load
3	Pressure (kPa)	3970	3111	2400
	Temperature (°C) from PEPSE curves	421.7	405.66	394.99
	Mass flow to next section (kg/s)	202	158.89	125.11
4	Pressure (kPa)	2513	1966	1549
	Temperature (°C)	358.9	345.2	338.7
	Mass flow to next section (kg/s)	180.11	141.46	111.03
5	Pressure (kPa)	1492	1176	934
	Temperature (°C)	292.4	281	276.2

	Mass flow to next section (kg/s)	169.56	133.8	105.38
6	Pressure (kPa)	832	660	529
	Temperature (°C)	223.5	212.5	210.7
	Mass flow to next section (kg/s)	155.35	123.52	98.575
7	Pressure (kPa)	294	233.5	184.5
	Quality	0.9855	0.985	0.9875
8	Pressure (kPa)	294	233.5	184.5
	Quality	0.9855	0.985	0.9875
	Mass flow to LPT (kg/s)	154.42	123.52	98.575
9	Pressure (kPa)	60.1	47.8	38.3
	Quality	0.9138	0.9167	0.9205
	Mass flow to next section (kg/s)	147.06	117.59	94.237
10	Pressure (kPa)	22.1	17.2	14.1
	Quality	0.8819	0.8831	0.8867
	Mass flow to next section (kg/s)	143.56	114.24	92.376
11	Pressure (kPa)	9.78	6.21	6.09
	Quality	0.8774	0.8723	0.8848

B.2: Results

Table B. 4: Analytical solution results for HPT for PP-C

Correlations\ Load	**80 %**		**60 %**		**46 %**	
	Mass flow (1) kg/s	**Pressure (3) kPa**	**Mass flow (1) kg/s**	**Pressure (3) kPa**	**Mass flow (1) kg/s**	**Pressure (3) kPa**
GE law ave	324.37	2783.7	248.46	2065.9	197.22	1576.7
GE law inlet	324.8	2735.7	249.09	2066.7	197.57	1615.8
Stodola T	327.31	3149	253.24	2635.2	202.46	2196.1
Stodola T ave	338.79	3061	259.05	2297.4	205.24	1810.1
Stodola v	324.35	2778.8	248.39	2054	197.1	1561.4
Stodola v ave	332.69	2908.4	249.23	2044.2	194.51	1527.6
Schegliaiev	328.69	2790.1	255.39	2184.3	203.94	1758.7

Table B. 5: Flownex solution results for PP-C

Correlations\ Load	**80 %**		**60 %**		**46 %**	
	Mass flow (1) kg/s	**Pressure (3) kPa**	**Mass flow (1) kg/s**	**Pressure (3) kPa**	**Mass flow (1) kg/s**	**Pressure (3) kPa**
GE law ave	400.34	5693.3	307.02	4342.3	243.52	3432.5
GE law inlet	324.81	2736.2	249.1	2067.3	197.58	1616
Stodola T	327.31	3149	253.24	2635.2	202.46	2196
Stodola T ave	406.68	6335.8	311.68	4835.7	247.27	3825.6
Stodola v	324.36	2780.4	248.4	2055.8	197.1	1562.3

Stodola v ave	403.02	6234.7	305.73	4667.6	240.73	3636.7
Schegliaiev	328.69	2790.1	255.39	2184.3	203.94	1758.6

Table B. 6: Analytical solution results for IPT section 6-7 for PP-C

Correlations	**GE law ave**		**GE law inlet**		**Stodola v**	
	Mass flow (6) kg/s	**Pressure (7) kPa**	**Mass flow (6) kg/s**	**Pressure (7) kPa**	**Mass flow (6) kg/s**	**Pressure (7) kPa**
80 % load	309.95	1391	309.44	1390.5	309.891	1391.1
60 % load	231.19	1042.9	230.57	1043.1	231.004	1042.8
46 % load	183.44	824.18	182.77	825.1	183.216	823.9

Table B. 7: Analytical solution results for IPT section 7-8 for PP-C

Correlations	**GE law ave**		**GE law inlet**		**Stodola v**	
	Mass flow (7) kg/s	**Pressure (8) kPa**	**Mass flow (7) kg/s**	**Pressure (8) kPa**	**Mass flow (7) kg/s**	**Pressure (8) kPa**
80 % load	298.937	757.34	298.775	750.86	299.066	762.26
60 % load	224.347	574.74	224.495	568.88	224.502	581.59
46 % load	179.247	463.06	179.54	457.02	179.378	469.83

Table B. 8: Analytical solution results for IPT section 8-10 for PP-C

Correlations	**GE law ave**		**GE law inlet**		**Stodola v**	
	Mass flow (8) kg/s	**Pressure (10) kPa**	**Mass flow (8) kg/s**	**Pressure (10) kPa**	**Mass flow (8) kg/s**	**Pressure (10) kPa**
80 % load	272.84	350.79	273.23	345.81	273	351.95
60 % load	202.75	260.48	202.9	257.46	202.94	261.19
46 % load	160.59	209.12	160.59	205.82	160.74	209.86

Table B. 9: Analytical solution results for LPT section 10-11 for PP-C

Correlations	**GE law ave**		**GE law inlet**		**Stodola v**	
	Mass flow (10) kg/s	**Pressure (11) kPa**	**Mass flow (10) kg/s**	**Pressure (11) kPa**	**Mass flow (10) kg/s**	**Pressure (11) kPa**
80 % load	129.001	138.55	128.694	137.58	128.961	139.76
60 % load	96.321	103.94	95.999	103.41	96.344	105.65
46 % load	76.499	85.133	76.232	83.83	76.615	86.92

Table B. 10: Analytical solution results for LPT section 10-12 for PP-C

Correlations	GE law ave		GE law inlet		Stodola v	
	Mass flow (10) kg/s	Pressure (12) kPa	Mass flow (10) kg/s	Pressure (12) kPa	Mass flow (10) kg/s	Pressure (12) kPa
80 % load	127.41	44.25	127.29	48.861	127.28	55.205
60 % load	95.62	34.025	95.23	36.328	95.275	39.778
46 % load	75.99	27.6	75.85	31.195	75.913	39.05

Table B. 11: Analytical solution results for LPT section 11-13 for PP-C

Correlations	GE law ave		GE law inlet		Stodola v	
	Mass flow (11) kg/s	Pressure (13) kPa	Mass flow (11) kg/s	Pressure (13) kPa	Mass flow (11) kg/s	Pressure (13) kPa
80 % load	115.88	18.635	115.794	21.403	115.8	28.429
60 % load	87.645	15.167	87.165	16.22	87.34	21.413
46 % load	70.253	11.922	69.699	13.982	69.932	19.678

Table B. 12: Analytical solution results for LPT section 13-14 for PP-C

Correlations	GE law ave		GE law inlet		Stodola v	
	Mass flow (13) kg/s	Pressure (14) kPa	Mass flow (13) kg/s	Pressure (14) kPa	Mass flow (13) kg/s	Pressure (14) kPa
80 % load	228.14	7.047	228.88	6.798	228.07	7.15
60 % load	176.53	6.635	174.2	6.086	176.75	6.78
46 % load	136.2	5.861	129.77	5.315	136.78	6.009

Table B. 13: Analytical solution results for HPT for PP-A

Correlations\ Load	80 %		60 %	
	Mass flow (1) kg/s	Pressure (3) kPa	Mass flow (1) kg/s	Pressure (3) kPa
GE law ave	392.96	3145.5	304.22	2431.1
GE law inlet	392.7	3147.5	304.04	2435.7
Stodola T	395.96	3470.2	309.35	2951.6
Stodola T ave	407.89	3497.8	316	2712.9
Stodola v	392.91	3141.9	304.15	2423.6
Stodola v ave	401.63	3360.6	305.47	2477.4
Schegliaiev	395.31	3212.1	309	2546.1

Table B. 14: Analytical solution results for IPT section 6-7 for PP-A

Correlations	GE law ave		GE law inlet		Stodola v	
	Mass flow (6) kg/s	Pressure (7) kPa	Mass flow (6) kg/s	Pressure (7) kPa	Mass flow (6) kg/s	Pressure (7) kPa
80 % load	371.76	1583.4	371.46	1582.5	371.75	1583.5
60 % load	286.21	1221.9	285.76	1221.6	286.22	1222

Table B. 15: Analytical solution results for IPT section 7-8 for PP-A

Correlations	GE law ave		GE law inlet		Stodola v	
	Mass flow (7) kg/s	Pressure (8) kPa	Mass flow (7) kg/s	Pressure (8) kPa	Mass flow (7) kg/s	Pressure (8) kPa
80 % load	347.89	562.38	347.73	558.12	347.88	563.05
60 % load	269.8	434.98	269.83	432.33	269.76	435.31

Table B. 16: Analytical solution results for IPT section 8-9 for PP-A

Correlations	GE law ave		GE law inlet		Stodola v	
	Mass flow (8) kg/s	Pressure (9) kPa	Mass flow (8) kg/s	Pressure (9) kPa	Mass flow (8) kg/s	Pressure (9) kPa
80 % load	317.05	240	316.94	239.73	317.07	240.02
60 % load	244.31	183.42	244.17	183.84	244.38	183.23

Table B. 17: Analytical solution results for LPT section 10-11 for PP-A

Correlations	GE law ave		GE law inlet		Stodola v	
	Mass flow (10) kg/s	Pressure (11) kPa	Mass flow (10) kg/s	Pressure (11) kPa	Mass flow (10) kg/s	Pressure (11) kPa
80 % load	302.08	108.13	301.37	108.1	302.17	108.1
60 % load	232.96	82.777	232.15	83.052	233.03	82.658

Table B. 18: Analytical solution results for LPT section 11-12 for PP-A

Correlations	GE law ave		GE law inlet		Stodola v	
	Mass flow (11) kg/s	Pressure (12) kPa	Mass flow (11) kg/s	Pressure (12) kPa	Mass flow (11) kg/s	Pressure (12) kPa
80 % load	291.1	40.675	290.86	38.57	290.8	40.21
60 % load	227.33	32.245	226.61	30.134	226.43	31.448

Table B. 19: Analytical solution results for LPT1 section 12-13 for PP-A

Correlations	GE law ave		GE law inlet		Stodola v	
	Mass flow (12) kg/s	Pressure (13) kPa	Mass flow (12) kg/s	Pressure (13) kPa	Mass flow (12) kg/s	Pressure (13) kPa
80 % load	137.15	9.337	137.06	8.027	137.09	9.283
60 % load	106.85	7.24	106.06	6.238	106.89	7.22

Table B. 20: Analytical solution results for LPT2 section 12-13 for PP-A

Correlations	GE law ave		GE law inlet		Stodola v	
	Mass flow (12) kg/s	Pressure (13) kPa	Mass flow (12) kg/s	Pressure (13) kPa	Mass flow (12) kg/s	Pressure (13) kPa
80 % load	137.04	7.961	136.55	5.81	136.97	7.681
60 % load	106.9	6.165	105.47	4.516	106.83	5.977

Table B. 21: Analytical solution results for HPT section 2-3 of PP-B

Correlations\ Load	80 %		60 %	
	Mass flow (1) kg/s	Pressure (3) kPa	Mass flow (1) kg/s	Pressure (3) kPa
GE law ave	152.65	2573.2	120.96	2035.1
GE law inlet	151.37	2712	120.23	2140.1
Stodola T	153.15	2576.9	121.82	2097.2
Stodola T ave	150.8	2900.7	119.96	2265.3
Stodola v	152.09	2458.7	120.42	1945.2
Stodola v ave	148.73	2843.2	117.22	2188.7
Schegliaiev	151.95	2913.5	120.38	2309

Table B. 22: Analytical solution results for IPT section 3-4 for PP-B

Correlations	GE law ave		GE law inlet		Stodola v	
	Mass flow (3) kg/s	Pressure (4) kPa	Mass flow (3) kg/s	Pressure (4) kPa	Mass flow (3) kg/s	Pressure (4) kPa
80 % load	159.71	1981.4	159.79	1978.9	159.74	1981.7
60 % load	121.83	1492.8	121.49	1497.5	121.95	1490.9

Table B. 23: Analytical solution results for IPT section 4-5 for PP-B

Correlations	GE law ave		GE law inlet		Stodola v	
	Mass flow (4) kg/s	Pressure (5) kPa	Mass flow (4) kg/s	Pressure (5) kPa	Mass flow (4) kg/s	Pressure (5) kPa
80 % load	141.37	1174.6	141.18	1172.9	141.38	1174.8
60 % load	111.06	934.35	110.77	931.08	111.09	934.86

Table B. 24: Analytical solution results for IPT section 5-6 for PP-B

Correlations	GE law ave		GE law inlet		Stodola v	
	Mass flow (5) kg/s	Pressure (6) kPa	Mass flow (5) kg/s	Pressure (6) kPa	Mass flow (5) kg/s	Pressure (6) kPa
80 % load	134.29	663.92	134.05	661.9	134.2	664.27
60 % load	106.24	537.3	105.96	533.39	106.25	538.09

Table B. 25: Analytical solution results for IPT section 6-8 for PP-B

Correlations	GE law ave		GE law inlet		Stodola v	
	Mass flow (6) kg/s	Pressure (8) kPa	Mass flow (6) kg/s	Pressure (8) kPa	Mass flow (6) kg/s	Pressure (8) kPa
80 % load	124.23	242.89	124.25	238.51	124.27	243.15
60 % load	99.84	200.48	99.84	193.17	99.67	198.52

Table B. 26: Analytical solution results for LPT section 8-9 for PP-B

Correlations	GE law ave		GE law inlet		Stodola v	
	Mass flow (8) kg/s	Pressure (9) kPa	Mass flow (8) kg/s	Pressure (9) kPa	Mass flow (8) kg/s	Pressure (9) kPa
80 % load	123.52	47.983	123.54	47.868	123.56	48.13
60 % load	98.14	34.089	98.05	36.732	98.18	34.697

Table B. 27: Analytical solution results for LPT section 9-10 for PP-B

Correlations	GE law ave		GE law inlet		Stodola v	
	Mass flow (9) kg/s	Pressure (10) kPa	Mass flow (9) kg/s	Pressure (10) kPa	Mass flow (9) kg/s	Pressure (10) kPa
80 % load	118.04	17.603	118.37	17.601	118.03	17.622
60 % load	94.72	14.502	94.69	14.333	94.71	14.541

Table B. 28: Analytical solution results for LPT section 10-11 for PP-B

Correlations	GE law ave		GE law inlet		Stodola v	
	Mass flow (10) kg/s	Pressure (11) kPa	Mass flow (10) kg/s	Pressure (11) kPa	Mass flow (10) kg/s	Pressure (11) kPa
80 % load	117.17	7.121	120.46	7.315	117.01	7.112
60 % load	93.084	6.294	93.483	6.279	93.14	6.303

B.3: Error analysis

- PP-C

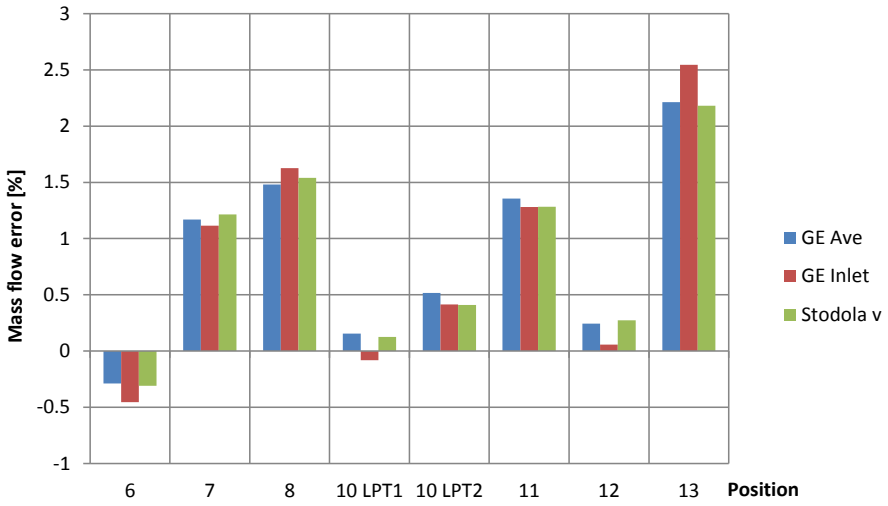

Figure B. 4: Mass flow error for 80 % load for PP-C

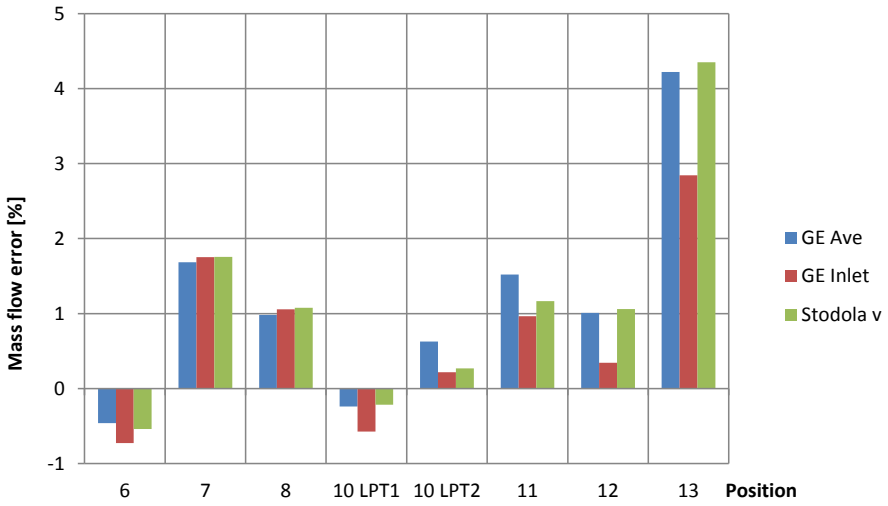

Figure B. 5: Mass flow error for 60 % load for PP-C

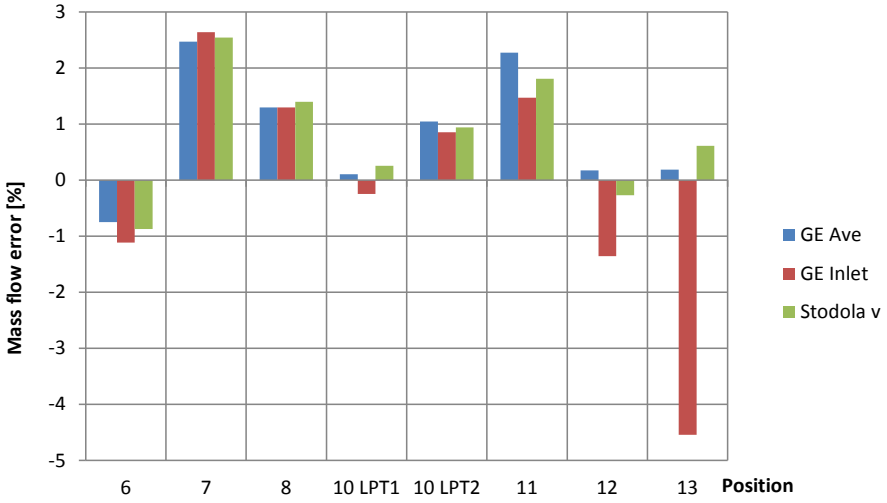

Figure B. 6: Mass flow error for 46 % load for PP-C

From Figure B. 4, Figure B. 5 and Figure B. 6, reflecting the mass flow error at various loads for PP-C, there is not much of a difference in the errors for the various correlations except for Figure B. 9 where "GE Ave" and "Stodola v" errors at position 13 (and position 12 to lesser degree) are much lower than for "GE Inlet".

This might be as a result of low load and the positions, being the last few stages of the LPT, having a greater effect on "GE Inlet".

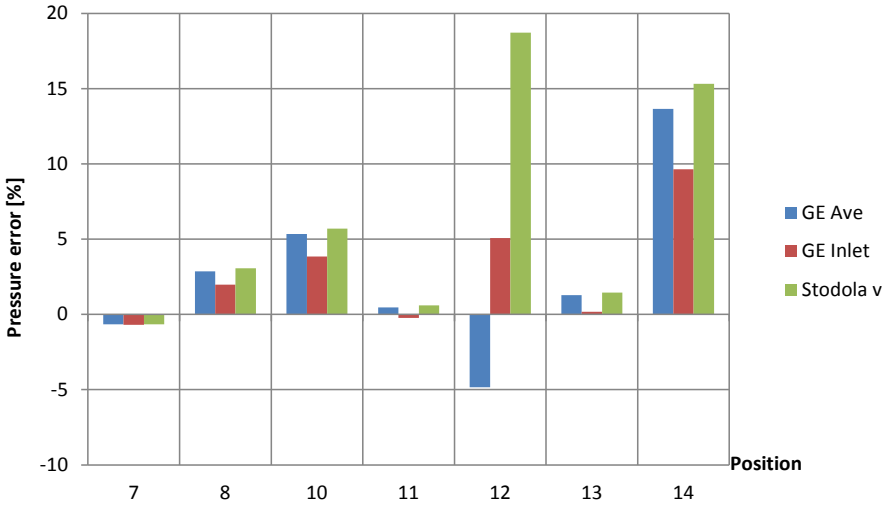

Figure B. 7: Pressure error for 80 % load for PP-C

Figure B. 8: Pressure error for 60 % load for PP-C

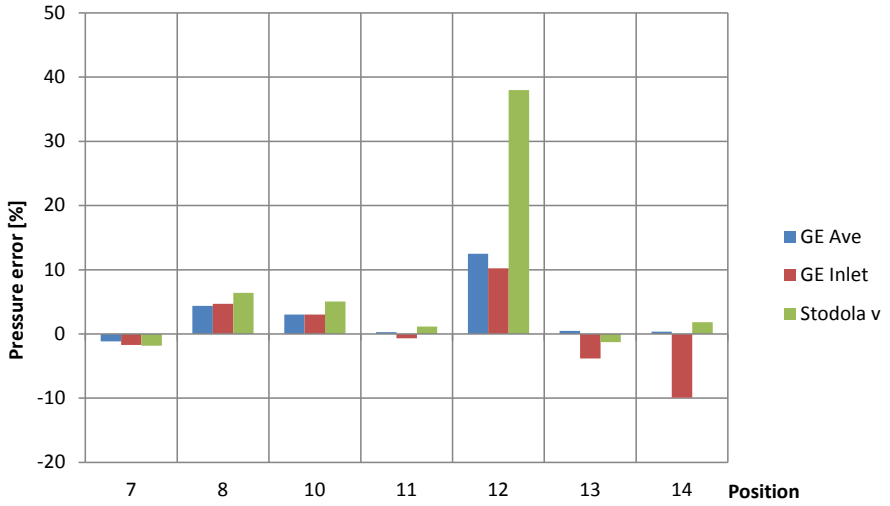

Figure B. 9: Pressure error for 46 % load for PP-C

From Figure B. 7, Figure B. 8 and Figure B. 9, reflecting the pressure error at various loads for PP-C, one notes that a small difference in pressure results can cause a large percentage error towards the LPT sections.

- PP-A

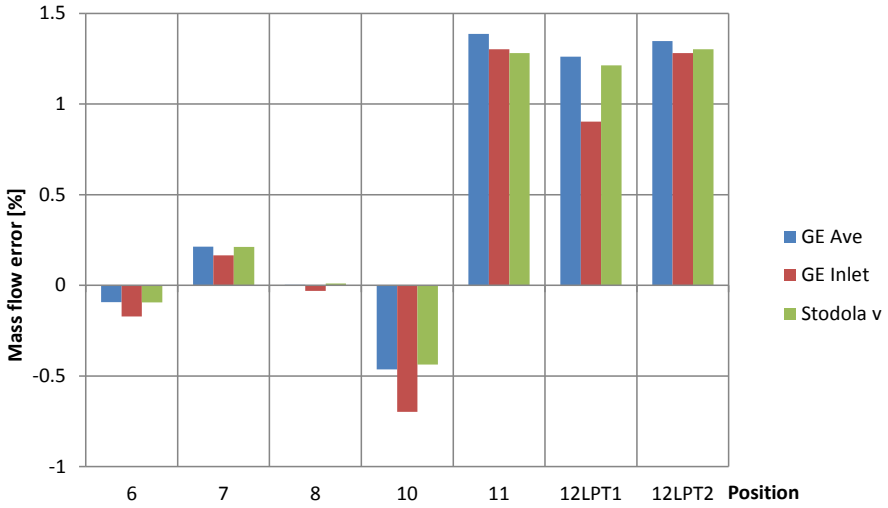

Figure B. 10: Mass flow error for 80 % load for PP-A

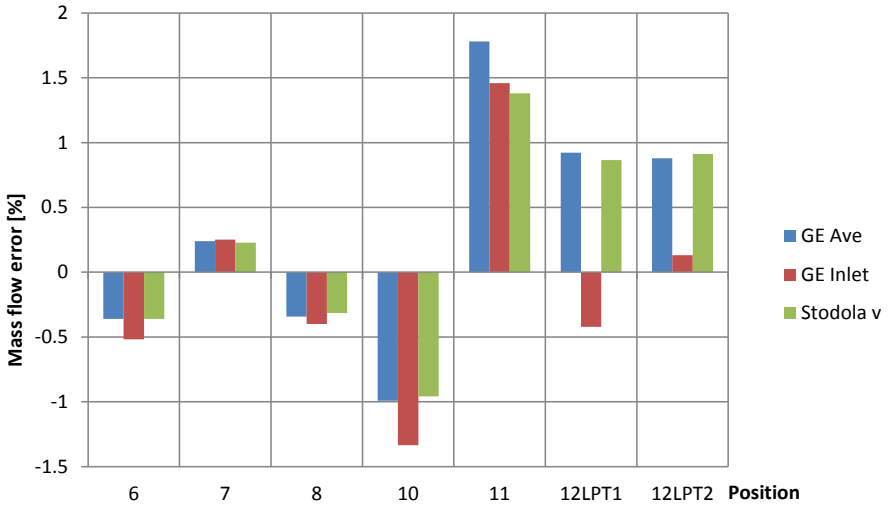

Figure B. 11: Mass flow error for 60 % load for PP-A

From Figure B. 10 and Figure B. 11, showing the mass flow error at various loads for PP-A, one notes that the difference in error for the various correlations relative to each other is small.

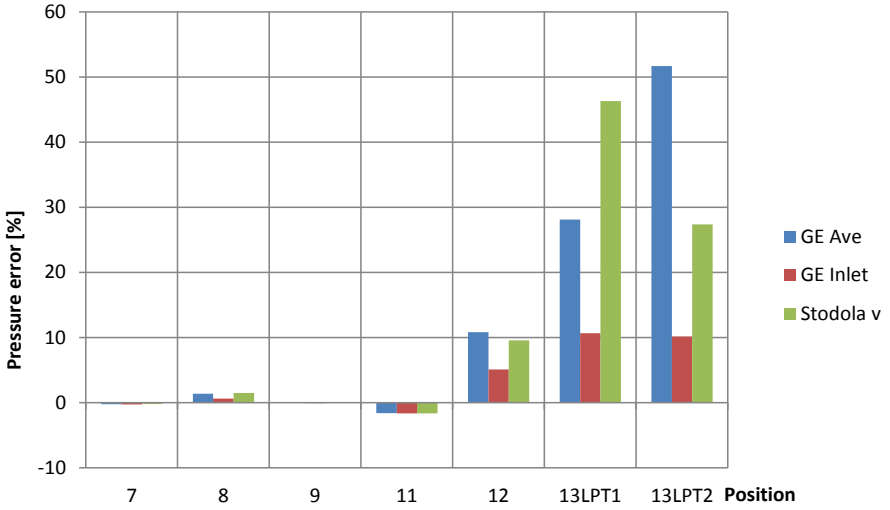

Figure B. 12: Pressure error for 80 % load for PP-A

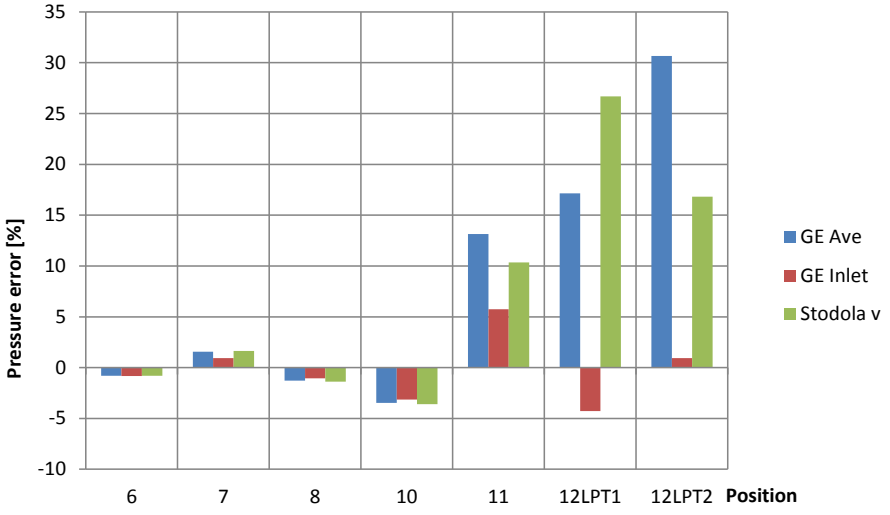

Figure B. 13: Pressure error for 60 % load for PP-A

From Figure B. 12 and Figure B. 13, reflecting the pressure error at various loads for PP-A, one notes the same trend of larger errors towards the LPT for the same reason i.e. a small difference in pressure results can cause a large percentage error towards the LPT sections.

- PP-B

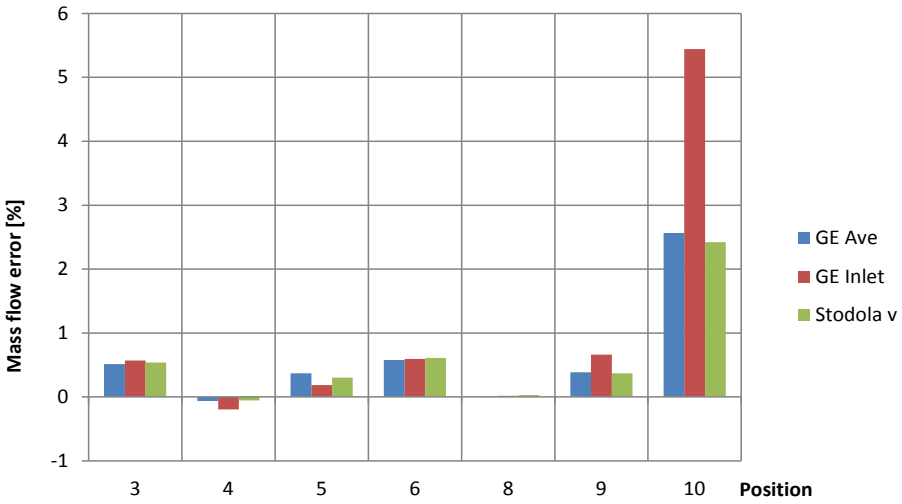

Figure B. 14: Mass flow error for 80 % load for PP-B

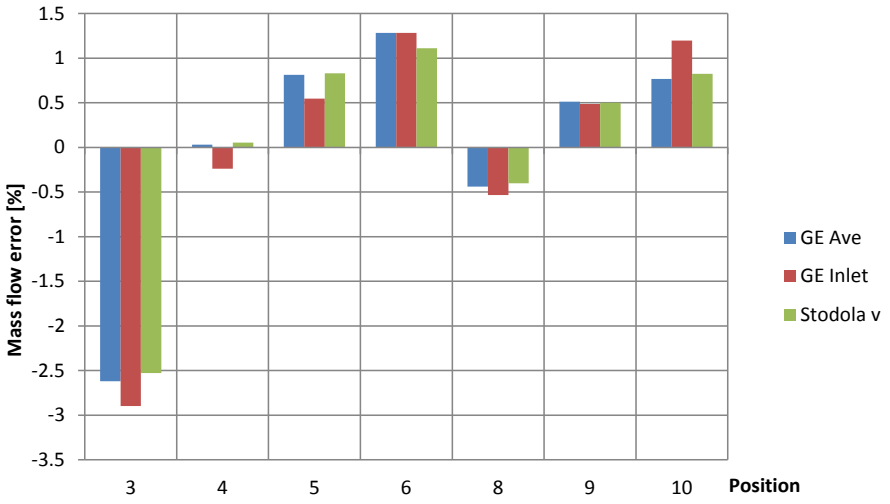

Figure B. 15: Mass flow error for 60 % load for PP-B

From Figure B. 14 and Figure B. 15, showing the mass flow error at various loads for PP-B, one notes the errors for the various correlations are similar except for Figure B. 14 where “GE Inlet” at position 10 is significantly larger than the other two correlations.

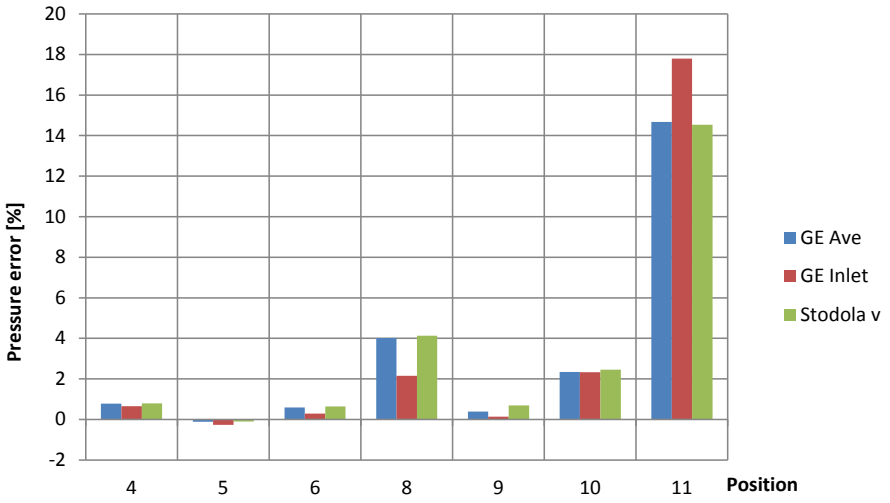

Figure B. 16: Pressure error for 80 % load for PP-B

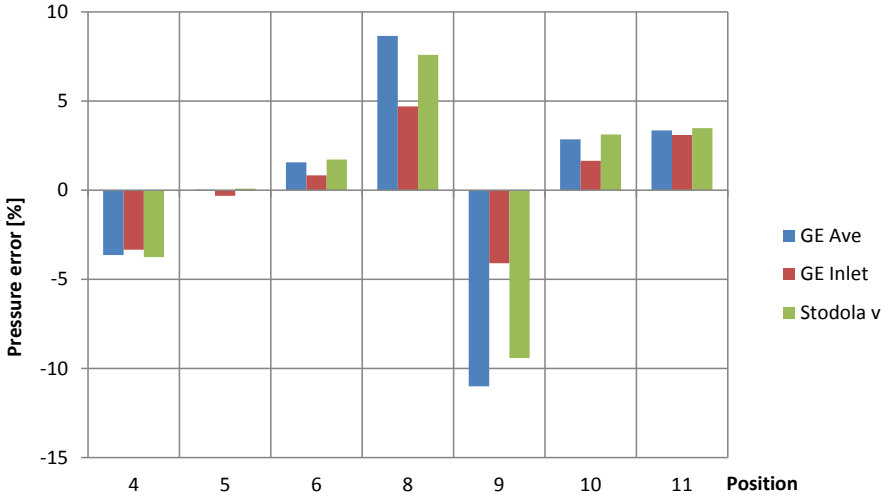

Figure B. 17: Pressure error for 60 % load for PP-B

From Figure B. 16 and Figure B. 17, showing the pressure error at various loads for PP-B, one notices that there is significant change at positions 9 and 11 of the two figures.

B.4. Mean and standard deviations of errors

Table B. 29: Mean error and standard deviation for HPT of various reference plants

Correlations	Mean	Standard Deviation
GE Ave	6.2461	6.694
GE Inlet	5.3251	4.8333
Stodola T	22.177	11.313
Stodola Tave	8.7801	1.5296
Stodola v	8.4390	7.8751
Stodola vave	7.4230	3.1396
Schegliaiev	6.4573	3.3375

Table B. 30: Mean error and standard deviation for selected methods for all turbine sections

Correlations	Mean	Standard Deviation
GE Ave – Mass error	0.86817	0.83455
GE Ave – Pressure error	6.0992	9.4563
GE Inlet – Mass error	1.0157	1.0982
GE Inlet – Pressure error	3.3346	3.6396
Stodola v – Mass error	0.86422	0.82728
Stodola v – Pressure error	7.1558	9.9329

Table B. 31: Overall mean error and standard deviation for selected methods

Correlations	Mean	Standard Deviation
GE Ave	6.2136	9.45857
GE Inlet	3.531	3.7598
Stodola v	7.2629	9.9272

Appendix C. Efficiency Correlations

C.1: Efficiency from acceptance test

Table C. 1: Actual efficiencies for PP-C

Load\ Turbine	HPT	IPT	LPT
100 %	91.72 %	92.23 %	89.91 %
80 %	91.6 %	91.58 %	90.84 %
60 %	91.7 %	91.6 %	90.03 %
46 %	92.15 %	91.9 %	86.8 %

Table C. 2: Actual efficiencies for PP-A

Load\ Turbine	HPT	IPT	LPT
100 %	89.47 %	94.8 %	91.03 %
80 %	89.66 %	94.81 %	91.01 %
60 %	89.69 %	94.74 %	91.68 %

NB: For PP-A, the efficiency of the LPT was not reported in the acceptance test. The efficiencies of the LPT were calculated with data from acceptance test and heat balance diagrams.

The acceptance test for PP-B does not contain efficiencies at various load and turbines. Expansion line diagrams were available, Figure C. 1. These expansion lines were digitised, data was extracted and the efficiencies were calculated from the data.

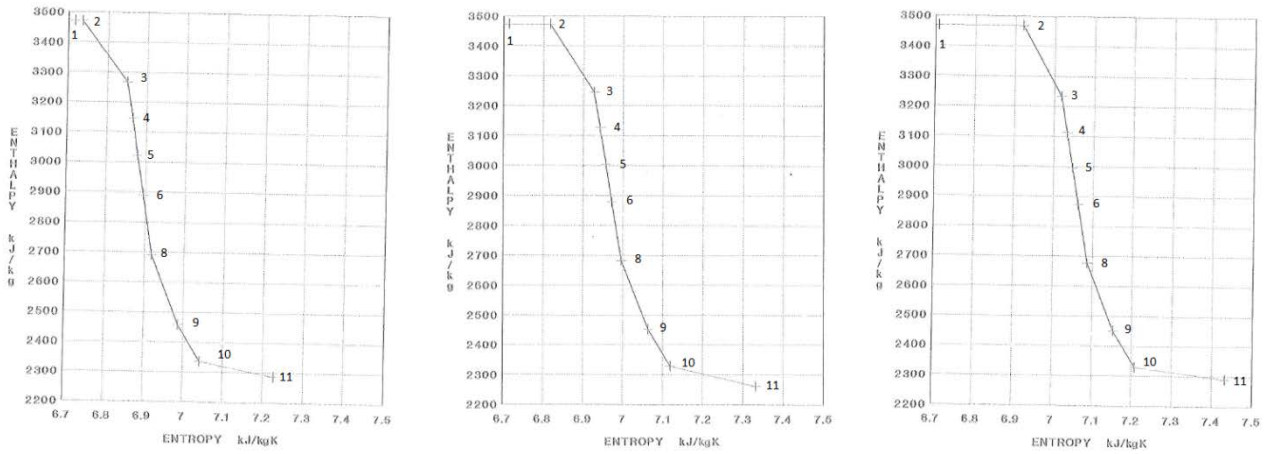

Figure C. 1: PP-B acceptance test expansion lines at 100 %, 80 % and 60 % load

Table C. 3: Actual efficiencies for PP-B

Load\ Turbine	HPT		LPT
	HPT (2-3)	IPT (3-8)	
100 %	76.26 %	95.19 %	80.08 %
80 %	88.28 %	95.32 %	80.47 %
60 %	89.62 %	95.8 %	78.46 %

C.2: Results

Table C. 4: Analytical results for efficiency methods for PP-C

Methods\ Turbine	HPT			IPT			LPT		
	80 % load	60 % load	46 % load	80 % load	60 % load	46 % load	80 % load	60 % load	46 % load
Ray	91.711	91.661	91.668	92.222	92.22	92.227	89.91	89.687	87.755
Darie	91.720	91.720	91.720	92.230	92.230	92.230	89.910	89.904	89.887
PEPSE	91.882	92.029	92.141	92.273	92.188	92.218	90.046	90.093	90.068
SCC	91.652	91.708	91.802	92.279	92.524	92.597	90.168	90.651	90.849

Table C. 5: Flownex results for efficiency methods

Methods\ Load	80 %	60 %	46 %
Ray	91.711	91.662	91.668
Darie	91.72	91.72	91.72
SCC	91.652	91.709	91.803

Table C. 6: Analytical results for efficiency for PP-A

Methods\ Turbine	HPT		IPT		LPT	
	80 % load	60 % load	80 % load	60 % load	80 % load	60 % load
Ray	89.465	89.470	94.800	94.800	90.968	90.446
Darie	89.470	89.470	94.800	94.800	91.024	91.019
PEPSE	89.616	89.731	94.797	94.801	91.086	91.130
SCC	89.386	89.436	94.878	94.989	91.283	91.627

Table C. 7: Analytical results for efficiency for PP-B

Methods\ Turbine	HPT				LPT	
	HPT (2-3)		IPT (3-8)			
	80 % load	60 % load	80 % load	60 % load	80 % load	60 % load
Ray	76.051	76.235	95.104	94.898	79.784	79.976
Darie	76.255	76.255	95.194	95.193	80.075	80.079
PEPSE	76.347	76.573	95.276	95.356	80.501	80.514
SCC	76.327	76.368	95.120	95.170	80.150	80.337

C.3: Error analysis

Table C. 8: Mean error and standard deviation for various efficiency methods

Methods\ Turbine	Mean	Standard Deviation
Ray	0.50126	0.42957
Darie	0.53795	0.71532
PEPSE	0.51051	0.80162
SCC	0.64547	0.90642

- PP-B's HPT (2-3)

In Table C. 3 one notes that there is a large difference between the nominal efficiency and the off-design efficiency. Comparing the "actual" HPT efficiency, Table C. 3, to the efficiencies calculated by the correlations, Table C. 7, one notices that there is huge discrepancy. The efficiency methods are based on a nominal efficiency, therefore if there is large difference between the nominal efficiency and the off-design efficiency the effect will be that the correlations will also produce a large difference.

As mentioned previously, efficiencies were determined from expansion diagrams. The enthalpy before as well as after the governor valves, $h_{2,}$ is the same and not dependent on the first stage pressure. The entropy at point 2 is dependent on the overall first stage pressure. The isentropic exhaust enthalpy, $h_{3s,}$ is a function of the entropy at point 2, hence the pressure at point 2.

$$\text{Efficiency, } \eta = \frac{h_2 - h_3}{h_2 - h_{3s}}$$

From the above equation, efficiency is a function of h_{3s}, hence the pressure at point 2. The pressure at point 2 in Figure C. 1 is less representative of the overall first stage pressure during off-nominal load conditions therefore off-design efficiency various by such a large margin from the nominal efficiency. It is unusual for off-design efficiency to be so much better than the nominal

efficiency. This puts the accuracy of the efficiency for PP-B's HPT (2-3) in doubt. Including the results of the PP-B's HPT (2-3) in the error analysis would have skewed the analysis. Therefore these results were excluded.

C.4: Algorithm to calculate outlet enthalpy for PEPSE method

expansion line eq.: $h(s) := M \cdot s + C_{int_3}$

1st stage inlet pressure: $p := p_{2_3}$

lower limit entropy guess: $sc_1 := 6.4 \frac{kJ}{kg \cdot K}$

upper limit entropy guess: $sc_2 := 6.8 \frac{kJ}{kg \cdot K}$

calculating outlet enthalpy:

$h_c :=$ err ← 2
while $|err| > 0.1$
$s \leftarrow \frac{sc_1 + sc_2}{2}$
$h_{sc} \leftarrow h(s)$
$h_p \leftarrow h_{steam}(p, "", "", "", s)$
$err \leftarrow (h_p - h_{sc}) \cdot \frac{kg}{kJ}$
$sc_2 \leftarrow s$ if $h_{sc} < h_p$
$sc_1 \leftarrow s$ otherwise
h_{sc}

outlet enthalpy: $h_c = 2958.2 \cdot \frac{kJ}{kg}$

Appendix D. Case Study Implementation of Models

D.1: Acceptance test data for PP-F

PP-F is a 686 MW reheat reaction machine. The turbine train consists of four cylinders (1 x HPT, 1 x double flow IPT and 2 x double flow LPT). The extractions on the IPTs are asymmetrical. The LPTs exhaust into an indirectly dry-cooled condenser.

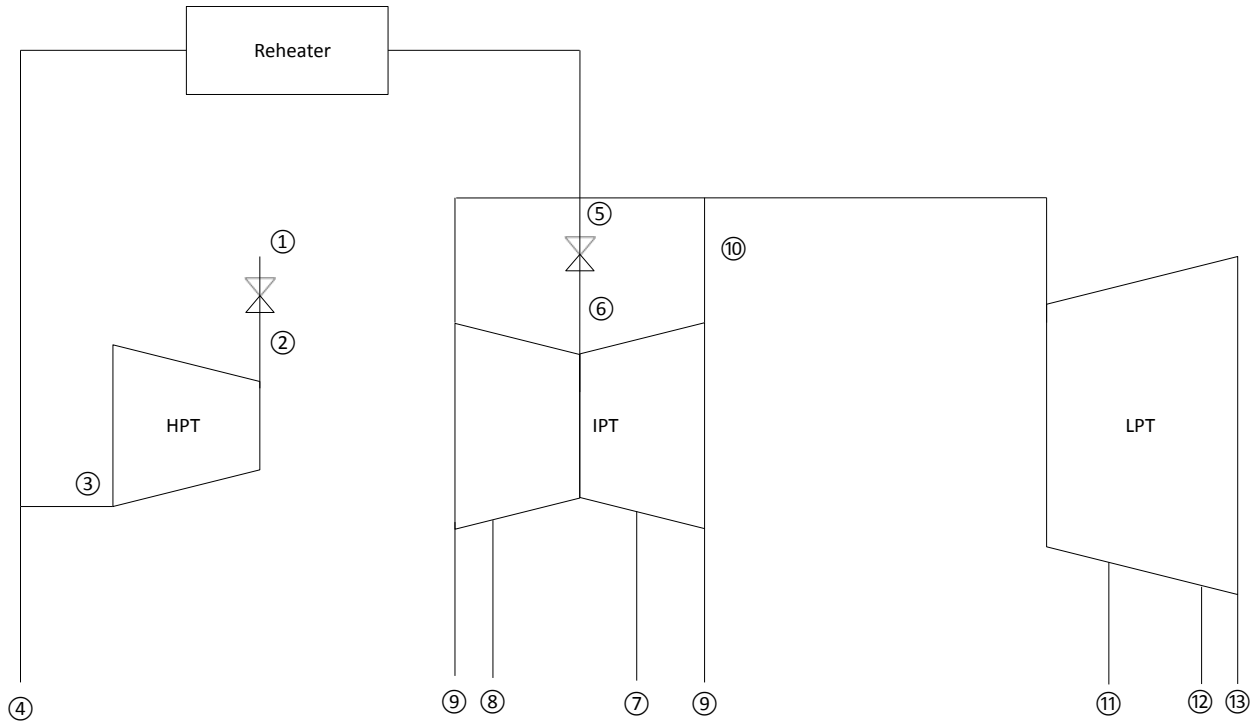

Figure D. 1: Schematic of PP-F

Table D. 1: Acceptance test data for PP-F at various condenser pressures

		8kPa	**15kPa**	**25kPa**
1	Pressure (kPa)	15940	15970	15960
	Temperature (°C)	529.1	532.1	532.3
	Mass flow (kg/s)	568.67	569.31	567.05
2	Pressure (kPa)	15790	15810	15820
3	Pressure (kPa)	4042	4048	4046
	Temperature (°C)	324.9	327.9	327.7
4	Pressure (kPa)	3941	3949.5	3943.5
	Temperature (°C)	324.6	327.5	327.3
	Mass flow to next section (kg/s)	514.26	515.54	512.68
5	Pressure (kPa)	3677	3688	3682
	Temperature (°C)	530.9	534.5	533.85

6	Pressure (kPa)	3595	3599	3591
	Mass flow (kg/s)	516.18	517.88	515.15
	Mass flow per flow (kg/s)	258.09	258.94	257.575
7	Pressure (kPa)	1610	1615	1614
	Temperature (°C)	408.8	412	412.3
	Mass flow to next section (kg/s)	234.12	234.46	233.675
8	Pressure (kPa)	962.5	968.2	968.3
	Temperature (°C)	341.9	345.1	345.4
	Mass flow to next section (kg/s)	235.73	236.87	235.595
9	Pressure (kPa)	476	478.6	478.9
	Temperature (°C)	254.6	257.1	257.5
10	Pressure (kPa)	466.1	469	469.4
	Temperature (°C)	257.7	256.2	256.55
	Mass flow to next section (kg/s)	447.469	449.068	447.578
11	Pressure (kPa)	221.15	224.3	226.55
	Temperature (°C)	162.5	168.7	174
	Mass flow to next section (kg/s)	421.253	424.677	424.502
12	Pressure (kPa)	63.49	69.93	75.3
	Temperature (°C)	86.2	89.095	91.42
	Mass flow to next section (kg/s)	391.392	399.569	406.263
13	Pressure (kPa)	8.23	14.75	25

D.2: Results

Table D. 2: Results for PP-C

		100% load		**80% load**		**60% load**		**46% load**	
		GE Inlet	**Stodola v**	**GE Inlet**	**Stodola v**	**GE Inlet**	**Stodola v**	**GE Inlet**	**Stodola v**
2	Pressure (kPa)	14187	14187	11354	11363	8694.7	8713.2	6925.9	6940.3
	Temperature (°C)	502.23	502.23	486.83	486.87	473.04	473.14	463.5	463.58
3	Pressure (kPa)	3373.6	3373.8	2678.5	2678.5	2019.3	2019.3	1609.7	1609.8
	Temperature (°C)	295.5	295.5	284.35	284.29	273.35	273.17	266.52	266.34
4	Temperature (°C)	294.61	294.61	283.63	283.57	272.87	272.68	266.16	265.98
	Mass flow to next section (kg/s)	374.17	374.1	301.19	301.19	233.41	233.43	186.38	186.36
5	Pressure (kPa)	3125	3125.3	2479	2479	1865.2	1865.2	1486.7	1486.8
	Mass flow to next section (kg/s)	393.79	393.73	312.48	312.49	233.41	233.43	186.38	186.36
7	Temperature (°C)	441.87	441.91	438.07	438.11	445.33	445.36	441.9	441.95
	Mass flow to next section (kg/s)	376.51	376.39	298.89	298.86	223.33	223.32	178.31	178.26
8	Temperature (°C)	352.13	352.15	349.96	350	356.65	356.92	353.33	353.11

	Mass flow to next section (kg/s)	341.05	340.86	271.4	271.32	202.57	202.56	161.48	161.41
10	Pressure (kPa)	421.64	421.67	336.54	336.59	254.03	254.04	200.86	200.78
	Temperature (°C)	245.36	245.35	244.54	244.55	250.56	250.56	246.67	246.62
	Mass flow to next section (kg/s)	323.27	323.00	257.74	257.54	192.84	192.79	152.51	152.65
11	Temperature (°C)	162.54	162.54	161.44	161.48	167.92	167.92	168.39	168.27
	Mass flow to next section (kg/s)	144.26	143.68	115.54	115.08	86.695	86.468	68.793	68.801
12	Temperature (°C)	85.278	85.278	79.52	79.52	77.715	77.452	82.501	81.847
	Quality	0.9897	0.98972	0.9929	0.99288				
	Mass flow to next section (kg/s)	148.18	148.48	118.28	118.49	88.71	89.09	69.85	70.46
13	Temperature (°C)	62.918	62.918	58.266	58.266	53.268	53.268	49.251	49.251
	Quality	0.9502	0.9502	0.953	0.953	0.9655	0.96487	0.9773	0.9759
	Total mass flow to next section (kg/s)	280.84	280.64	225.45	225.19	169.46	170.38	132.33	134.32

Table D. 3: Results for PP-A

		100% load		**80% load**		**60% load**	
		GE Inlet	**Stodola v**	**GE Inlet**	**Stodola v**	**GE Inlet**	**Stodola v**
2	Pressure (kPa)	15115	15115	12308	12302	9545.6	9542.4
	Temperature (°C)	532.54	532.54	518.59	518.56	507.11	507.1
3	Pressure (kPa)	3873.3	3873.3	3169.3	3169.2	2454.3	2454.2
	Temperature (°C)	331.92	331.92	322.83	322.86	315.38	315.41
4	Temperature (°C)	331.15	331.16	322.23	322.26	314.95	314.99
	Mass flow to next section (kg/s)	446.71	446.72	365.28	365.34	284.85	284.92
5	Pressure (kPa)	3588.6	3588.6	2937.2	2937	2273.2	2273
6	Pressure (kPa)	3505.7	3505.7	2869.4	2869.2	2220.9	2220.6
	Temperature (°C)	536.4	536.4	534.81	534.82	534.01	534.02
	Mass flow to next section (kg/s)	456.73	456.74	373.19	373.25	288.15	288.22
7	Temperature (°C)	445.81	445.77	444.83	444.79	444.71	444.69
	Mass flow to next section (kg/s)	424.21	424.38	346.93	347.16	268.48	268.64
8	Temperature (°C)	300.81	300.82	300.56	300.57	300.59	300.59
	Mass flow to next section (kg/s)	385.32	385.46	315.77	316.01	243.77	243.98
10	Pressure (kPa)	289.43	289.33	238.55	238.35	184.76	184.54
	Temperature (°C)	200.78	200.74	200.9	200.82	201.13	201.03
	Mass flow to next section (kg/s)	366.94	367.16	300.92	301.33	232.28	232.66
11	Temperature (°C)	132.07	132.05	132.73	132.74	133.28	133.28

	Mass flow to next section (kg/s)	346.15	346.47	286.78	287.2	222.4	222.84
12	Temperature (°C)	78.076	78.076	73.801	73.801	67.921	67.921
	Quality	0.97389	0.97389	0.97865	0.97861	0.98477	0.98519
	LPT1 mass flow to next section (kg/s)	162.82	163	135.76	135.91	105.06	105.52
	LPT2 mass flow to next section (kg/s)	162.85	163	135.32	135.81	104.53	105.48

Table D. 4: Results for PP-B

		100% load		**80% load**		**60% load**	
		GE Inlet	**Stodola v**	**GE Inlet**	**Stodola v**	**GE Inlet**	**Stodola v**
2	Pressure (kPa)	9257	9274	7288.1	7411.8	5735.2	5746.4
	Temperature (°C)	535.15	535.22	527.33	527.88	518.84	518.89
3	Pressure (kPa)	3970	3832.2	3122.9	3271.3	2457	2371.6
	Temperature (°C)	405.92	400.81	402.16	406.59	394.06	389.07
4	Temperature (°C)	342.81	342.96	339.16	336.93	331.89	332.04
	Mass flow to next section (kg/s)	180.11	179.75	140.58	140.58	110.62	110.52
5	Temperature (°C)	275.77	275.87	273.01	270.99	266.9	267.03
	Mass flow to next section (kg/s)	169.56	169.14	132.75	132.75	104.96	104.84
6	Temperature (°C)	209.5	209.56	207.42	205.66	202.4	202.56
	Mass flow to next section (kg/s)	155.35	154.96	122.54	122.46	97.939	97.684
8	Pressure (kPa)	287.9	287.5	226.3	226.26	179.97	179.57
	Temperature (°C)	132.12	132.08	124.16	124.15	116.91	116.84
	Mass flow to next section (kg/s)	154.42	154.05	121.89	121.81	97.378	97.139
9	Temperature (°C)	85.969	85.969	80.2	80.2	74.816	74.816
	Quality	0.92153	0.92151	0.92776	0.9266	0.93373	0.93373
	Mass flow to next section (kg/s)	147.06	146.79	117.21	116.81	93.47	93.301
10	Temperature (°C)	62.232	62.232	56.834	56.834	52.693	52.693
	Quality	0.89183	0.89023	0.89648	0.89581	0.90475	0.90477
	Mass flow to next section (kg/s)	143.56	143.38	115.95	114.74	91.641	91.488

Table D. 5: Results for PP-F at various condenser pressures

		8 kPa		**14.75 kPa**		**25 kPa**	
		GE Inlet	**Stodola v**	**GE Inlet**	**Stodola v**	**GE Inlet**	**Stodola v**
2	Pressure (kPa)	15790	15789	15848	15864	15795	15809
	Temperature (°C)	528.7	528.7	531.71	532.52	531.91	532.72

3	Pressure (kPa)	4042	4039.3	4053.5	4047.5	4044.7	4038.7
	Temperature (°C)	325.02	324.94	327.31	327.63	327.66	327.99
4	Temperature (°C)	324.05	324.00	326.33	326.71	326.71	327.11
	Mass flow to next section (kg/s)	514.26	515.99	513.31	517.16	512.69	516.63
5	Pressure (kPa)	3677	3671.9	3688.0	3694.8	3679.8	3686.6
6	Pressure (kPa)	3619.9	3614.3	3630.7	3640.5	3622.7	3632.5
	Temperature (°C)	531.02	531.01	534.62	534.80	534.93	535.09
	Mass flow to next section (kg/s)	258.92	260.03	259.03	261.21	258.30	260.52
	Mass flow to next section (kg/s)	259.19	259.82	259.25	260.92	258.54	260.26
7	Temperature (°C)	414.31	414.80	417.58	417.84	417.99	418.22
	Mass flow to next section (kg/s)	234.95	235.54	234.99	236.21	234.46	235.75
8	Temperature (°C)	345.85	346.26	349.03	349.19	349.49	349.61
	Mass flow to next section (kg/s)	236.83	237.10	237.09	238.10	236.55	237.67
10	Pressure (kPa)	468.24	468.91	471.42	477.05	472.57	477.30
	Temperature (°C)	257.24	257.58	260.24	261.62	260.94	262.13
	Mass flow to next section (kg/s)	449.40	449.95	449.47	451.84	448.15	451.02
11	Temperature (°C)	184.53	184.78	187.87	187.62	189.36	188.63
	Mass flow to next section (kg/s)	423.18	423.50	423.03	425.76	421.10	425.73
12	Temperature (°C)	87.383	87.383	89.905	89.905	92.805	91.864
	Mass flow to next section (kg/s)	393.32	393.56	397.16	404.12	393.74	409.64

D.3: Error analysis

- PP-C

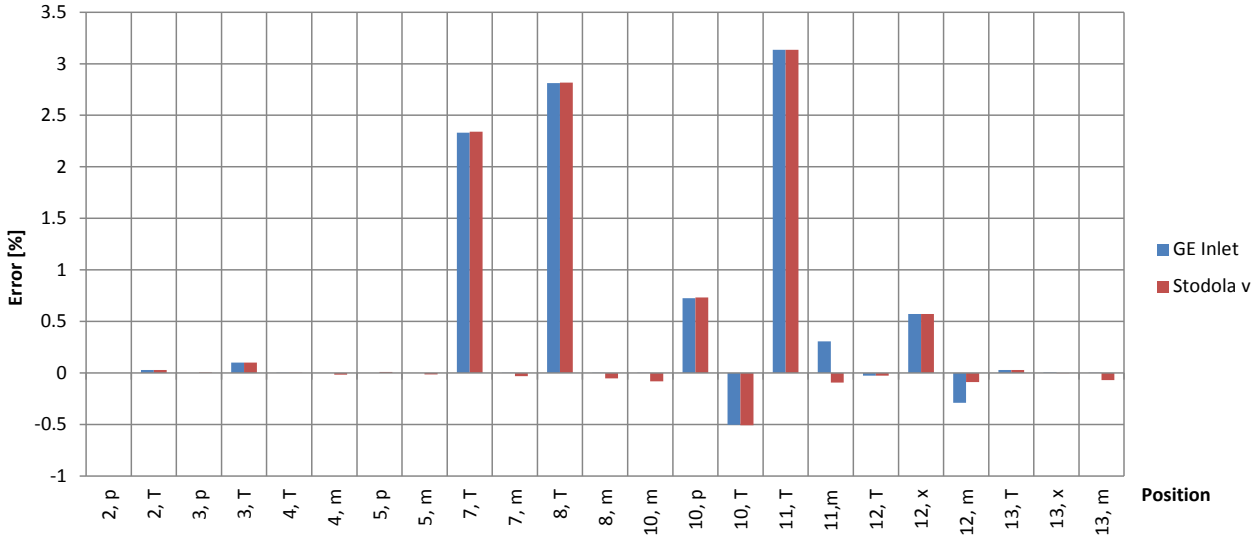

Figure D. 2: Error for PP-C at calibration

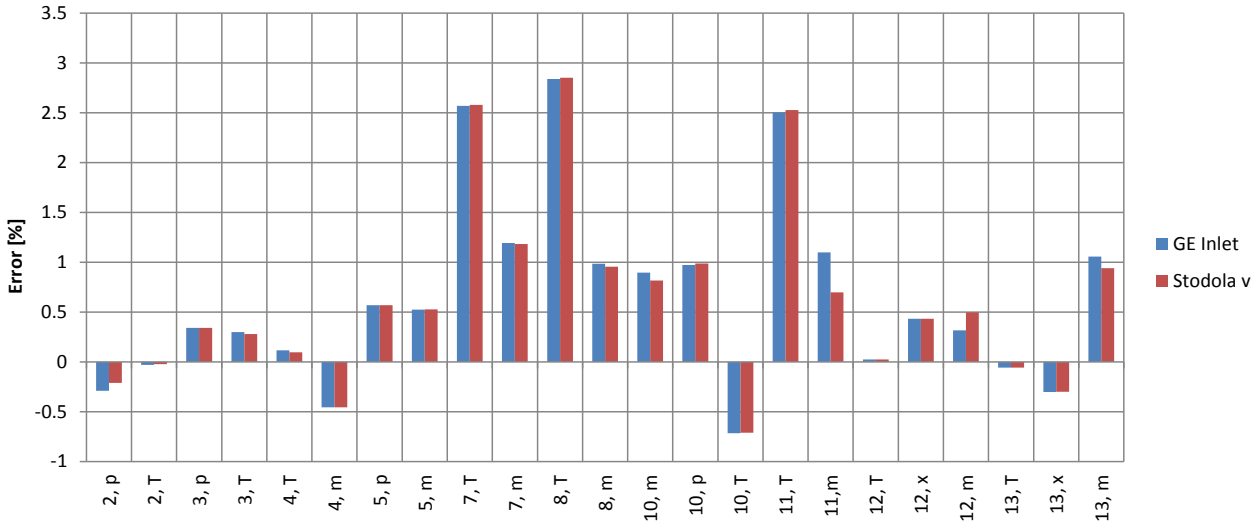

Figure D. 3: Error for PP-C at 80 % load

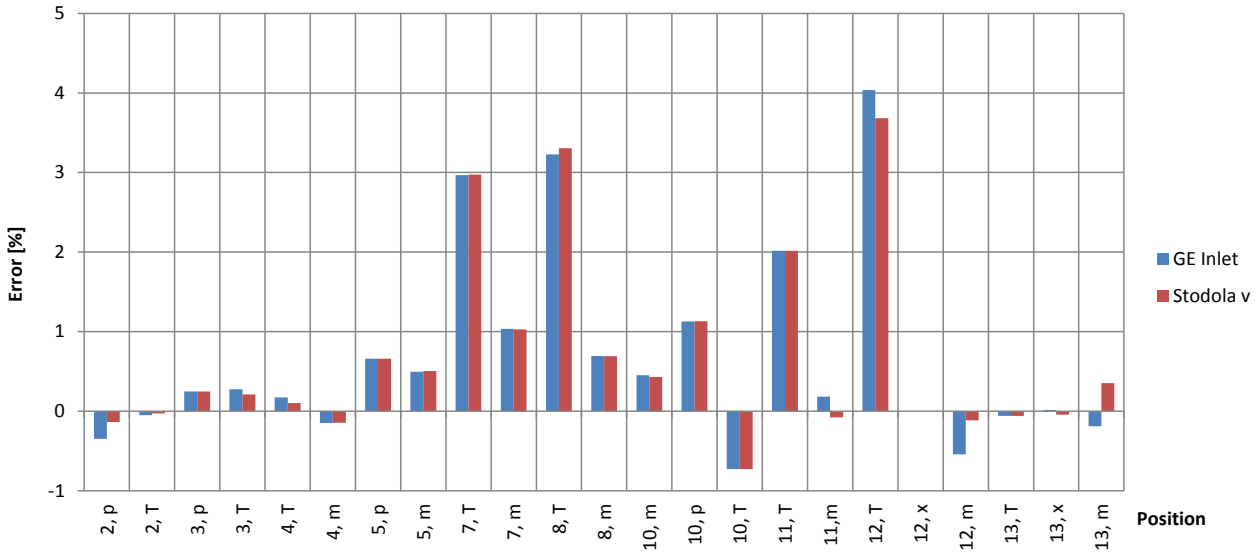

Figure D. 4: Error for PP-C at 60 % load

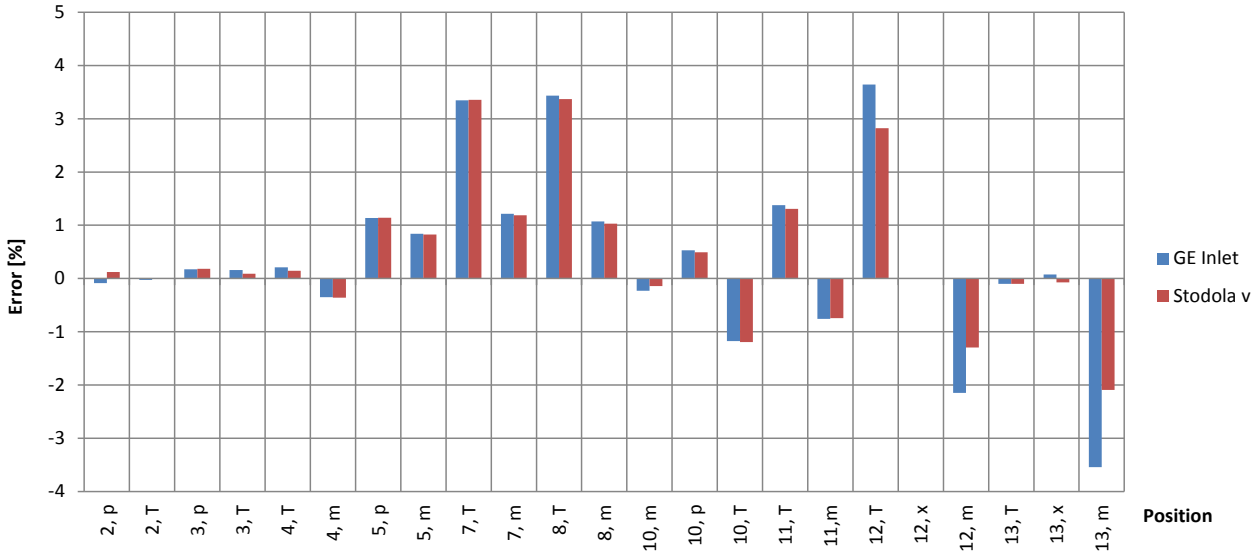

Figure D. 5: Error for PP-C at 46 % load

In Figure D. 2, Figure D. 3, Figure D. 4 and Figure D. 5, one notices a similar trend to that of PP-A i.e. the temperature errors. The errors are larger for the same reason i.e. the overall efficiency of the IPT and LPT was applied to individual turbine sections instead of applying individual efficiencies to each turbine section.

- PP-B

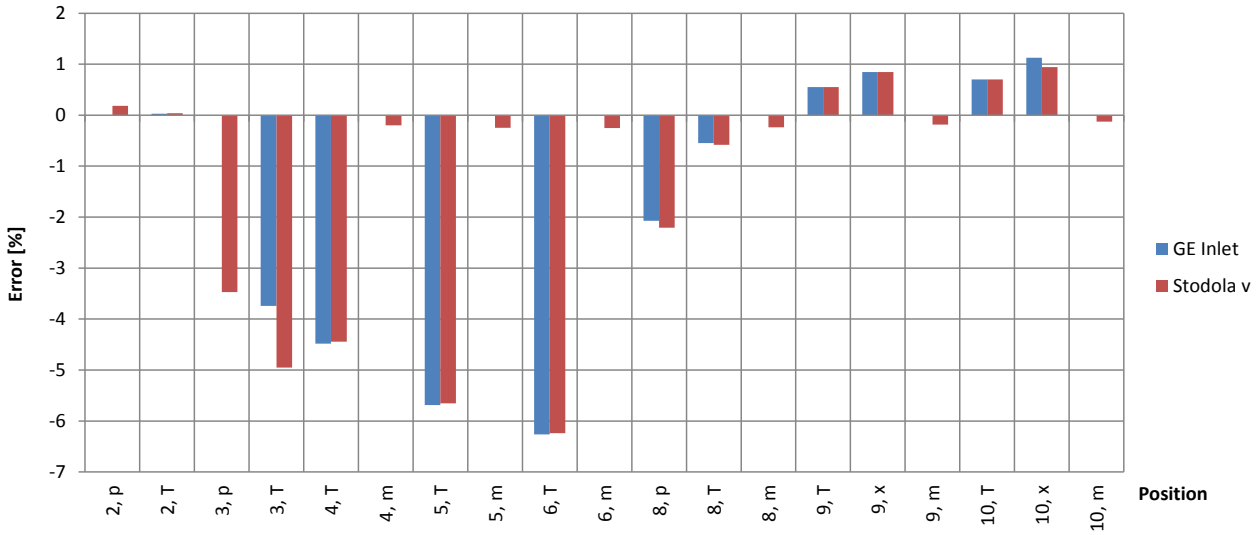

Figure D. 6: Error for PP-B at calibration

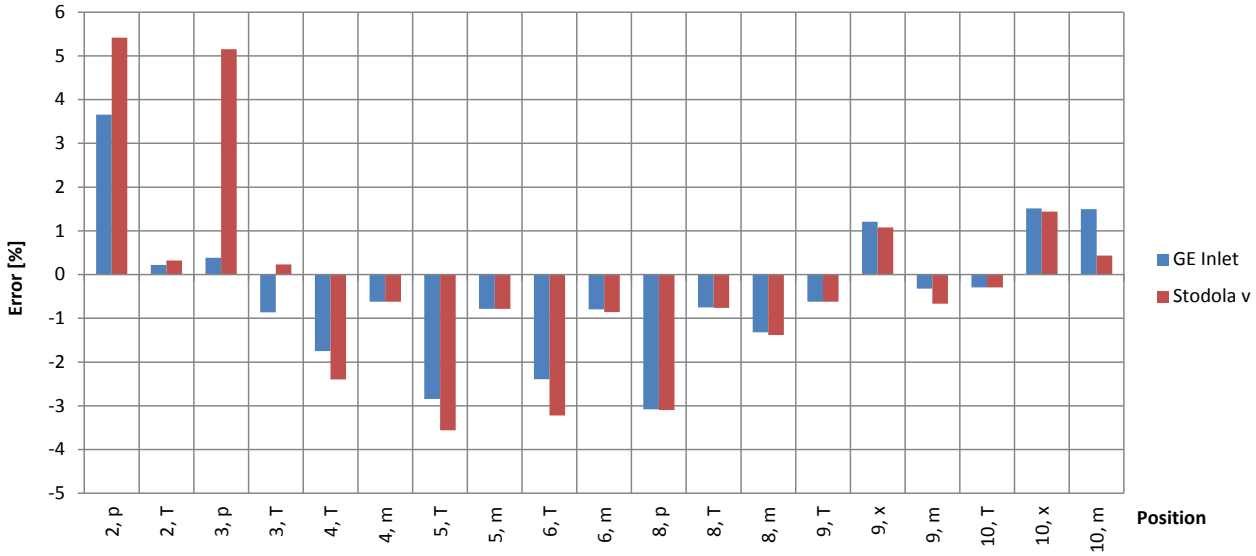

Figure D. 7: Error for PP-B at 80 % load

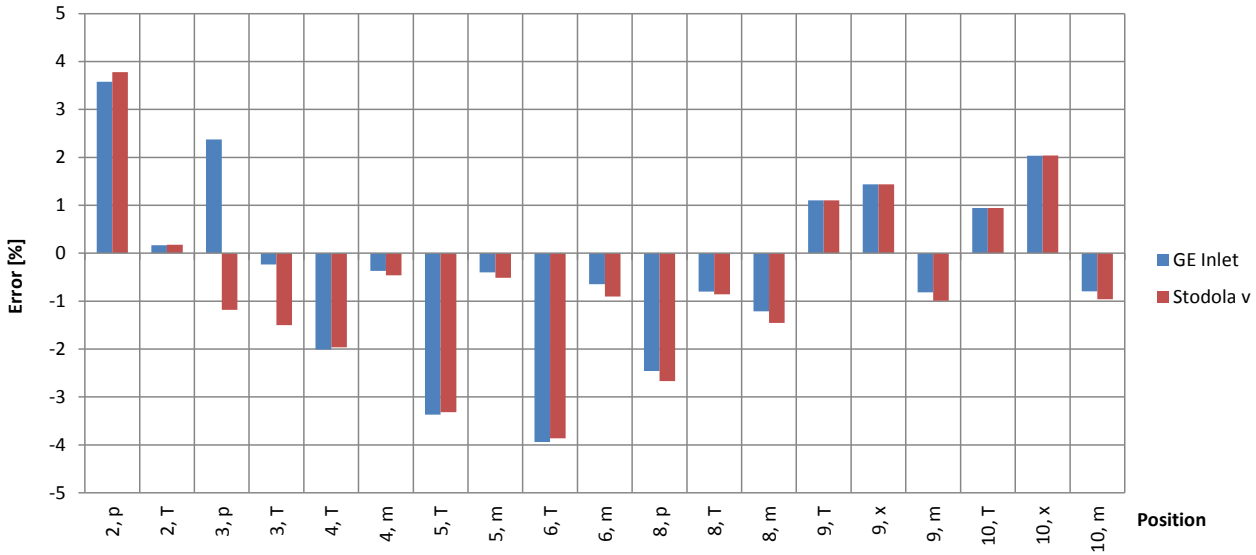

Figure D. 8: Error for PP-B at 60 % load

The temperature error trend in Figure D. 7 and Figure D. 8 is similar to that of PP-A and PP-C for the same reason i.e. the overall efficiency of the IPT and LPT was applied to individual turbine sections instead of applying individual efficiencies to each turbine section. In addition, the inlet and redirection chamber pressure error is larger. As previously mentioned, in Appendix C, there is some doubt regarding the HPT (2-3) data for PP-B.

- PP-F

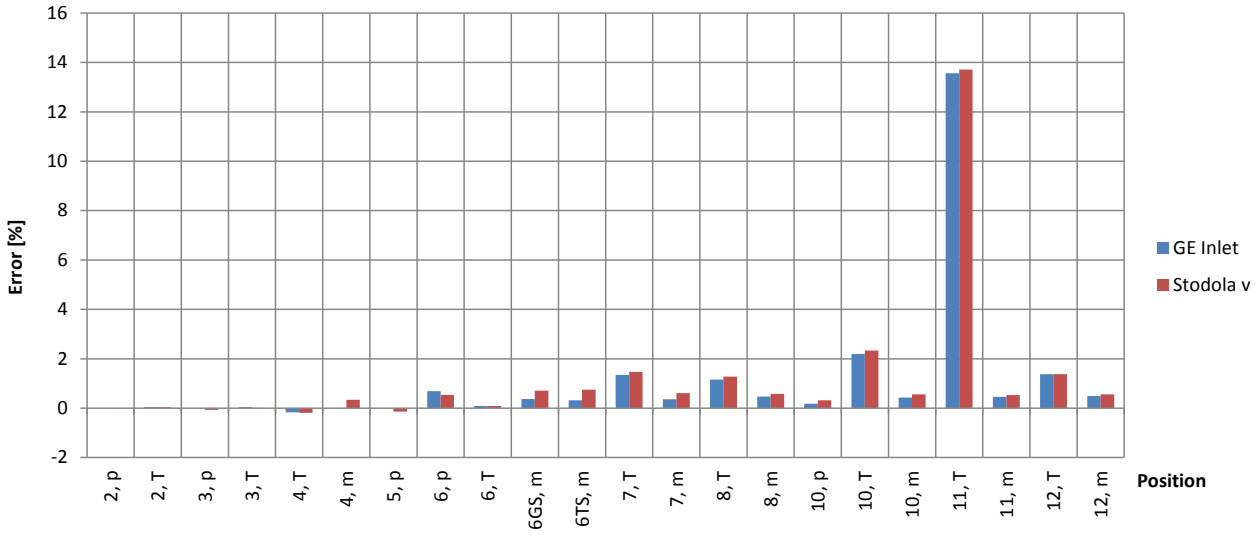

Figure D. 9: Error for PP-F at calibration

The reason for the much large error at point 11 is that the acceptance test data did not provide the efficiency for the LPT or sufficient detail to calculate the efficiency. Therefore the efficiency for the LPT was estimated. Also, as at the other plants, the overall efficiency of the IPT and LPT was applied to individual turbine sections instead of applying the individual efficiencies of each turbine section, which compounds the situation.

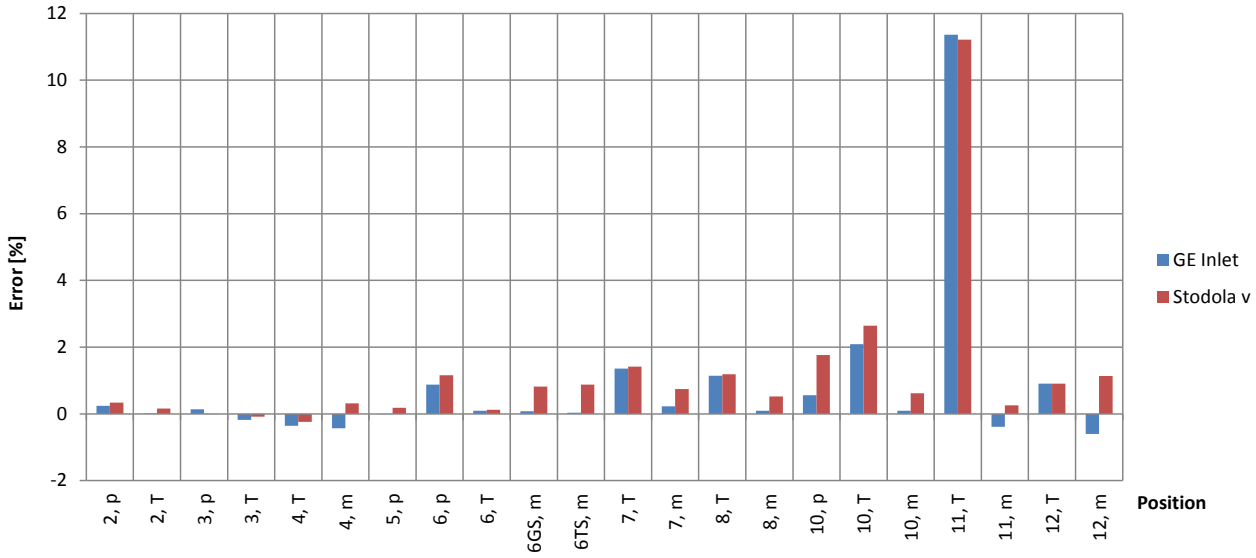

Figure D. 10: Error for PP-F at 14.75 kPa back pressure

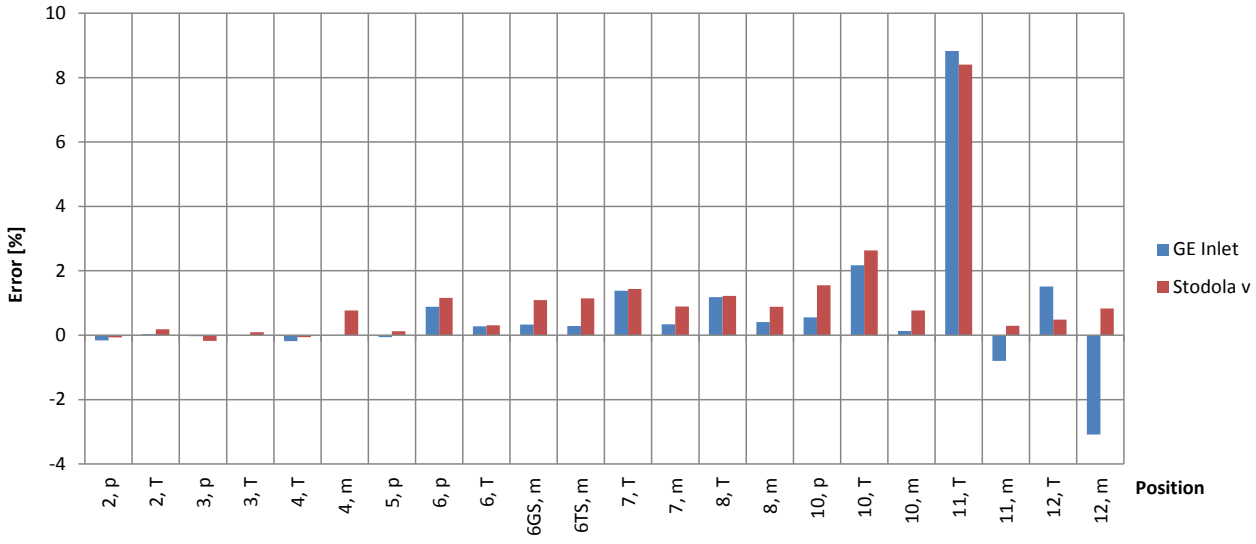

Figure D. 11: Error for PP-F at 25 kPa back pressure

In Figure D. 10 and Figure D. 11, one notes that the temperature error at point 11 is dominant for the same reason i.e. the overall efficiency of the IPT and LPT was applied to individual turbine sections instead of applying individual efficiencies to each turbine section. At point 12 in Figure D. 11, the mass flow predicted by “Stodola v” is much better than that predicted by “GE Inlet”. This could be that “Stodola v” outperforms “GE Inlet” at higher back pressures; however, there is insufficient data available to verify this. A similar trend is noted for PP-A at 60 % load, Figure 46, and for PP-C at 46 % load, Figure D. 5; however, their back pressure is very low.

Appendix E. Compound Component

E.1: Compound component script

Below is an extract of the C# code, showing the parameter definitions as main calculation block only.

```
public class Script: IPS.Scripting.IComponentScript
{
   IPS.Properties.Double _Pin; //total nominal inlet pressure (user input)
   IPS.Properties.Double _Pout; //total nominal outlet pressure (user input)
   IPS.Properties.Double _Massin; //nominal inlet mass flow rate (user input)
   IPS.Properties.Double _Rhoin; //nominal inlet density (user input)
   IPS.Properties.Double _Etan; //nominal efficiency (user input)
   IPS.Properties.Double _hndelta; //nominal enthalpy drop (user input)
   IPS.Properties.Double _hin; //inlet enthalpy (internal calculation)
   IPS.Properties.Double _houts; //outlet isentropic enthalpy (internal calculation)

   IPS.Properties.Double _Ck; //turbine loss constant (internal calculation)
   IPS.Properties.Double _Eta; //off design efficiency (internal calculation)

 //script main execution function - called every cycle
   public override void Execute(double Time)
   {
      //calculates the turbine loss constant
      _Ck.Value = (_Pin.Value - _Pout.Value)/(Math.Pow(_Massin.Value, 2)/_Rhoin.Value);

      //calculates the efficiency
      _Eta.Value = _Etan.Value - 2 * Math.Pow((_hndelta.Value/(_hin.Value - _houts.Value) - 1), 2);
   }
…

…

}
```